PRODUCTION OF TITANIUM DIOXIDE THIN FILMS WITH IMPROVED PHOTOCATALYTIC ACTIVITY: THE USE OF BACTERIA AS 3D TEMPLATES

A THESIS SUBMITTED TO
THE GRADUATE SCHOOL OF NATURAL AND APPLIED SCIENCES
OF
MIDDLE EAST TECHNICAL UNIVERSITY

BY

BURCU KOÇ HASKILIÇ

IN PARTIAL FULFILLMENT OF THE REQUIREMENTS
FOR
THE DEGREE OF MASTER OF SCIENCE
IN
MICRO AND NANOTECHNOLOGY

JULY 2009

Approval of the thesis:

PRODUCTION OF TITANIUM DIOXIDE THIN FILMS WITH IMPROVED PHOTOCATALYTIC ACTIVITY: THE USE OF BACTERIA AS 3D TEMPLATES

submitted by **BURCU KOÇ HASKILIÇ** in partial fulfillment of the requirements for the degree of **Master of Science in Micro and Nanotechnology, Middle East Technical University by**,

Prof. Dr. Canan Özgen _____
Dean, Graduate School of **Natural and Applied Sciences**

Prof. Dr. Raşit Turan _____
Head of Department, **Micro and Nanotechnology**

Prof. Dr. Gürkan Karakaş _____
Supervisor, **Chemical Engineering Dept., METU**

Prof. Dr. Mehmet Parlak _____
Co-supervisor, **Physics Dept., METU**

Examining Committee Members:

Prof. Dr. Ufuk Bakır _____
Chemical Engineering Dept., METU

Prof. Dr. Gürkan Karakaş _____
Chemical Engineering Dept., METU

Prof. Dr. Mehmet Parlak _____
Physics Dept., METU

Prof. Dr. Deniz Üner _____
Chemical Engineering Dept., METU

Prof. Dr. Zekiye Suludere _____
Biology Dept., Gazi University

Date: 03.07.2009

I hereby declare that all information in this document has been obtained and presented in accordance with academic rules and ethical conduct. I also declare that, as required by these rules and conduct, I have fully cited and referenced all material and results that are not original to this work.

Name, Last Name: Burcu Koç Haskılıç

Signature:

ABSTRACT

PRODUCTION OF TITANIUM DIOXIDE THIN FILMS WITH IMPROVED PHOTOCATALYTIC ACTIVITY: THE USE OF BACTERIA AS 3D TEMPLATES

Koç Haskılıç, Burcu
M.S., Department of Micro and Nanotechnology
Supervisor: Prof. Dr. Gürkan Karakas
Co-supervisor: Prof. Dr. Mehmet Parlak

July 2009, 139 pages

Transition metaloxide semiconductor, such as TiO_2, SnO_2, and ZnO have taken more attention as multifunctional materials with their unique physical and chemical properties. TiO_2 photocatalysts with anatase structure generate strong oxidizing power under UV irradition which corresponds to lower wavelength than its edge energy (385 nm) as a result of charge separation. The photocatalytic efficiency of many synthetically produced TiO_2 samples depend on many factors such as band gap, surface area, particle size, crystallinity etc. In recent years, much effort has been devoted to increase the photocatalytic efficiency of TiO_2 materials. Charge recombination is the major side reaction which limits the photocatalytic efficiency of TiO_2 materials. The crystal defects and impurities are usually attributed as charge recombination centers and larger particle size contributes to the loss of efficiency by increasing the charge recombination probability. The photocatalytic performance of TiO_2 materials might be improved by reducing the particle size or by increasing the porosity. In general, both methods have been applied to achieve higher photocatalytic activity by

synthesizing powders of highly dispersed fine particles and the thin films over the structural substrates such as glass panels, ceramic plates or textiles.

In the present study, porous and dispersed TiO_2 thin films were obtained over the Pyrex glass substrates by dip coating from a colloidal solution which was obtained by sol-gel method. The porosity and surface morphology of the thin films were modified by utilizing *Esherichia coli* as 3D templates. For this purpose, the colloidal solution of TiO_2 synthesized by sol-gel method is properly mixed with the *E. coli* culture and the precleaned glass substrates were coated by using dip-coating technique. The photocatalytic activities of the samples were measured against methylene blue degradation. Contact angle, band gap, surface area measurement and AFM, SEM were employed to characterize the coated samples. The contact angle of the samples between 2-5^o indicated the superhydrophilic structure which is necessary for antifogging applications. The relative surface area of the samples as measured by evaluating the methylene blue adsorption data with Langmuir adsorption isotherm. It was found that, the surface area of the catalysts increased proportionally with the addition of *E. coli* and the highest relative surface area was observed for the film with the 1.71 ratio of *E. coli* content as 19.69 cm^2/cm^2. The highest decomposition rate was achieved for the film with the composition of 0.83 : 1 for TiO_2 and *E. coli*, respectively which yields 6 times higher activity than the pure TiO_2 surface. However, the surface area of the samples enhanced by 3.5 times with the addition of *E. coli* in the same proportion. This indicates the importantce of other photocatalytic surface parameters such as reflection, transparency, etc.

Keywords: Semiconductor, thin films, TiO_2, SiO_2, sol-gel, photocatalytic activity, bacterial template, surface area, roughness, *E. coli*

ÖZ

FOTOKATALİTİK AKTİVİTESİ GELİŞTİRİLMİŞ TİTANYUM DİOKSİT İNCE FİLMLERİN ÜRETİMİ: BAKTERİLERİN 3 BOYUTLU ŞABLON OLARAK KULLANILMASI

Koç Haskılıç, Burcu
Yüksek Lisans, Mikro ve Nanoteknoloji Bölümü
Tez Yöneticisi: Prof. Dr. Gürkan Karakas
Ortak Tez Yöneticisi: Prof. Dr. Mehmet Parlak

Temmuz 2009, 139 sayfa

TiO_2, SnO_2, and ZnO gibi geçiş metal oksit yarıiletkenler benzersiz kimyasal ve fiziksel özellikleri ile çok işlevli malzemeler olarak ilgi çekmektedir. Anataz yapıda olan TiO_2 fotokatalizi sınır enerjisinden (385 nm) daha düşük dalga boyuna sahip UV ışıması ile uyarıldığında güçlü oksitleme potansiyeli oluşturur. Sentetik yöntemlerle elde edilen TiO_2 örneklerinin fotokatalitik verimliliği bant aralığı, yüzey alanı, partikül boyu, kristal yapısı gibi bir çok faktöre bağlıdır. Son yıllarda fotokatalitik aktivitenin verimliliğini arttırmak için çok fazla çaba harcanmıştır. Oluşan yüklerin tekrar biraraya gelmesi, TiO_2 malzemesinin düşük fotokatalitik verimliliğine sebep olan en önemli ikincil reaksiyonlardır. Kristal yapıdaki kusurlar ve safsızlıklar genellikle yüklerin tekrar bir araya geldiği bölgelerdir ve partikül boyutunun büyük olması da yüklerin bir araya gelme olasılığını arttırdığı için verimliliğin düşmesinde payı vardır. TiO_2 malzemenin fotokatalitik performansı partikül boyutunu azaltarak veya yüzey alanın artırarak geliştirilebilir. Genel olarak daha iyi fotokatalitik aktiviteye ulaşmak için, tamamen birbirinden ayrılmış ince partikül olarak sentezleme ve cam, seramik

veya tekstil malzemelerin yüzeyinde ince film olarak sentezleme yöntemlerinin her ikisi de uygulanabilir.

Bu çalışma ile sol-gel metodu kullanılarak elde edilen koloidal yapıdaki çözeltiye daldırarak kaplama yöntemi kullanılarak camların üzerine gözenekli yapıda ve tamamen yüzeye yayılmış TiO_2 ince filmler oluşturulmuştur. *Esherichia coli* bakterilerinin üç boyutlu şablon şeklinde kullanılması ile ince filmlerin yüzey gözenekliliği ve morfolojisi geliştirilmiştir. Bu amaç doğrultusunda sol-gel metodu kullanılarak hazırlanan TiO_2 çözeltisi *E. coli* bakteri kültürü ile tamamen karıştırılmış ve ön temizleme işleminden geçirilen cam altlıklar, elde edilen bu çözeltiye daldırarak kaplama yöntemi yardımıyla kaplanmıştır. Örneklerin fotokatalitik etkinliği metilen mavisinin bozunma reaksiyonu ile test edilmiştir. Yüzey yapısını karakterize etmek için yüzeyin saf su ile yaptığı temas açısı ölçümleri, bant aralığı ölçümleri, yüzey alanı ölçümleri, AFM ve SEM analizleri yapılmıştır. Örneklerin 2-5^o aralığında bulunan temas açısı ölçümleri filmlerin süper susever olduğunu göstermektedir ve bu özellikleri ile de filmler yüzeyde buharlaşmanın istenmediği alanlarda uygulama alanı bulabilirler. Örneklerin karşılaştırmalı yüzey alanı Langmuir soğurma izotermisi kullanılarak metilen mavisinin soğurganlık ölçümü ile hesaplanmıştır. Katalizlerin yüzey alanının *E. coli* konsantrasyonu ile orantılı olarak arttığı bulunmuştur ve hazırlanan örnekler arasında 1.71 oranında *E. coli* içeren filmin yüzey alanının en fazla olduğu gözlemlenmiştir (19.69 cm^2/cm^2). Ancak, en yüksek bozunma değeri 0.83 oranında TiO_2 ve 1 oranında *E. coli* içeren ince filmlerde gözlemlenmiştir. Bu filmlerin verimliliği saf TiO_2 ile kaplanan filmlerden 6 kat fazla iken aynı oranda *E. coli* eklenmesi ile elde edilen örneklerin yüzey alanı da 3.5 kat fazladır. Bu durum saydamlık ve yansıma gibi diğer fotokatalitik yüzey parametrelerinin önemini göstermektedir.

Anahtar Kelimeler: Yarı iletken, ince film, TiO_2, SiO_2, sol-gel, fotokatalitik aktivite, bakteriyel şablonlar, yüzey alanı, pürüzlülük, *E.coli*

To My Mother and Father

ACKNOWLEDGEMENTS

First of all I wish to express here my deep and sincere gratitude to my supervisor Prof Dr. Gürkan Karakaş and cosupervisor Prof. Dr. Mehmet Parlak for their valuable guidance and encouraging supports during this research.

I wish to express my gratitude to Prof. Dr. Ufuk Bakır for his valuable advises on growth mechanism and properties of *Escherichia coli* bacteria. I also would like to thank to Prof. Dr. Zekiye Suludere for SEM investigations and contribution.

Many thanks to Gizem Seber, Erinç Bahçegül and Merve Çınar for their help in cultivation of *Escherichia coli* under laboratory conditions. I am grateful to the members of my research group for their valuable help and discussions.

Additionally, I would like to thank my colleagues at The Scientific and Technological Research Council of Turkey (TUBITAK) for their suggestion and comments while writing this thesis.

I would like to thank my dear family for their endless love, patience and support. I wish to express my special appreciation to my mother Pakize Koç and my brother Burak Koç for their encouragement and motivation throughout my life.

Finally, I am thankful to my husband Hakan Haskılıç, for his patience, being there for me to share the life and especially for his love.

TABLE OF CONTENTS

ABSTRACT iv
ÖZ vi
ACKNOWLEDGEMENTS ix
TABLE OF CONTENTS x
LIST OF TABLES xiii
LIST OF FIGURES xv
CHAPTERS 1
1. INTRODUCTION 1
2. LITERATURE SURVEY 6
2.1. Semiconductors 6
2.1.1. Semiconductor Materials 6
2.1.2. Optical Absorption of Semiconductors 7
2.2. Photocatalysts 8
2.3. Hydrophilicity and Hydrophobicity 13
2.4. Mechanism for Photocatalytic Reaction and Superhydrophilicity of TiO_2 Thin Films 15
2.5. Improve the Photocatalytic Activity 20
2.5.1 Effect of Surface Morphology 21
2.5.2. Effect of Light Intensity, Wavelength and Noble Metals 23
2.5.3 Effect of Crystallographic Phase 25
2.5.4 Effect of Adsorption and pH 27
2.5.5 Transparency of TiO_2 Thin Films 27
2.7. Sol-Gel Method 29
2.8. Coating Methods 30
2.8.1. Spin Coating 31
2.8.2. Dip Coating 31
2.9. Heat Treatment 34

2.9.1. Drying 34
2.9.2. Calcination 35
2.10. Aging 35
2.11. Applications of Titania Thin Films 36
3. EXPERIMENTAL 44
3.1. Materials 44
3.1.1. Chemicals 44
3.2. Pretreatment of Substrate 45
3.3. Preparation of *Esherichia coli* Doped TiO_2 Solution 46
3.4. Coating the Films 50
3.5. Analysis of the Films 51
3.5.1. Spectroscopic Analysis 51
3.5.2. Surface Area Analysis of the Films 52
3.5.3. Self Cleaning Activity 55
3.5.4. Measurement of Photocatalytic Activity 56
3.5.5. Contact Angle Measurement 57
3.5.6. Surface Morphology and Thickness Measurement 57
3.5.7. Film Roughness Measurement 58
3.5.8. Surface Area, Pore Size Distribution, XRD and TGA Analysis for Powder Form 58
4. RESULTS AND DISCUSSION 60
4.1. Measurements of Photocatalytic Activities 60
4.2. Optical Absorption of the Films 69
4.3. Surface Area Measurements 70
4.3.1. Surface Area Determination of the Powders 70
4.3.2. Surface Area Determination of the Films 70
4.4. Film morphology 75
4.4.1. Surface SEM Images of the *E. coli* doped TiO_2 Thin Films 75
4.4.2. Cross Sectional SEM Images of Thin Films 85
4.5. Film roughness 86
4.6. Characterization of Hydrophilic Property 89

4.7. Thermal Analysis of the *E. coli* Doped Thin Films 92
4.8. Crystalline Film Formation 94
4.9. Pore Size Distribution Measurements 96
5. CONCLUSIONS 98
6. FURTHER SUGGESTIONS 100
REFERENCES 101
APPENDICES 117
A. SAMPLE CALCULATIONS FOR THE TITANIUM DIOXIDE AND *E. COLI* CONCENTRATION IN THE SOLUTIONS 117
A.1. Titanium Dioxide Rate Calculation in the Solution 117
A.2. *E. coli* Rate Calculation in the Solution 119
B. CALCULATIONS FOR SURFACE AREA MEASUREMENTS 121
C. DATA OF PHOTOCATALYTIC ACTIVITY MEASUREMENTS 133
D. PREPARATION OF NUTRIENT BROTH 143
E. GROWTH CURVE 144

LIST OF TABLES

Table 2.1 Band gap energy of various catalysts 9
Table 2.2 Degrees of wetting 14
Table 3.1 Preparation of *E. coli* doped TiO_2 solutions of different concentrations 49
Table 4.1 *E. coli* doped TiO_2 solutions of different concentrations 67
Table 4.2 Relative Surface area of the thin films with different concentrations.. 73
Table 4.3 Surface area of the powder samples with different concentrations..... 75
Table 4.4 *E. coli* doped TiO_2 film thickness with three dip coating layers..... 86
Table 4.5 Contact angle measurements of pretreated substrate 89
Table 4.6 Contact angle measurements of *E. coli* doped TiO_2-SiO_2 coated cracked thin films 91
Table 4.7 Contact angle measurements of *E. coli* doped TiO_2-SiO_2 coated crack free thin films 91
Table B.1 Data required to calculate surface area measurement for the sample of TiO_2 rate is 0.71 and *E. coli* rate is 1.71..... 125
Table B.2 Data required to calculate surface area measurement for the sample of TiO_2 rate is 0.91 and *E. coli* rate is 0.54..... 127
Table B.3 Data required to calculate surface area measurement for the sample of TiO_2 rate is 0.95 and *E. coli* rate is 0.29..... 128
Table B.4 Data required to calculate surface area measurement for the sample of TiO_2 rate is 0.98 and *E. coli* rate is 0.12..... 130
Table B.5 Data required to calculate surface area measurement for the sample of TiO_2 rate is 1 and *E. coli* rate is 0..... 131
Table C.1 Concentration change of methylene blue stain with the concentartion of 170 mg/lt for the *E. coli* doped titanium dioxide coated thin films subjected to 300 W/m^2 artificial solar irradiation.....133

Table C.2 Concentration change of methylene blue stain with the concentartion of 180 mg/lt for the *E. coli* doped titanium dioxide coated thin films subjected to 300 W/m^2 artificial solar irradiation.....135
Table C.3 Concentration change of methylene blue stain with the concentartion of 190 mg/lt for the *E. coli* doped titanium dioxide coated thin films subjected to 300 W/m^2 artificial solar irradiation.....137
Table C.4 Concentration change of methylene blue stain with the concentartion of 210 mg/lt for the *E. coli* doped titanium dioxide coated thin films subjected to 300 W/m^2 artificial solar irradiation.....139
Table C.5 Concentration change of methylene blue solution for the *E. coli* doped (x0-x0.12-x0.29) titanium dioxide (x1-x0.98-x0.95) coated thin films subjected to 300 W/m^2 artificial solar irradiation.....140
Table C.6 Concentration change of methylene blue solution for the *E. coli* doped (x0.54-x1-x1.71) titanium dioxide (x0.91-x0.83-x0.71) coated thin films subjected to 300 W/m^2 artificial solar irradiation.....141
Table C.7 Mean, standart deviation and error value of the *E. coli* doped (x0.54-x1-x1.71) titanium dioxide coated thin films.....142
Table C.8 Mean, standart deviation and error value of the *E. coli* doped (x0.12-x0.29-x0.54-x1-x1.71) and undoped titanium dioxide coated thin films.....142

LIST OF FIGURES

Figure 2.1 Simplified diagram of the electronic band structure of metals, semiconductors, and insulators 7
Figure 2.2 Optically generated electron hole pair formation in a semiconductor.. 8
Figure 2.3 Generation of photocatalytic active species at the surface of photocatalyst..... 10
Figure 2.4 Schematic representations of selected low-index faces of rutile: (a) (110); (b) (100); and (c) (001)..... 11
Figure 2.5 Schematic representations of selected low-index faces of anatase: (a) (101); (b) (100); and (c) (001)..... 12
Figure 2.6 Wetting of different fluids 14
Figure 2.7 Mechanism of photocatalysis..... 17
Figure 2.8 Mechanism of photoinduced superhydrophilicity of TiO_2 18
Figure 2.9 Self-cleaning mechanism of hydrophilic TiO_2 thin films..... 20
Figure 2.10 Mechanism of photocatalysis improved by noble metals..... 25
Figure 2.11 Stages of the dip coating process; (a) dipping, (b) wet layer formation and (c) evaporation..... 32
Figure 2.12 Schematic drawing of evaporation of the solvent and subsequent destabilization of the sol..... 33
Figure 2.13 Industrial applications of TiO_2..... 36
Figure 2.14 Self-cleaning test for a PVC tent material manufactured by Taiyo Kogyo done in the Photocatalyst Museum, KAST. The left half part of the tent material was coated with TiO_2. (a) Picture taken in July 22, 2004. (b) Picture taken in April 23, 2007 38
Figure 2.15 Finished sample for the usage of TiO_2-based photocatalytic material on roadway surfaces with the coated surface showing a lighter color..... 40
Figure 3.1 Flow chart for the preparation of titanium dioxide-silicon dioxide ludox colloidal solution..... 47

Figure 3.2 *E. coli* doped TiO_2-SiO_2 coating solution of (a)*E. coli* x 1, (b)*E. coli* x 0.29 and (c)*E. coli* x 0 50
Figure 3.3 Experimental setup for dip coating 51
Figure 3.4 The structure of methylene blue 52
Figure 3.5 Photographs of the (a) adsorbing solutions in the presence of solid after 24 hours and (b) the solids removed from the MB solution after 24 hours 55
Figure 3.6 Thin films (a) maintained in methylene blue solution for 24 hours and then dried (b) radiated with Suntest solar simulator until the recorded absorbance data reached to constant value. 57
Figure 4.1 Thin films which contained *E. coli*:TiO_2 at a rate of 1:0.83, were stained with the methylene blue solution which had concentrations between the range of 150 mg/lt-210 mg/lt (a) kept in dark place (b) radiated with Suntest solar simulator for 4 hours. 62
Figure 4.2 Concentration change of methylene blue for the *E. coli* doped titanium dioxide coated thin films subjected to 300 W/m^2 artificial solar irradiation. 63
Figure 4.3 Concentration change of methylene blue stained on the surface of the thin films with different *E. coli* and titania content under 300W/m^2 irradiation. 64
Figure 4.4 Concentration change of methylene blue solution on the surface of the thin films with different *E. coli* and titania content under 300W/m^2 irradiation 66
Figure 4.5 The initial degradation rate of methylene blue which is the avarage of four different data for various *E. coli* (x0.54-x1.71) contents. 68
Figure 4.6 The initial degradation rate of methylene blue which is the avarage of two different data for various *E. coli* (x0-x1.71) content. 68
Figure 4.7 Absorbance spectra of *E. coli* doped and undoped TiO_2 - SiO_2 coated films. 70
Figure 4.8 Adsorption isotherm for the sample of TiO_2 rate is 0.71 and *E. coli* rate is 1.71 72

Figure 4.9 Relationship between the initial rate of MB degredation and the surface area of the thin films. 74
Figure 4.10 Cluster of *E. coli* cells magnified 5,000 times 76
Figure 4.11 SEM surface image of TiO_2–SiO_2 layer of pH≈2 78
Figure 4.12 SEM surface image of the cracked titania layer of pH≈8 78
Figure 4.13 SEM surface image of the cracked titania layer doped with *E. coli* x 0.29 79
Figure 4.14 SEM surface image of the cracked titania layer doped with *E. coli* x 0.54 79
Figure 4.15 SEM surface image of the cracked titania layer doped with *E. coli* x 1 80
Figure 4.16 SEM surface image of the crack free titania layer of pH≈8, indicating a low porosity level 81
Figure 4.17 SEM surface image of the crack free titania layer doped with *E. coli* x 0,12 81
Figure 4.18 SEM surface image of the crack free titania layer doped with *E. coli* x 0,29 82
Figure 4.19 SEM surface image of the crack free titania layer doped with E coli x 0,54 82
Figure 4.20 SEM surface image of the crack free titania layer doped with *E. coli* x 1 83
Figure 4.21 SEM surface image of the crack free titania layer doped with *E. coli* x 1.71 indicating a high porosity level 83
Figure 4.22 SEM surface view of the overlaped *E. coli* bacteria sink into three-layered film. 84
Figure 4.23 AFM image of the (a) interior part of the *E. coli* gap and (b) outer part of the *E. coli* gap for the film with the rate of 1.71(*E. coli*) and 0.71 (TiO_2). 87
Figure 4.24 AFM image of the (a) interior part of the *E. coli* gap and (b) outer part of the *E. coli* gap for the film with the rate of 0.12 (*E. coli*) and 0.98 (TiO_2). 88

Figure 4.25 Differential thermal analysis (DTA) and thermogravimetric analysis (TGA) curves of *E. coli* doped TiO_2 powders with composition of *E. coli* x 1 and TiO_2 x 0.83 93
Figure 4.26 Differential thermal analysis (DTA) and thermogravimetric analysis (TGA) curve of *E. coli* doped TiO_2 powders with composition of *E. coli* x 0.29 and TiO_2 x 0.95 93
Figure 4.27 Differential thermal analysis (DTA) and thermogravimetric analysis (TGA) curve of *E. coli* doped TiO_2 powders with composition of *E. coli* x 0 and TiO_2 x 1 94
Figure 4.28 Powder X-ray diffraction patterns for (a) *E. coli* x 1 and TiO_2 x 0.83 and (b) *E. coli* x 0.29 and TiO_2 x 0.95 95
Figure 4.29 Pore size distribution curves of TiO_2 films which include: (a) *E. coli* x 0 and (b) *E. coli* x 1 97
Figure B.1 Adsorption isotherm for the sample of TiO_2 rate is 0.83 and *E. coli* rate is 1 124
Figure B.2 Adsorption isotherm for the sample of TiO_2 rate is 0.71 and *E. coli* rate is 1.71 126
Figure B.3 Adsorption isotherm for the sample of TiO_2 rate is 0.91 and *E. coli* rate is 0.54 127
Figure B.4 Adsorption isotherm for the sample of TiO_2 rate is 0.95 and *E. coli* rate is 0.29 129
Figure B.5 Adsorption isotherm for the sample of TiO_2 rate is 0.98 and *E. coli* rate is 0.12 130
Figure B.6 Adsorption isotherm for the sample of TiO_2 rate is 1 132
Figure C.1 Concentration change of methylene blue (170 mg/lt) solution on the surface of the thin films with different *E. coli* and titania content.....134
Figure C.2 The initial degradation rate of methylene blue solution (170 mg/lt) for various *E. coli*content.....134
Figure C.3 Concentration change of methylene blue solution (180 mg/lt) on the surface of the thin films with different E. coli and titania content.....136

Figure C.4 The initial degradation rate of methylene blue solution (180 mg/lt) for various *E. coli* content.....136
Figure C.5 Concentration change of methylene blue solution (190 mg/lt) on the surface of the thin films with different *E. coli* and titania content.....138
Figure C.6 The initial degradation rate of methylene blue solution (190 mg/lt) for various *E. coli* content.....138
Figure D.1 Flow chart for the preparation of *E. coli* culture.....143
Figure E.1 Growth curve of *E. coli* XL1-blue.....144

CHAPTER 1

INTRODUCTION

Photocatalysis is the enhancement of photoinduced reaction rate by the presence of a catalyst. Semiconductor materials absorb the light and respond by the generation of electron-hole (e^-/h^+) pairs. The electron-hole pairs formed in the solid materials are very active and either recombine in bulk, diffuse to the surface, recombine over the surface, or trapped by the surface adsorbed species and generate free radicals by electron transfer. The free radicals have great potential to initiate many reduction and oxidation reactions. However, only small proportion of electron-hole pairs can reach to the outer surface and trapped by surface ad-species. The photocatalytic efficiency is limited by the side reactions which results with charge recombination in a great extend and only 10-12 % of photons that are absorbed can be converted to free radicals.

Among the many photocatalysts, such as ZnO, CdS and WO, titanium dioxide are the widely used semiconductor catalyst in photocatalysis processes since it is chemically and biologically inert, photocatalytically stable, relatively easy to produce, has high-dielectric constant, high refractivity, able to efficiently catalyse reactions, inexpensive and without risks to environment or humans [1]. Bulk TiO_2 exists primarily in three different crystalline phases named as anatase, rutile and brookite. It has been reported that anatase phase which has a tetragonal structure, develops at temperature below 573-873 ^oC has shown greater photocatalytic efficiency for the degradation of organic pollutants. At higher temperature above 573-873 ^oC, anatase is transformed into rutile phase that has tetragonal structure [2, 3] Despite that it has been found that the rutile (stable phase) photoactivity may not be negligible regarding the preparation method [4], TiO_2 in anatase phase (metastable phase) has shown the greater photocatalytic efficiency for the degradation of organic pollutants [5]. On the other hand, the

brookite phase that has an orthorhombic structure, has many defects in the crystal structure and so it has not been used as a photocatalyst. In addition, formation of a particular phase not only depends upon the annealing temperature but also it depends on nature of starting material, its composition and deposition [6].

Starting in the late 1960s, titanium dioxide (TiO_2) material has been studied in different areas. TiO_2 uses both as photocatalytic materials and structural materials which were applied in exterior construction materials and interior furnishing materials, such as cement mortar, exterior tiles, paving blocks, glass and PVC fabric is attributed to the properties including air purification, self-cleaning and selfdisinfecting [7]. Wastewater effluents from the textile industry are one of the major pollutants of the environment since they contain considerable amounts of non-fixed dyes and a huge amount of inorganic salts. Using TiO_2 is an effective method for the degradation/decoloration of various dyes in solution [8]. Thin TiO_2 films are broadly used optical applications ranging from dielectric interference filters to antireflective coatings [9]. In addition surfaces of a controlled hydrophilicity have many useful applications such as anticlouding effect of bathroom mirrors, car windows and full wetting conditions for dehumidifying heat exchangers [9, 10].

Because of the fact that, TiO_2 is one of the most powerful oxidant due to the high oxidizing potential of holes in the valence band formed by photoexcitation, it has been studied in various areas as explained. However, TiO_2 has some restrictions in terms of technological application. The most restrictive concern is the need for the excitation source because TiO_2 is photoactive only under about wavelength of smaller than 380 nm due to its large band gap ($E_g \approx 3.2$ eV). Thus photocatalytic activity of TiO_2 is expected to be low under visible light irradiation since UV light is about < 10 % of the over-all solar intensity [11].

There are several aspects that influencing efficiency of the TiO_2 material. One of the important factor is crystallographic phase of titanium dioxide. The meta stable anatase phase exhibits a higher efficiency than the thermodynamic stable rutile phase. A further aspect concerning the efficiency is the lifetime of electron hole pairs which should be as long as possible which can be reached by a low recombination rate and therefore a low defect density within the layers [12]. It is declared that amorphous titanium dioxide layers show no photocatalytic activity, because no e^-/h^+ pairs with satisfactory lifetime are generated. Furthermore the size of the surface area plays a significant role since a larger surface area increases the adsorption of more molecules and therefore maximize the photocatalytic efficiency [13]. In addition, the photocatalytic activity is influenced by structure and morphology which are determined by the deposition parameters [14]. Other common way to enhance the quantum efficiency improvement and thus photocatalytic activity of TiO_2 under UV irradiation is to load metal. Metal deposition particles can act as electron trapping to reduce the recombination rate of photogenerated electron-hole pairs. Within the related dopant metals the most suitable one would also be convenient for industrial applications due to its low cost and easy preparation [15].

It has been notified that TiO_2 has various application areas such as air cleaning, water purification, self cleaning effect. In order to avoid problems that were experienced while applying titania powder to different areas, developing immobilise TiO_2 particles in film form on pyrex glass was studied. A number of techniques have been reported in literature to obtain thin films of TiO_2. Among these sol-gel process is one of the industrially promising technique for the preparation of thin films onto the large scale substrates.

Sol-gel process offers advantages in terms of low consumption of energy, low material consumption rate, simplicity and speedy deposition on small as well as large area or curved substrates with good homogeneity and tailored inhomogeneity without the requirement of expensive and complicated

equipment. On the other hand, the only drawback of this technique is that the post deposition heat treatment (calcination) of the substrate at several hundred degrees Celsius is required to remove hydroxyl and organic functional groups, which limit the substrate to be a thermostable material. [16, 17]

Sol-gel method can be used to fabricate almost any single- or multi-component oxide coating which has been classified as two different methods named as dip and spin coating. The dip coating has been used for preparation TiO_2 nanostructured thin films in accordance with several studies.

The aim of the current study is to improve the photocatalytic and hydrophilic properties by developing a simple and repeatable procedure. In order to improve the activity, porosity and the surface area was changed. For this purpose, *Esherichia coli* doped TiO_2-SiO_2 coatings were studied for increasing the visible light absorption of TiO_2 materials. The multi-layered TiO_2 films on glass substrates were deposited by sol-gel dip coating technique in the present study. Then photocatalytic activity, hydrophilicity and surface area of the films were determined.

The multiple dip coated mesoporous TiO_2 thin films were characterized by using CAM, SEM and UV-Visible Spectrophotometer. In order to reveal the porosity of the films surface area measurements were carried out by using the adsorption of methylene blue. Then, the adsorption data were analyzed according to the Langmuir equation. Moreover, the photocatalytic activities of the films were measured with the degradation of organic materials when subjected to the artificial solar light irradiation.

In order to obtain the crystallographic structure of the films, XRD was used however no particular peak could be observed. The parallel situation was experienced for the BET analysis. Moreover, sample preparation of the films was almost unfeasible for some analysis such as TGA. Therefore, experimental

investigations of BET, pore size distribution, XRD and TGA were performed on titanium dioxide powders. TiO_2 powders were synthesized by drying the stock solution prepared for dip-coating procedure and grinding to obtain powdered samples. These samples were calcinated at the same temperature and time.

CHAPTER 2

LITERATURE SURVEY

2.1. Semiconductors

2.1.1. Semiconductor Materials

According to band theory of solids, instead of having discrete energies as in the case of free atoms, the available energy states form bands. Solids have two energy bands which are conduction band and valence band. The valence band is the lower energy band where electrons are normally present at absolute zero. On the other hand, conduction band which is the range of electron higher than that of the valence band, is empty at absolute zero. The energy difference between the valence and the conduction band is called the band gap. As the temperature rises or light is introduced, electrons absorb the energy and leave the valence band to rise up to the conduction band if they gain enough energy which is greater than the band gap energy [18].

At the temperatures different from absolute zero, electrical conductivity of solids depends on the magnitude of the band gap. As shown in Figure 2.1 in insulators the electrons in the valence band are separated by a large gap from the conduction band, in conductors like metals the valence band overlaps the conduction band, and in semiconductors there is a small enough gap between the valence and conduction bands that might be conveyed by the photons. Therefore in a semiconductor electrons can be more easily excited from the valence band to the conduction band which leads to higher electrical conductivity when compared with an insulator [19].

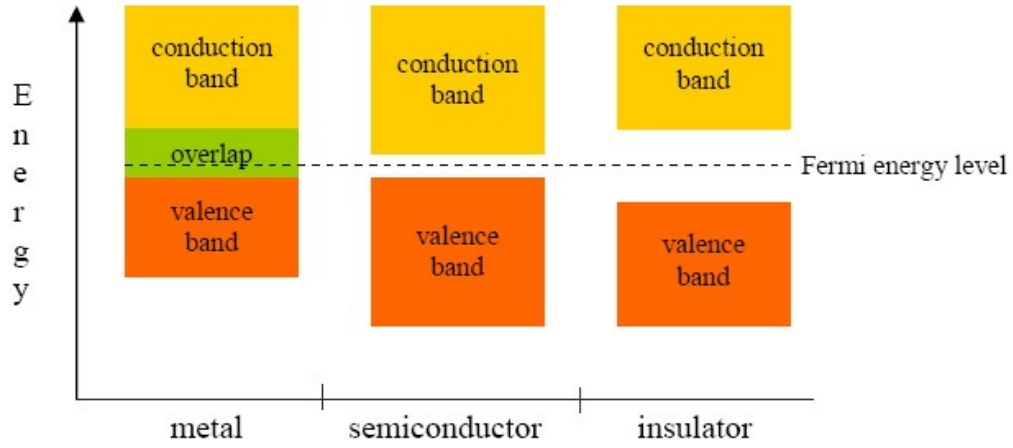


Figure 2.1 Simplified diagram of the electronic band structure of metals, semiconductors, and insulators

2.1.2. Optical Absorption of Semiconductors

The energy of photon is;

$$E = h\nu \quad \textbf{(2.1)}$$

where h is Plank's constant and ν is the frequency. The relation between the wavelength and energy can be given as follows

$$\lambda = c/\nu = hc/E \quad \textbf{(2.2)}$$

where E is the photon energy in eV and c is the speed of light.

Depending on the photon energy and bandgap energy, when a semiconductor is illuminated with light the photons may be absorbed or propagated through the semiconductor. If photon energy is less than bandgap energy, the photons are not readily absorbed. Under these circumstances the light is transmitted through the material or scatter back and the semiconductor appears to be transparent. Inversely, the photon can interact with a valence electron and elevate it into the conduction band. This interaction creates an electron in the conduction band and

a hole in the valence band namely electron hole pair. The basic absorption process for different values of hν shown in Figure 2.2 [20].

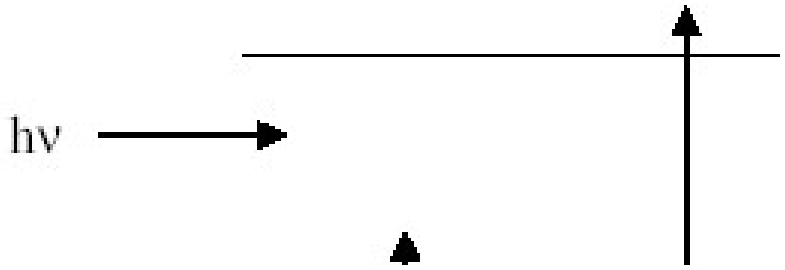


Figure 2.2 Optically generated electron hole pair formation in a semiconductor

2.2. Photocatalysts

The prefix photo, defined as "light" and catalysis is the process where a substance participates in modifying the rate of a chemical transformation of the reactants without being altered in the end. Hence, photocatalysis is a change in the rate of chemical reactions which uses light to activate a substance (photocatalysis) that increase the rate of a chemical reaction without being involved itself [20]. A good catalyst should be photoactive, able to utilize visible or near UV light, biologically and chemically inert material, non-toxic and inexpensive [21].

Photocatalysis uses semiconductor materials as catalysts. It is a promising technique that utilizes nano-sized semiconductors like TiO_2, ZnO, CdS, WO_3, $FeTiO_3$, V_2O_5, CeO_2 and $SrTiO_3$ which have a narrow gap between the valence and conduction bands to carry out photo induced oxidation process to disassemble VOCs into CO_2 and H_2O, and completely mineralize. Table 2.1 give band gap energies for some of these catalysts. However, some of the semiconductors may be unfavourable according to their application areas.

Exemplifying, CdS and ZnO do not have long term stability in aqueous media and photooxidation kinetics are poor in n-Si. Metal sulfide semiconductors are unstable since they undergo photoanodic corrosion [22].

Table 2.1 Band gap energy of various catalysts

Photocatalyst	**Bandgap Energy (eV)**
Si	1.1
TiO_2 (rutile)	3.0
TiO_2 (anatase)	3.2
ZnO	3.2
WO3	2.7
CdS	2.4
ZnS	3.7

The structure of energy levels in semiconductor materials is well described by the quantum theory of solids [23]. Electron-hole pairs are generated upon interband electronic transitions as an effect of interaction with photons having energy equal or higher to the band gap that is separating the conduction and valance bands (Figure 2.3).

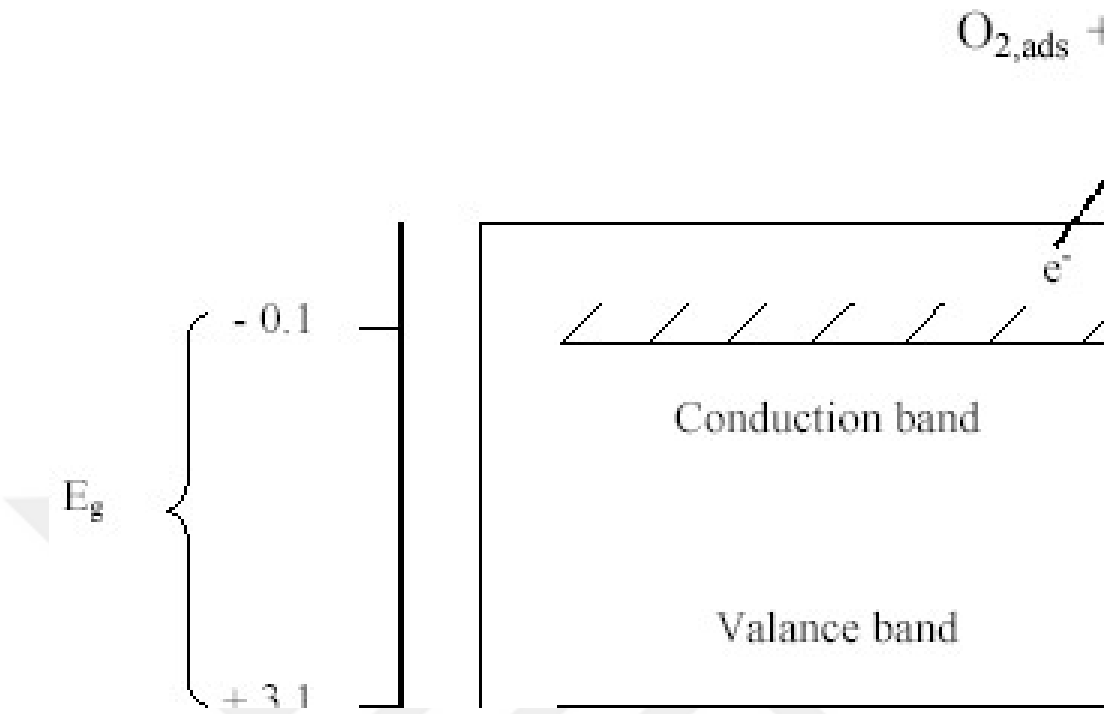


Figure 2.3 Generation of photocatalytic active species at the surface of photocatalyst

Titanium dioxide, also known as titanium (IV) oxide or titania (TiO_2), is the naturally occurring oxide of titanium. There are three main types of TiO_2 structures that are rutile, anatase and brookite. Rutile is the most stable phase for particles above 35 nm in size [24] and anatase is the most stable phase for nanoparticles below 11 nm. Brookite has been found to be the most stable for nanoparticles in the 11-35 nm range [25]. It has been reported that, commonly rutile and anatase are used in photocatalysis, with anatase showing a higher photocatalytic activity [26].

Rutile has three main crystal faces which of two are quite low in energy and are thus considered to be important for practical polycrystalline or powder materials [27]. These two crystal faces are (110) and (100) which is demonstrated from the

Fig. 2.4 (a), (b). Furthermore, within them the most thermally stable one is (110), and therefore it has been the most practically studied [25].

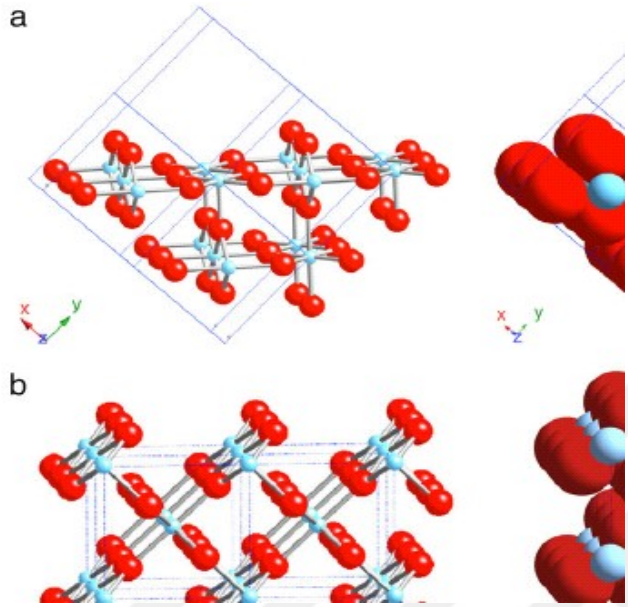


Figure 2.4 Schematic representations of selected low-index faces of rutile: (a) (110); (b) (100); and (c) (001) [23] .

Anatase has two low energy surfaces, (101) and (001) (Fig.2.5 (a), (b)), which are common for natural crystals. The (101) surface is the most prevalent face for anatase nanocrystals while the (100) surface is less common on typical nanocrystals but is observed on rod-like anatase grown hydrothermally under basic conditions [28, 29].

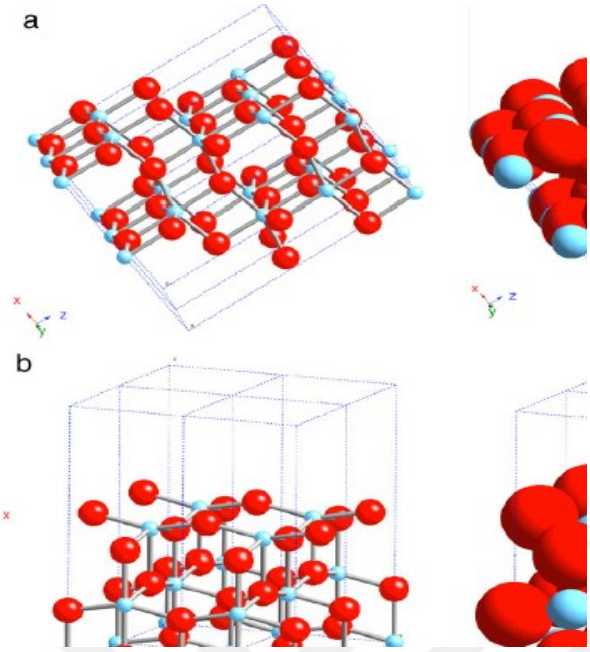


Figure 2.5 Schematic representations of selected low-index faces of anatase: (a) (101); (b) (100); and (c) (001) [23].

The brookite phase, which is rare and more difficult to prepare, has also been studied as a photocatalyst has three crystal face that are (010), (110) and (100) [25].

TiO_2 is a semiconductor with a band gap of 3.2 eV (380 nm) which is the energy difference between the valence band and the conduction band as noticed before. When photocatalyst titanium dioxide (TiO_2) absorbs ultraviolet (UV) radiation from sunlight or illuminated light source (fluorescent lamps) with the electrons can be excited from the valence to the conduction band [30]. This property promoted titanium dioxide as a good and promising candidate for use as a photocatalyst using solar light as energy source.

TiO_2 is usually supplied in the form of powder. Some of the particle properties which are known to affect the photocatalytic activity are particle size, crystal

structure, absolute crystallinity, quantity and the identity of defects, optical properties etc. Also the incident light intensity, adsorption of pollutants, pH of the solution, and preparation method have an important role on photocatalytic activity [31-34]. Semiconductor powders are not acceptable as photo catalyst because of the difficulties of separation, mixing and irraditation problems of nanostructured powders. There is a great interest on the immobilzation of photocatalysts over a support material having a proper irradiation geometry and stability and a suitable method to fix the semiconductors into a solid supporting material has being considered for a long time [35]. Immobilization of TiO_2 particles by using binders, coating surfaces with vacuum deposition techniques such as CVD [36], PVD [37], pyrolytic coating techniques [38], spray coating [39] or dip coating [40] of colloidal solutions are some of these methods.

2.3. Hydrophilicity and Hydrophobicity

Wetting is the contact between a liquid and a solid surface, resulting from intermolecular interactions including the surface tensions or energies between two surfaces. The degree of wetting is described by the angle at which the liquid-vapor interface meets the solid-liquid interface that is called contact angle [41].

When the wetting is very favorable, the fluid will spread to cover a larger area on the surface as a conclusion contact angle will be low, demonstrated from the Figure 2.6 (A). Inversely, the fluid will form a compact droplet on the surface, if the wetting is unfavorable which can be seen from the Figure 2.6 (B). [41]

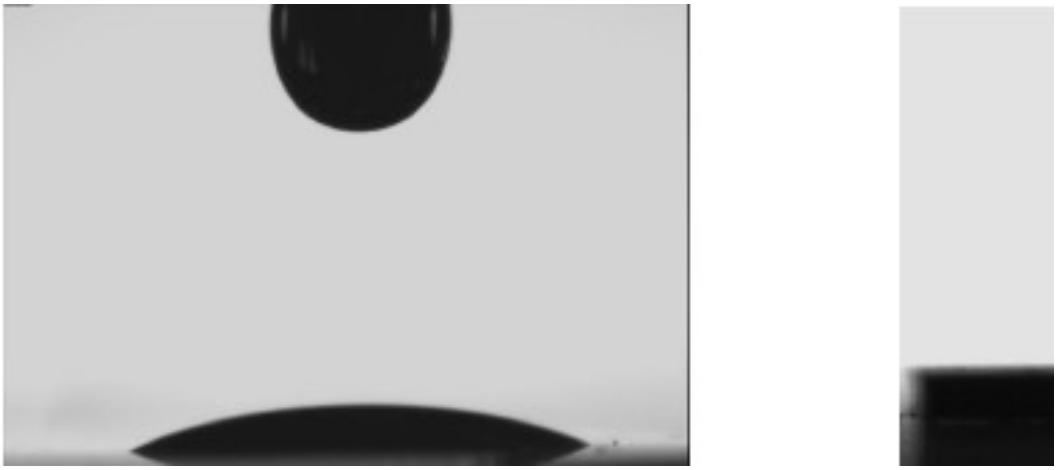


Figure 2.6 Wetting of different fluids

A table describing varying contact angles and their corresponding solid/liquid and liquid/liquid interactions can be seen as follows. A contact angle of 0° indicate complete/perfect wetting, contrarily a contact angle of 180° corresponds to complete/perfectly non-wetting [41]. In the context of water, a wettable surface may also be termed hydrophilic and a non-wettable surface hydrophobic.

Table 2.2 Degrees of wetting

Contact Angle	**Degree of Wetting**	**Strength of:**	
		S/L Interactions	**L/L Interactions**
$\theta = 0^o$	perfect wetting super-hydrophilic	strong	weak
$0^o < \theta < 90^o$	high wettability	strong	strong
		weak	weak
$90^o \leq \theta < 180^o$	low wettability	weak	strong
$\theta = 180^o$	perfectly non-wetting super-hydrophobic	weak	strong

In 1805 Thomas Young defined the contact angle θ which by analyzing the forces acting on a fluid droplet resting on a solid surface surrounded by a gas. The contact angle, θ, is the angle formed by a liquid at the three phase boundary where the liquid, gas, and solid intersect. The contact angle which depends on the interfacial tensions between the gas & liquid, liquid & solid, and gas & solid, can be expressed analytically by using Young's Relation:

$$\gamma_{SG} = \gamma_{SL} + \gamma_{LG} \cos\theta \quad \textbf{(2.3)}$$

where

γ_{SG} = Interfacial tension between the solid and gas

γ_{SL} = Interfacial tension between the solid and liquid

γ_{LG} = Interfacial tension between the liquid and gas

The consequence of this equation is that the complete wetting occurs when $\gamma_{SG} > \gamma_{SL} + \gamma_{LG}$ and zero wetting forms when $\gamma_{SL} > \gamma_{SG} + \gamma_{LG}$ [42].

θ can be measured using a contact angle goniometer. Contact angle goniometers measure a droplet's contact angle by assuming the droplet fits the geometry of a sphere, ellipsoid, or the Young-Laplace equation.

2.4. Mechanism for Photocatalytic Reaction and Superhydrophilicity of TiO_2 Thin Films

The excess energy of excited electron promoted the electron to the conduction band of titanium dioxide therefore creating the negative-electron (e^-) at the conduction band and positive-hole (h^+) at the valence band.

Electron-hole (e^-/h^+) pair formation:

$$TiO_2 \xleftrightarrow{h\nu} e_{cb}^- (TiO_2) + h_{vb}^+ (TiO_2) \quad \textbf{(2.4)}$$

The mobile charge carrier species may either recombine or reach the semiconductor surface where they can be trapped by the surface adsorbates or other sites. Under ambient conditions, oxygen (O_2) and water (H_2O) molecules in air are the primary adorbed species over the surface. The relative concentrations of O_2 and H_2O depends on the reaction medium and the reaction takes place under air or aquaeous conditions, the relative amount of O_2 and H_2O species varies. The photogenerated electrons react with molecular oxygen (O_2) to produce superoxide radical anions ($O_2^{\bullet -}$), and the photogenerated holes react with water molecule adsorbed on the TiO_2 surface to produce hydroxyl ($OH^{\cdot}$) radicals [30].

Semiconductor valence band hole and conduction band electron [43]:

$$TiO_2^{-} + O_2 + H^+ \rightarrow TiO_2 + HO_2 \quad \textbf{(2.5)}$$

$$TiO_2^{-} + H_2O_2 + H^+ \rightarrow TiO_2 + H_2O + OH^{\bullet} \quad \textbf{(2.6)}$$

Electron removal from the conduction band [43]:

$$TiO_2^{-} + 2H^+ \rightarrow TiO_2 + {}^{\bullet}H_2 \quad \textbf{(2.7)}$$

$$TiO_2^{-} + 2O_2 \rightarrow TiO_2 + O_2^{-\bullet} \quad \textbf{(2.8)}$$

Hole trapping [146]:

$$H^+ + H_2O \rightarrow OH^{\bullet} + H^+ \quad \textbf{(2.9)}$$

$$H^+ + HO^{-} \rightarrow OH^{\bullet} \quad \textbf{(2.10)}$$

Oxidation of organic pollutant molecules [43]:

$$OH^{\bullet} + O_2 + C_xO_yH_{(2x-2y+2)} \rightarrow xCO_2 + (x-y+1)H_2O \quad \textbf{(2.11)}$$

Non-productive radical reactions [43]:

$$TiO_2^{-} + OH^{\bullet} + H^+ \rightarrow TiO_2 + H_2O(\text{recombination}) \quad \textbf{(2.12)}$$

$$2OH^{\bullet} \rightarrow H_2O_2 \quad \textbf{(2.13)}$$

$$2HO_2^{-} \rightarrow H_2O_2 + O_2 \quad \textbf{(2.14)}$$

$$2OH^{\bullet} + H_2O_2 \rightarrow H_2O + O_2 \quad \textbf{(2.15)}$$

$$2OH^{\bullet} + HCO_3^{-} \rightarrow CO_3^{\bullet} + H_2O \quad \textbf{(2.16)}$$

These highly reactive species are able to decompose a variety of pollutants and kill microorganisms such as bacteria and viruses [44]. This cycle that continues when light is available is demonstrated at the Figure 2.7 [45].

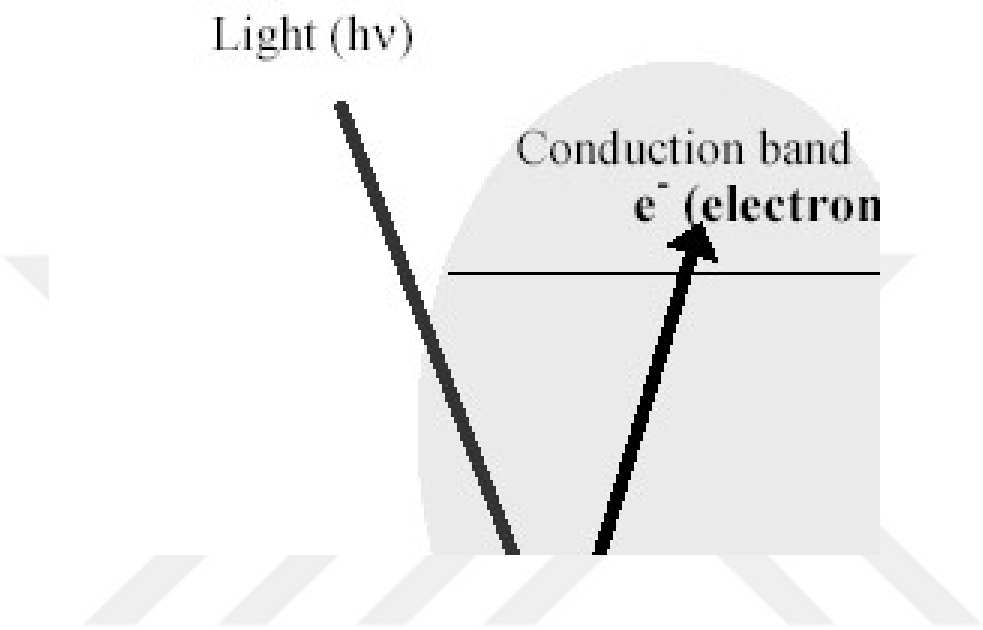


Figure 2.7 Mechanism of photocatalysis

Apart from the photocatalytic properties, TiO_2 films exhibit superhydrophilicity, after UV illumination [46]. As in the case of photocatalysis, in superhydrophilicity electrons and holes are still produced, but they react in a different way. The superhydrophilicity mechanism occurs in three steps.

In the first step, as in the case of photocatalysis mechanism when the surface of TiO_2 is irradiated by UV light, an electron–hole pair is created by excitation.

$$h\nu \longrightarrow e^- + h^+ \qquad \textbf{(2.17)}$$

Then, the Ti on the TiO_2 crystal surface is reduced by a surface trapped electron and the oxygen vacancies are created.

$$e^- + Ti^{4+} \longrightarrow Ti^{3+} \quad \textbf{(2.18)}$$

$$4h^+ + 2O^{2-} \longrightarrow O_2 \quad \textbf{(2.19)}$$

Finally, Ti^{3+} is immediately oxidized by oxygen in the air and the oxygen vacancies that are formed bond with water molecules forming a chemisorbed water layer [46, 47]. In the process created oxygen vacancies produced -OH groups which leads to an increase interactions with H_2O and water can easily spread across the surface.

The reduced sites can be reoxidized by air and the weakly bound hydroxyl groups reactively desorb from the surface that returns to a more hydrophobic form when maintained over some time in the dark. On the other hand, the longer the surface is illuminated with UV light, the smaller the contact angle for water becomes [48, 49]. The mechanism of photoinduced superhydrophilicity of TiO_2 is exhibited in the Figure 2.8. It is desirable that the contact angle rises slowly in a dark place, and stays low for a long time. This condition is esential especially when actual use is considered, it is not always irradiated by UV light, such as sunlight in rainy or cloudy days.

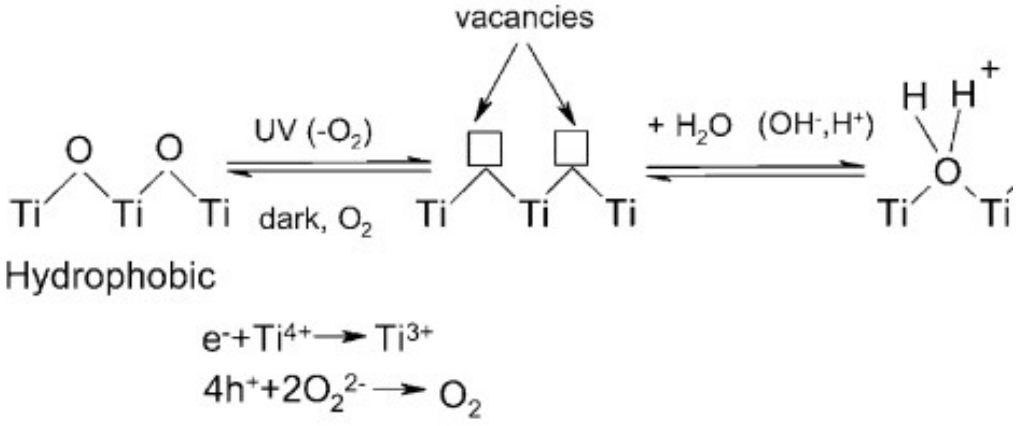


Figure 2.8 Mechanism of photoinduced superhydrophilicity of TiO_2 [49]

It was found out that depending upon the content by adding SiO_2 into TiO_2, the contact angle of water can decrease and the maintenance of hydrophilicity in a dark place is also improve [50-52]. Not only the improved hydrophilic property but also improved photocatalysis have been found for TiO_2/SiO_2 composite films [53-55]. According to Guan et al. [55] the addition of SiO_2 in TiO_2 film can enhance the acidity of the composite oxide which is thought to be the main reason for improving the photocatalysis and hydrophilicity. The surface improved acidity can adsorb more OH radicals.

According to Zhao et al. [56], the important factors that influence both photocatalytic activity and also the photoinduced hydrophilicity of TiO_2 thin films can be arranged as surface microstructure, including morphology of surface, grain size of TiO_2, chemical state of Ti, pore size and distribution and surface OH^- contents.

One of the most interesting aspects of TiO_2 is that the photocatalysis and hydrophilicity can take place simultaneously on the same surface even though the mechanisms are completely different as noticed before [30]. The relationship between photocatalysis and hydrophilicity can be summarized by the help of their characteristic mechanism. It has been reported that hydrophilicity enhance the photocatalytic activity because more OH groups can be adsorbed on the surface due to hydrophilicity [57, 58]. In addition, if it is considered that photocatalysis can decompose the organic compounds on the surface resulting in the restoration of hydrophilicity, one can determine that photocatalysis can also improve hydrophilicity even maintain this characteristic for a long time [59].

The role of photocatalysis and hydrophilicity to sustain the self-cleaning effect is expressed in the Figure 2.9. Due to hydrophilicity of the film a layer of chemisorbed H_2O which can further absorb layers of water by Van der Waals forces is formed on the film. The hydrogen bounds hold up the close contact between surface and adsorbed contaminants. Therefore when the soiled

substance adsorbed on the surface can be easily removed by spread water, the glass shows self-cleaning effect. In other words, the self-cleaning effect can stay a long time due to the synergetic effect of photocatalysis and hydrophilicity.

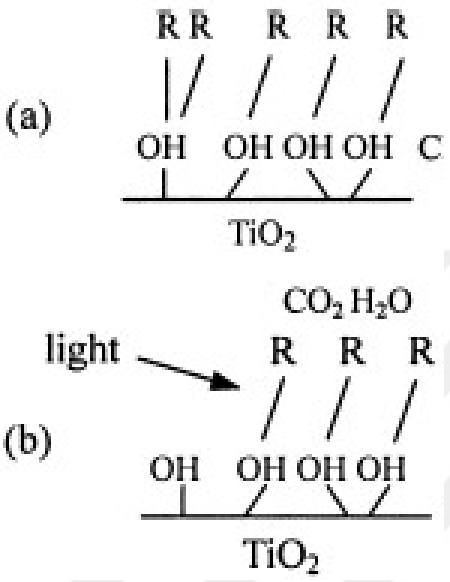


Figure 2.9 Self-cleaning mechanism of hydrophilic TiO_2 thin films [59].

To sum up photocatalysis plays an important role in maintain the self-cleaning effect through two ways. The first one is that by the aid of photocatalysis decomposition of the soiled compounds into H_2O, CO_2 and organic compounds act on self-cleaning effect directly. Second one is that when the soiled compounds decompose to recover the hydrophilicity the self-cleaning effect indirectly improve.

2.5. Improve the Photocatalytic Activity

The large forbidden band of TiO_2 only activated with the energy of more than 3.2 eV and fast charge carrier recombination stimulate the photocatalytic action of TiO_2 [60]. Moreover, the immobilization process of titanium dioxide

nanocrystaline generally lowers the surface area and increases the band gap of TiO_2 wich are the factors for decreasing the photocatalytic activity [61].

There are several aspects that influence the photocatalytic efficiency of titanium dioxide and the most significant ones will be presented in this section. To enhance the photocatalytic activity of TiO_2, it is necessary to prevent the combination of electrons with holes and increase the surface area of the photocatalyst. There has been studies concerning the photocatalytic activity of titania-based mixed oxides such as ZrO_2/TiO_2 and SiO_2/TiO_2 and silica-titania mixed oxides have attracted much attention since many researchers reported that silica-titania nanocomposites have higher photoactivity than pure TiO_2 [62]. When titania is mixed with a suitable amount of silica, the increase in photocatalytic efficiency has been attributed to enhanced thermal stability which results in the inhibition of the phase transformation from anatase to rutile, surface area and surface acidity [63]. Moreover, the increase in surface area with a reduction in particle size means an increase in the number of active sites on which the electron acceptor and donor are adsorbed and participate in the redox reaction. It has been reported that mesoporous titanium dioxide with a high specific surface area shows higher activity than usual TiO_2 [64]. Also, the addition of noble metals substantially enhances the photocatalytic activity of titanium dioxide since the deposited metal increases charge separation and reduces the recombination of electron–hole pairs [49].

2.5.1 Effect of Surface Morphology

Morphological control of materials involves regulation of the outer shape and size as well as inner structure, pore size and connectivity, the colloidal dimensions, and crystal phase of the components. In order to improve photocatalytic performance, efforts have been made to increase the number of attainable surface activation sites by making porous mirostructure. Organic materials of numerous structures and forms, which can be regulated and easily

removed by calcination, are applied as templates for formation of porous inorganic structures with catalytic and photocatalytic properties. In fact, to achieve high photoconversion efficiency, both high crystallinity and accessible ordered mesoscopic structures are essential. After combustion of residual organic components, an open cellular structure consisting of anatase nanoparticles is obtained In order to create tunable pore structures, block copolymers and surfactants, lattices of variable diameters and polymer gels can be employed.

A larger surface area enables the simultaneous adsorption of more molecules and therefore a higher efficiency [13]. In addition, Robert et al [65] studied TiO_2 prepared by sol-gel method with surface areas of 160 m^2/g and 300 m^2/g. They experienced that the latter showed higher photocatalytic activity as it possesed higher surface area.

Y. Ao et al. [66], prepared porous titania thin films by using carbon spheres as pore-forming materials. 0.05 g of carbon spheres which were added into 100ml titania sols, were dispersed by ultrasonic. Then the carbon spheres-titania suspension was spin-coated on glass substrates and the photocatalytic properties of the films were evaluated by degrading Reactive Brilliant Red dye under UV light irradiation. Results showed that photocatalytic performance of as-prepared porous film was much higher than that of corresponding smooth films as it is expected since the porous structure can provide more surface activation sites for photocatalytic reaction.

Another method that have been reported to increase photocatalytic efficiency is the modification of photocatalysts with polyethyleneglycol (PEG). It has been reported that PEG acts as a surfactant stabilizer, suppresses coagulation and increases the homogeneity of the final product. Kuo and Lin observed that the TiO_2 powder that is prepared without the addition of PEG is non uniform and has cracks,whereas that prepared by adding PEG into the sol is uniform with a granular texture and without cracking [67].

The electron hole pairs generated by absorption have to diffuse to the surface where they can catalyze chemical reactions. Lattice defects are reactive sites in terms of adsorption. In addition more important aspect concerning the efficiency is the lifetime of charge carriers or the lifetime of electron hole pairs which should be as long as possible. Yet, grain boundaries, lattice defects and impurities are potential recombination centers which generate undesired case. This case can be prevented by deriving low defect density within the layers and thus maintaining low recombination rate [68].

Particle size is an important parameter for photocatalytic efficiency since the electron-hole recombination may be different depending on particle size. For instance in the nanometer-size range, physical and chemical properties of semiconductors are modified. Small variations in particle diameters lead to great modifications in the surface and thus modify the surface electron–hole recombinations [49].

2.5.2. Effect of Light Intensity, Wavelength and Noble Metals

For semi conductor metal oxide photocatlayts, the electron transfer from valence band to conduction band of the photocatalyst is provided by UV light required to the photons. The electromagnetic spectrum of UV light can de subdivided into three categories. According to the standards (ISO-DIS-21348) UV-A (long wave) has the wavelength in the range of 400-320 nanometers, UV-B (medium wave) has the wavelength in the range of 320-280 nanometers and UV-C (short wave) has the wavelength in the range of 280-100 nanometers. The energy required for the electron transfer is related to the wavelength of the photon and overall energy input which is less than 380 nm for TiO_2. Therefore the light intensity and wavelength are considerable factors for the photocatalytic process [69].

Titanium dioxide can only be activated by UV light which is about < 10 % of the over-all solar intensity. As the lighting contains little UV it is therefore usually impractical to apply TiO_2 to interior or exterior living spaces. For this reason, large number of researches aimed at activating TiO_2 photocatalyst using visible light. Doping TiO_2 with metal ions, attaching photosentizers. Another semiconductor material that absorb visible light and formation of reduced TiO_2 photocatalyst are some methods for activating TiO_2 photocatalyst using visible light.

It has been reported that photocatalytic activity of TiO_2 can be improved by noble metals such as Pt, Au, Pd, Rh, Ni, Cu and Ag [70]. As an example the deposition of silver has been studied because of its potential applications in order to improve the photocatalytic activity of TiO_2 under UV irradiation and Ag species were dispersed in the body of the film uniformly. Silver acts as electron traps to enhance photocatalytic activity of Ag/TiO_2 thin films and also shift the visible region of absorbance spectra of the films [71]. Anoher study done by Uddin et al. [72] was aimed to improve the self cleaning properties by developing Au/TiO_2 nanophase on cotton fibres. It has been reported that in case of 0.16 wt.% Au content, the activity of the Au-modified TiO_2 is approximately double that of the unmodified support [73, 74].

These results can be clarified by the help of two aspects. The first one is that the metal nanoparticles which act as sensitizer, absorb the light in the visible range and transfer the excitation to TiO_2 photocatalyst [72]. The second one which is the most encountered explanation of this result is the electron trapping ability of the metal particles which can increase excitation lifetime and stability of generated electrons, thus reducing the tendency to recombine hole (h^+) and electron (e^-). As the Fermi levels of the noble metals are lower than that of TiO_2, photo-excited electrons can be transferred from CB to metal particles deposited on the surface of TiO_2. Since the electrons are transferred from TiO_2 while the photo-generated VB holes remain on the TiO_2, the possibility of electron-hole

recombination is reduced that leads stronger photocatalytic reactions (Figure 2.10) [70]. In other words, the role of the metal nanocrystal is to enhance the charge separation at the nanocrystal surface.

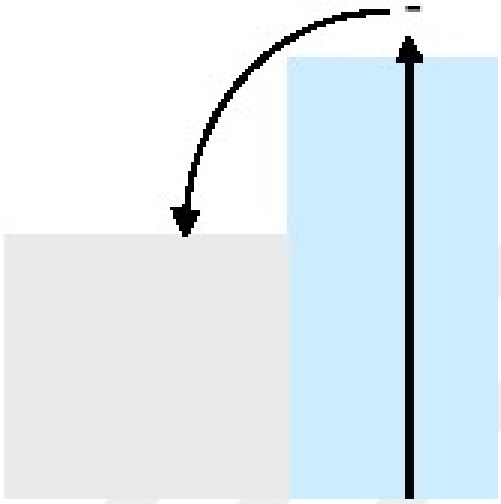


Figure 2.10 Mechanism of photocatalysis improved by noble metals

2.5.3 Effect of Crystallographic Phase

The photocatalytic activity is influenced by structure and morphology, which are determined by the production parameters for titanum dioxide. The band gap of semiconductor strongly depends on the crystalline structure as well as light-absorption properties of TiO_2 [75]. Therefore, crystallographic phase of titanium dioxide is a notable factor influencing the efficiency. Anatase has the advantage because it has a higher adsorptive activity for oxygen and water than rutile. On the other hand, anatase shows an indirect interband tarnsition and has larger optical bandgap (E_g=3.2 eV) than rutile (E_g=3.0eV) [76].

It has been reported that the meta stable anatase phase exhibits a higher photocatalytic efficiency than the thermally stable rutile phase due to the fact that

the conduction band of anatase has a higher energetic level than rutile, which enables a higher reduction potential [47, 77]. However, rutile phase has also been shown to be more active than anatase phase in few examples such as photodecomposition of H_2S [78].

The preparation of TiO_2 by using sol–gel method mostly involve calcination step to remove organic precursors that are employed on the synthesis. At the same time, calcination step improves the crystallinity and phase purity of metal oxide and enables the control on crytal size and surface area to limited extend. [79]. However very high calcination temperature results in aggregation and/or phase transformation and affects either the micostructure and the properties of titanium dioxide [80].

Porter et al., practiced the annealing temperature of the TiO_2 powder from 600 to 1000 ^oC. It has been reported that with the increasing calcination temperature the apparent crystallite size and rutile content in the catalyst increased, whereas the specific surface area and so the rate of phenol photodecomposition under UV irradiation decreased [79]. Inagaki et al. studied four different TiO_2 samples calcinated in the range from 400 to 900 ^oC for different periods of time. According to this study the rate of methylene blue degradation under UV light increase with increasing calcination temperature from 400 to 700 ^oC due to partial transformation of anatase to rutile above 700 ^oC [81].

The addition of LaO_2, CeO_2, Fe_2O_3, Nb_2O_3, SiO_2, or other oxides was found to improve the thermal stability and photocatalytic activity of titanium dioxide. In the study carried out by Li et al., little rutile phase appeared for the silica modified TiO_2 samples calcinated at 1073 although the phase transformation of anatase to rutile took place at 573–873 K for pure titanium dioxide in general [80]. Thus, it was remarked that the crystallinity and sizes strongly depend on the silica content in the silica modified TiO_2 samples, and that small silica content

could effectively suppress the formation of rutile phase and the growth of titanium dioxide crystals [82].

The existence of the anatase phase is not solely sufficient for high efficiency. Beside the crystallographic orientation of the phases is important since it influences the bonding of the surface oxygen atoms and the adsorption of water on the surface [77, 83, 84]. Moreover, since no electron hole pairs with satisfactory lifetime are generated by amorphous titanium oxide layers, they show no photocatalytic activity [85].

2.5.4 Effect of Adsorption and pH

It has been reported that degradation occurs on the surface of the photocatalyst. Since the degradation of a substance is a function of adsorbed concentration of the organic or inorganic substance, it is reasonable to conclude that the extent of adsorption is an important factor. In addition surface charge, ionization and adsorption on the photocatalyst are effected by the pH that should also be considered. [86]

It was supposed that increased surface acidity and therefore increased TiO_2 adsorption affinity is another factor responsible for photocatalytic activity. X. Y. Deng et al. [87] prepared H_2SO_4 treated TiO_2 samples using the sol–gel method and demonstrated that the sulfated samples had a higher conversion and stability during the photocatalytic oxidation. This situation was explained by the two simultaneous trends: the increase of the surface area of sulfated samples and the increase of their surface acidity.

2.5.5 Transparency of TiO_2 Thin Films

For the preparation of films, the combination of surface roughness and low surface energy is required. From a viewpoint of surface roughness, activity and

wetting are competitive with its transparency because surface roughness becomes a scattering source of light. Thus, the precise control of roughness is required to satisfy the desired properties. [88]

Eventhough, film-type photocatalysts normally have lower surface areas than powdered ones, and the intrinsic photocatalytic activity of films is usually smaller than that of powders, in recent years some researches into semiconductor photocatalysis showed that these nanocrystalline films may be as photochemically active as, and more physically and chemically robust than, the 'standard' Degussa P25 films. This result is due to the fact that TiO_2 thin films are transparent and scatter less light than the Degussa P25 TiO_2 [89]. Therefore, control of the surface structure of titanium dioxide thin film photocatalysts should be successfully carried out.

2.6 Synthesis Methods of Titania Thin Films

The thin films of semiconductor metal oxides might be produced by vacuum deposition techniquies and wet methods. The vacuum deposition techniques may be further classified into several groups depending on the type of precursor (metal targets, organo metallic precursors etc.), the method of stimulation to evaporate precursor (thermal, magnetron, RF, electron beam etc.) and vacuum level, etc. On the other hand, wet chemistry methods such as precipitation, sol-gel etc might be eployed with suitable coating technique such as dip coating, spin coating and spray coating. The vacuum deposition techniques requires expensive equipment and advanced process control technology yielding very precise film thickness, and homogeneous composition [90]. However, size limitations, the weak adherence and mechanical strenght of the film are the major drawbacks. The vacuum deposition techniques are beyond the focus of this study no further information will be presented here. The sol gel techniques have many chemical steps which might be used to fine tune the final physical

and chemical properties of the oxide layer. Moreover, dip coating and spray coating methods are very advantageous over the vaccum deposition. [91]

2.7. Sol-Gel Method

The sol-gel process is a wet-chemical technique for the fabrication of materials (typically a metal oxide) starting either from a chemical solution (sol short for solution) or colloidal particles (sol for nanoscale particle) to produce in dense film, ceramic, aerogel or fiber structure. The starting materials (precursor) used in the preparation of the sol are usually inorganic metal salts or metal organic compounds such as metal alkoxides. Generally titanium alkoxides (Ti(OR)n) with C2-C4 alcohols are used as a precursor to form titanium dioxide [92]. In a typical sol-gel process, the precursor is subjected to a series of hydrolysis and condensation reactions to form a colloidal suspension or a solution of metal oxide. Providing titanium alkoxide used as a precursor, the reaction series to form titanium dioxide sol or suspension are given as follows:

$$\text{Ti-O-R} + H_2O \longrightarrow \text{Ti-OH} + \text{R-OH (hydrolysis)} \quad \textbf{(2.20)}$$

$$\text{Ti-OH} + \text{HO-Ti} \longrightarrow \text{Ti-O-Ti} + H_2O \text{ (water condensation)} \quad \textbf{(2.21)}$$

$$\text{Ti-O-R} + \text{HO-Ti} \longrightarrow \text{Ti-O-Ti} + \text{R-OH (alcohol condensation)} \quad \textbf{(2.22)}$$

During the hydrolysis reaction, alcohol molecules in the structure of metal alkoxides are eliminated with the replacement of water**.** In the condensation reactions, alcohol is eliminated directly in the alcohol condensation reaction while water is eliminated in the water condensation reaction. Metal alkoxide compounds are not completely hydrolyzed and form polymeric chains since hydrolysis and condensation reactions compete with similar reaction rates. At the end of these reactions, the product metal oxide is obtained.

Further processing of the "sol" enables one to make ceramic materials in different forms. Thin films can be produced on a piece of substrate. When the "sol" is cast into a mold, or a film, a wet "gel" will form. With further drying and

heat-treatment, the "gel" is converted into dense ceramic. If the liquid in a wet "gel" is removed under a supercritical condition, a highly porous and extremely low density material called "aerogel" is obtained. As the viscosity of a "sol" is adjusted into a proper viscosity range, ceramic fibers can be drawn from the "sol". Ultra-fine and uniform ceramic powders are formed by precipitation, spray pyrolysis, or emulsion techniques.

The sol-gel approach is interesting in that it is economically more favorable than vacuum deposition techniques. Sol-gel methods are low-temperature processes to produce ceramics and allow fine control on the product's chemical composition and physical properties. Coating processes which depend on sol-gel processing have advantages over conventional methods include the ability to coat large, curved substrates in a cost effective method using simple deposition equipment, the ability to obtain coatings with high homogeneity and tailored inhomogeneity, low firing temperatures, and the ability to prepare materials which cannot be prepared by other methods such as organic-inorganic hybrid materials. Moreover, sol-gel methods can be used to fabricate almost any single- or multi-component oxide coating. [93, 94]

Besides the advantages, sol-gel method also has some disadvantages. The most important difficulties of this process is that because the sol–gel process includes heat-treatment higher than 450 ^{o}C after coating for the elimination of organic components and for the achievement of a crystallized TiO_2 phase, it is a complex process and generally constrained to flat-substrates. [95]

2.8. Coating Methods

Sol–gel coating has been classified as two mostly employed methods which are named as dip and spin coating. To obtain proper characteristics some requirements must be fulfilled. Some of them are reported that the initial compounds must have an adequate solubility, the contact angles formed with the solution have to be sufficiently small to obtain good wetting of the substrate, the

solution must have an adequate durability, the processing conditions must be maintained constant and drying and heating must be carried out carefully to obtain reproducible solid and homogeneous oxide films [96].

Surfaces exposed to the atmosphere are generally contain unwanted material and/or energy on a surface which may cause the film not adhere well or not adhere at all. Therefore, before a surface is coated with thin films, substrates cleaned with appropriate methods. Prior treatment of the surface changes either the structure of the surface by providing detrimental effects on adhesion and sufficient wettability. Among the variety of cleaning processes, cleaning with solvents such as diluted acids is a widespread procedure [96].

2.8.1. Spin Coating

To perform the spinning process, the coating solution which is poured onto the horizontal rotating substrates spreads out on the substrate surface. Spreading out the coating solution in the form of a liquid film followed by subsequent heat treatment to produce oxide films [97]. The spin coating process have some problems which need to be solved such as the difficulty to produce spin-on coatings of multicomponent compositions, drawback in production of multiple coatings and coating of non-planar samples [96].

2.8.2. Dip Coating

The dip coating which has considerably been used for preparation TiO_2 nanostructured thin films can be made by two different process technologies. The first technologie is the lifting processes in which the parts to be coated are withdrawn from the solution and simultaneously covered with a liquid film (Figure 2.12), and the second one is the lowering processes, in which the parts to be coated remain at rest and the liquid level is lowered [96].

It has been reported that the lifting process is the more economical way for coating large substrates and it is also universally applicable. The substrates that are first optimally cleaned are inserted into a tank containing coating material at a constant speed preferably judder free. Then the substrate remains for a specific time fully immersed and motionless to allow for the coating material to apply itself to the substrate. Finally, the substrate carefully pulled out again at a constant speed to avoid any judders. The lifting operation has to be so slow that the liquid film adhering to the substrate surface is left in a flow zone which is very short. The coating thickness is mainly defined by the withdrawal speed, by the solid content and the viscosity of the liquid and can be calculated by the Landau-Levich equation [96, 98].

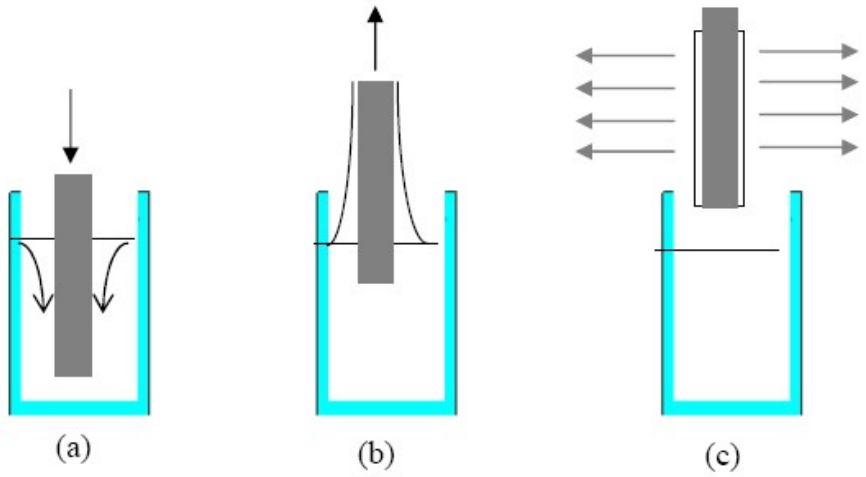


Figure 2.11 Stages of the dip coating process; (a) dipping, (b) wet layer formation and (c) evaporation

After coating process, evaporation of the solvent and the subsequent destabilization of the sols by solvent evaporation, leads to a gelation process and the formation of a transparent film due to the small particle size in the sols which can be demonstrated from the Figure 2.12. Since the solvent is evaporating and draining, the fluid film terminates at a well-defined drying line (x = 0, in Figure

2.12). Due to the geometrical factors affecting the diffusion of solvent vapor from the liquid surface, non-constant evaporation rate in the vicinity of the drying line formed which results in a parabolic thickness profile:

$$h(x) \alpha x^{1/2} \quad \textbf{(2.23)}$$

where *h(x)* is the film thickness as a function of position x below the drying line [99].

It could be noted that the thickness of the layers is mainly a function of the lifting speed, the viscosity, concentration and temperature of the solution, humidity of the atmosphere and the angle of inclination between the substrate and surface of the liquid. [100]

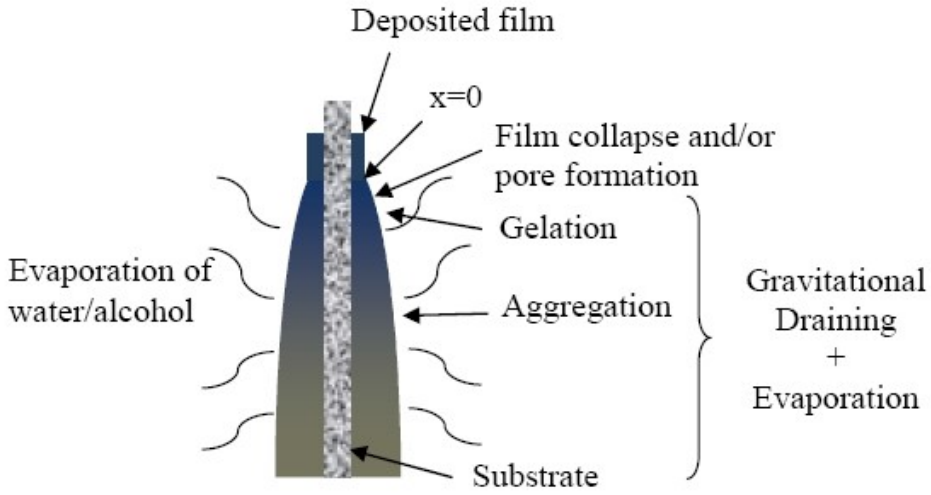


Figure 2.12 Schematic drawing of evaporation of the solvent and subsequent destabilization of the sol

Experimental results have shown that the preparation of high transparent TiO_2 thin film by dip coating method needs to control morphology, thickness of the

film and the phase transformation [101, 102]. Therefore, it is necessary to optimize the pH, concentration ratio of the reactants, and peptization process [103].

Both sides of the substrate are coated simultaneously by dipping which is preferable and easier way than to coat both sides for most products with antireflective coatings. It is the most economical method for large substrates. Dip coatings can be hard and scratch resistant and very durable against enviromenal influences. Generally, the dip coating process is confined to oxide layers since as an example metal films are difficult to produce with this methods. [100]

2.9. Heat Treatment

Heat treatment of the resultant films such as drying and calcination was considerable to finalize the process since the condensation that pulls together the constitute particles of the gel into a compact mass, thus building up the metal oxide crystal is usually accomplished by gelization and calcination. [104]. The conditions of heat treatment procedure influence the properties of the films. For instance, treating in air or in a reducing gas atmosphere can lead to the different oxidation stages depend on the composition of the atmosphere [100].

2.9.1. Drying

The drying procedure is necessary in order to form gel-like stable films on the substrate when the solvent evaporates. Furthermore, drying accompanies both the dip- and spin-coating processes and largely establishes the shape of the fluid film profile. Scherer divides the drying of gels into two stages: a constant rate period and a falling rate period. During the constant rate period, mass transfer is limited by convection away from the gel surface, whereas during the falling rate period, mass transfer is limited by the permeability of the gel [94]. According to Brinker et al. constant rate period would mostly obtain throughout the deposition

process, since for thin films the liquid-vapor interface remains located at the exterior surface [105].

When drying procedure begins, the coated substrate shrinks with the evaporated liquid by remaining the liquid-vapor interface at the surface. Then, further shrinkage of the coated substrate is observed since condensation reactions take place. Further shrinkage is prevented as the coated substrate becomes stiff. Once the film is attached to the substrate and unable to shrink in that direction, the reduction in volume is accommodated completely by a reduction in thickness. When the film has solidified and stresses can no longer be relieved by flow, tensile stresses develop in the plane of the substrate. Therefore at the end of drying stage, there could be cracks on the amorphous thin film.

2.9.2. Calcination

Calcination (annealing), is a heat treatment that cause changes in material properties. Annealing process can be summarized that heating to a suitable temperature, maintaining at that temperature, and then cooling. Calcination temperature is important for removing the organic molecules from the thin film and completing the crystallization. However, very high calcination temperature results in aggregation and/or phase transformation, and affects the microstructures as well as the properties of TiO_2 nanoparticles. It was mentioned that anatase phase TiO_2 crystallites are generally found to be more active than rutile which was due to the fact that the photocatalytic activity of TiO_2 strongly depends on its crystal structure. [106, 107]

2.10. Aging

When the process ended generally film-substrate system is not totally stable since it continues to change physically and chemically until it reaches a stable condition [108]. During the aging time chemical reactions in the interfacial layer

area, solid body diffusion across the interfacial layer and the crystal structure can alter that are strongly dependent on temperature [96].

2.11. Applications of Titania Thin Films

Due to the excellent photocatalytic properties as well as the high transparency, excellent mechanical and chemical durability of TiO_2 films in the visible and near-infrared region of the spectrum, TiO_2 photocatalyst thin film can commercialize in different industrial applications, such as, used as antibacterial ceramic tile and self-cleaning glass (Figure 2.13).

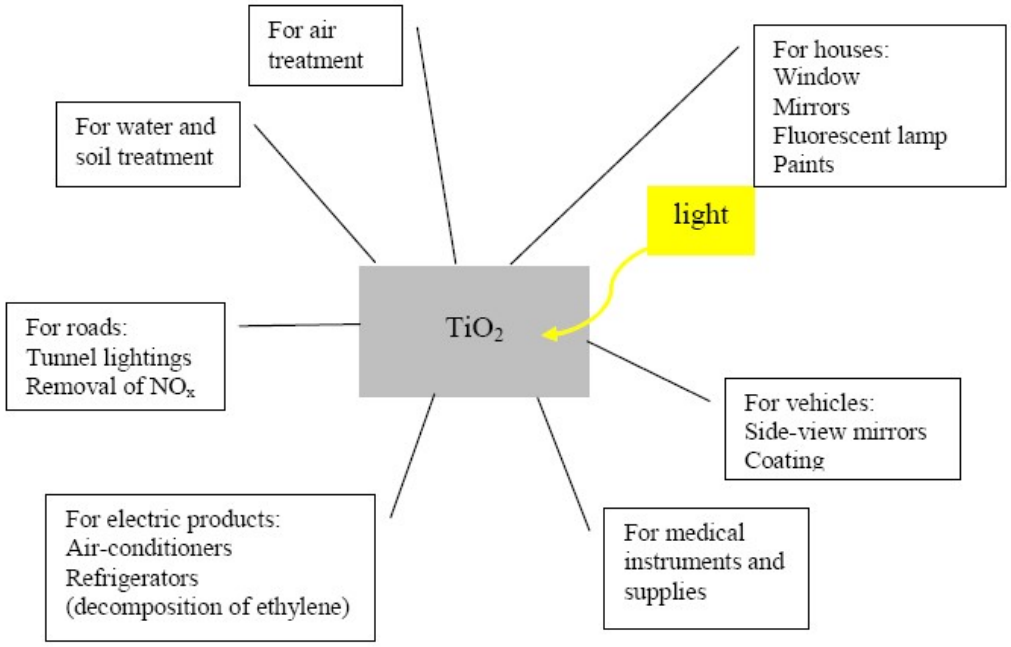


Figure 2.13 Industrial applications of TiO_2

Since TiO_2 surface decompose organic pollutants by the help of ultraviolet light, surfaces coated with titanium dioxide can be applied as self cleaning surfaces under UV light. This important property provide enviromental, maintenance and

cost benefit, since by the use of solar light or ultraviolet emission such as from the fluorescent lamp the surface can clean itself without utilizing detergents [25].

Moreover, according to Wang et al. [109] when water flow, such as natural rainfall, was applied to the TiO_2 surface, the self-cleaning effect could be enhanced. This phenomenon can be clarified that as the self-cleaning function of TiO_2 photocatalysis set by the number of incident photons, even the number of photons may be insufficient to decompose the adsorbed stain, when water is supplied there the surface is maintained clean. Therefore, it can be reported that the TiO_2 surface coated materials could be one of the best exterior construction equipments, since these materials could be exposed to abundant sunlight and natural rainfall. [47, 86, 110]

Watanabe, Hashimoto and Fujishima first demonstrated the self-cleaning concept on a titania-coated ceramic tile in 1992. The self-cleaning cover glass for highway tunnel lamps were one of the commercialized product improved by utilizing this unique property [47, 110]. Such materials have already been commercialized in Japan since the late 1990s and in other countries in recent years [86]. Moreover, TiO_2-coated textiles are another promising application of selfcleaning technology. Kiwi and co-worker swere shown that coffee and wine stains on TiO_2-treated cotton or synthetic textiles can be decolorized under sunlight [111, 112].

Fujshima, Zhang and Tryk experienced the efficiency of self-cleaning technology by testing a self-cleaning tent material. The tent material, made from PVC film, was coated with TiO_2 photocatalyst material on the left half. The test was started on July 22nd, 2004 and the first photo was taken on that day (Figure 2.14 (a)). It can be seen that both the non-coated and TiO_2-coated halves had the same white appearance. Figure 2.14 (b) which was taken on April 23rd, 2007 demonstrate that the TiO_2-coated part remains white in the photo, whereas the non-coated part is dark grey [25].



Figure 2.14 Self-cleaning test for a PVC tent material manufactured by Taiyo Kogyo done in the Photocatalyst Museum, KAST. The left half part of the tent material was coated with TiO_2. (a) Picture taken in July 22, 2004. (b) Picture taken in April 23, 2007 [25].

Zhang et al. [112, 113] reported that TiO_2-SiO_2 self-cleaning coatings may find application for the cover glass of solar cells. Nanoporous TiO_2-SiO_2 coatings that have a low refractive index were prepared. These coatings enhanced the transmission of the glass to exceed 97% for visible light, greater than the 90-92% for bare glass.

In 1977 Frank and Bard [114, 115] setup the earliest report about the cleaning properties of TiO_2. This study performed for suspensions of TiO_2 powder in contaminated water which were able to photocatalyze the conversion of cyanide to cyanate, thus detoxifying the water.

For water decontamination only the TiO_2 photocatalyst and UV light, either from solar light or artificial light sources, are needed and thus its cost can be lower than other kinds of advanced oxidation techniques. In addition, no toxic intermediate products are generated in the photocatalytic decontamination process. Therefore it can be concluded that TiO_2 ensure advantages for cleaning the water environment, even for cleaning drinking water [116].

There have been several types of water-purification facilities for various purposes as some of which are given as an example above. However, it is generally accepted in most of the studies that TiO_2 photocatalysis is feasible only for the treatment of wastewater that contains low to medium pollutant concentrations, because of its relatively low efficiency and the limited flux of ultraviolet photons [117, 118].

Another application of TiO_2 photocatalysis is to decontaminate, deodorize, and disinfect indoor air. Indoor air of public facilities, which is normally contaminated with bacteria, fungi, etc., interior furnishings and construction materials emmitted the low-concentration volatile organic compounds can be purified by the help of conventional air-purification systems often adapt filter-type components for the cleaning of polluted air.

In the case of the active carbon filters pollutants are accumulated into the filter which then becomes saturated with adsorbed substances and loses its function after a certain period of use. On the contrary photocatalytic air-cleaning filters can decompose the organic substances instead of accumulating them and, as a result, exhibit better performance [25].

The available air-cleaning application groups of the photocatalytic filters include air cleaners, air conditioners, air-cleaning units for refrigerators, etc. In addition, photocatalytic TiO_2 has the capability of removing nitrogen oxides exhausted from automobiles and became a serious source of air pollution in urban areas.

[119, 120]. Hence some companies created TiO_2-coated photocatalytic highway that are termed as``photo-road'' technology, to convert NOx and SOx molecules to more environmentally benign forms. [25]. This technology, has been tested in more than fourteen places in Japan over the past nearly ten years. As an example, lighter part of the surface coated roadway (Figure 2.15) was being prepared by mixing colloidal TiO_2 solutions with cement.



Figure 2.15 Finished sample for the usage of TiO_2-based photocatalytic material on roadway surfaces with the coated surface showing a lighter color

TiO_2 photocatalysts can kill bacteria on their surfaces, and therefore self-sterilizing surfaces can be prepared [47, 117]. The most important advantage for these surfaces is that they operate only with light and oxygen instead of electrical power or chemical reagents. Since TiO_2 surfaces are non-poisonous and will not result in environmental pollution unlike chemical antibacterial agents in the near future self-sterilizing TiO_2 materials may have many medical applications such as hospital room walls, medical instruments, and hospital uniforms. Moreover according to some studies metallic Ag is deposited on the TiO_2 surface to enhance the antibacterial action under dark conditions [25].

When moist air cools down on the surfaces, forming many water droplets ranging from micrometer to millimeter size the fogging on the surfaces of mirrors and glass occurs. In both Watanabe and co-workers were discovered that TiO_2-SiO_2 surfaces could become extremely hydrophilic under UV illumination [121, 122]. This property is based on the result that when water spreads evenly across the surface, if the amount of water is relatively small, the water layer becomes very thin and evaporates quickly and inversely a sheet-like layers formed if the amount of water is larger [25].

Automobile side-view mirrors have been the first commercial application of this property. Other familiar applications are adhesive TiO_2-coated plastic films or TiO_2-containing sprays for the conversion of existing mirrors. Moreover, another application area is air conditioners. When an air conditioner is operating to cool during the summer, air that is cooled on the heat exchanger of the air conditioner often has moisture condensing out of it. These condensed water droplets fog the fins by forming large water droplets often bridging between the adjacent fins which reduce the heat exchange efficiency and increase the resistance to air flow. According to the Takata et al. [120] coating the heat exchanger surface with superhydrophilic TiO_2, however, can hinder the fogging and the formation of water bridging, and remove the condensed water more effectively.

Takata et al., studied the heat transfer properties of superhydrophilic TiO_2 surfaces, were suggested that the superhydrophilic surface could be an ideal heat transfer surface and would be applicable to various heat transfer phenomena that are affected by surface wettability [123-125].

Hashimoto et al. reported recently the cooling of the exterior walls of buildings with a falling-water film to reduce the electricity consumption by air conditioners in summer According to their experiments, when water was continuously sprinkled onto the surfaces of buildings that were covered with TiO_2 films due to the superhydrophilic property of the material, water was able to spread on the surfaces in the form of a thin film either cooling the building

surface and also the surrounding air or also helps in maintaining the building surface clean by the self-cleaning effect [110]. Therefore, it can be expected that TiO_2-coated building materials could contribute much to energy-saving tchnologies in the future.

Several ways are available to protect metals from corrosion such as painting the metal compound or coating with a metal having a less positive corrosion potential. Recently, the application of photocatalytic technology in anticorrosive effect has been examined. As to study done by the Koyo Electrical Construction Co. and Ohko et al., when TiO_2 electrons were injected into the steel, it was protected from corrosion under UV irradiation, while the photogenerated holes decomposed organic contaminants to provide a self-cleaning function [126]. Later, the same group observed that TiO_2, when coupled with WO_3, maintained an anticorrosion effect even in the dark for a period of time [127-129]. In addition, recent studies have shown that phosphotungstic acid (PWA) exhibits a longer self-discharge time than WO_3 [130] which is a very promising result for the development of practical semiconductor coatings for metal corrosion protection.

During the photocatalytic process the active oxygen species such as the hydroxyl radical or singlet O_2 generated are so active that they can oxidize not only organic materials but also inorganic materials such as copper, silicon, carbon, and SiC etc. [131-133]. By the help of these reactions, it is possible to develop a novel photocatalytic lithographic method. This novel method would have the advantages of simplicity and low cost: it does not require expensive photo-resist materials and special equipment.

Photochromic materials, which change their colors reversiblyin response to light, would find a great number of applications, including a rewritable color copy paper or electronic paper and a high-density multi-wavelength optical memory. Ohko et al. recently studied the multicolor photochromism of TiO_2 films loaded

with silver nanoparticles [134-137]. The film color, initially brownish-grey, changed under monochromatic visible light to almost the same color as that of the light. Another important aspect for this study these processes were found to be repeatable.

They clarified that when Ag nanoparticles irradiatiated with monochromatic visible light, they adsorb the light. Then the electrons excited are accepted by O_2, resulting in oxidation of the Ag nanoparticles to Ag+ and an absorption decrease appears at the corresponding wavelength, i.e., the color of the excitation wavelength. The most important role of the TiO_2 film is that the repeatable generation of Ag nanoparticles with diverse sizes and shapes due to the ``molding effect'' of the nanoporous TiO_2 film which is resulted in different plasmon resonance absorption wavelengths of the Ag particles in the whole visible light spectrum [25].

CHAPTER 3

EXPERIMENTAL

In this study, glass substrates were first pretreated, then coated with colloidal solutions synthesized by sol-gel process, dried and finally calcinated. A special care has been paid to solution preparation, coating and heat treatment processes for reproducibility. The samples were characterized by using CAM (Contact Angle Meter), SEM (Scanning Electron Microscope), UV/Visible Spectrophotometer, BET (Brauner Emmett Teller), TGA (Thermogravimetric Analysis), AFM (Atomic Force Microscope) and Stylus Profiller.

3.1. Materials

3.1.1. Chemicals

All chemicals used for the synthesis of sol-gel solutions, were analytical reagent grade and used without further purification. The chemicals that have been used and their supplier are given below.

Glass substrates, Pyrex, microscope slides by Sailing Boat, (CAT No: 7102)
Titanium n-butoxide [Titanium(IV) n-butoxide, $C_{16}H_{36}O_4Ti$, 99%], by Acros Organics (CAS number: 5593-70-4)
Ethanol [C_2H_5OH, 99.9%,], by Merck (CAS number: 64-17-5)
Chloroform [$CHCl_3$, 99%], by LAB-SCAN Analytical Sciences (CAS number: 67-66-3)
Potassium hydroxide pellets [KOH, >84%] by Merck (CAS number: 1310-58-3)
Poly (ethylene glycol) [average M.W. 600, density=1.126 kg/lt] by Acros, (CAS Number: 25322-68-3)

Ammonia Solution 25% [by Merck (CAS Number: 1336-21-6)
Hydrochloric Acid 37% by Merck (CAS Number: 7647-01-0)
Ludox SM-30 colloidal silica [30 wt % suspension in water] by Sigma (CAS Number: 420794-1L)
Titanium (IV) isopropoxide 97% [$C_{12}H_8O_4Ti$,] by Acros (CAS Number: 546-68-9)

3.1.2. Microorganisms

E. coli strain (XL1-blue) was cultured aerobically in Luria–Bertani (LB) broth at 35 ^oC on a rotary shaker (170 rpm) overnight and were maintained on LB agar plates. The plates were incubated at 35 ^oC overnight and then stored at 4 ^oC until use [137]. The composition and preparation of nutrient broth is described in the Appendix D.

3.2. Pretreatment of Substrate

In this study, the pyrex microscope slides were used as glass substrates. In order to have succesful coating step and assess adhesion, the glass surface should be perfectly wetted by colloidal solution and the surface must be free from any contamination. In order to improve the wetting properties of the glass surface and attain cleaning, glass substrates were treated on several steps. The pyrex glass plates (25mm × 75mm × 1mm) which were used as the substrate during the experiments were first washed with detergent (anionic active material) solution and rinsed with distilled water. In order to improve wettability, the glass substrates were chemically etched under alkaline conditions. In order to prevent the contamination of glass surface with Na ions, which is poison for the TiO_2 photocatlysts [138], KOH solution were prefered. The pyrex glass plates were etched for 6 hours in 1N KOH solution and again rinsed with distilled water. Afterwards plates were first ultrasonicated with ethanol:chloroform mixture which had 1:1 concentration by volume and then with distilled water for 10

minutes. Finally, plates were dried at 110 ºC overnight and kept in the furnace for further use [139].

3.3. Preparation of *Esherichia coli* Doped TiO_2 Solution

The films were obtained by dip-coating technique from the sols derived from sol-gel procedure. So as to obtain the best photocatalyic activity and hydrophilicity, different solution recipes were experienced using the same coating technique.

In order to perform indendation by *E. coli* cells, a special recepie was developed to keep E.coli cells alive or at least intact till coating and drying operation to achieve 3D indentation. The former recepies were alcohol based which is very hostile environment for microorganisms. The new water based recepie, exhibited in the Figure 3.1, is applied by mixing 2.5 ml titanium tetra-isopropoxide (TTIP), 0.5 ml acetic acid and 0.35 ml nitric acid added very slowly to 100 ml of distilled water by stirring. Subsequently, mixture was heated to 80 ºC for 30 minnutes under refluxing. The resulting TiO_2 sol was kept under stirring for 1 hour at room temperature to warm up and SiO_2 ludox of 3.2 ml was added to obtain the desired $TiO_2 – SiO_2$ ratio [140].

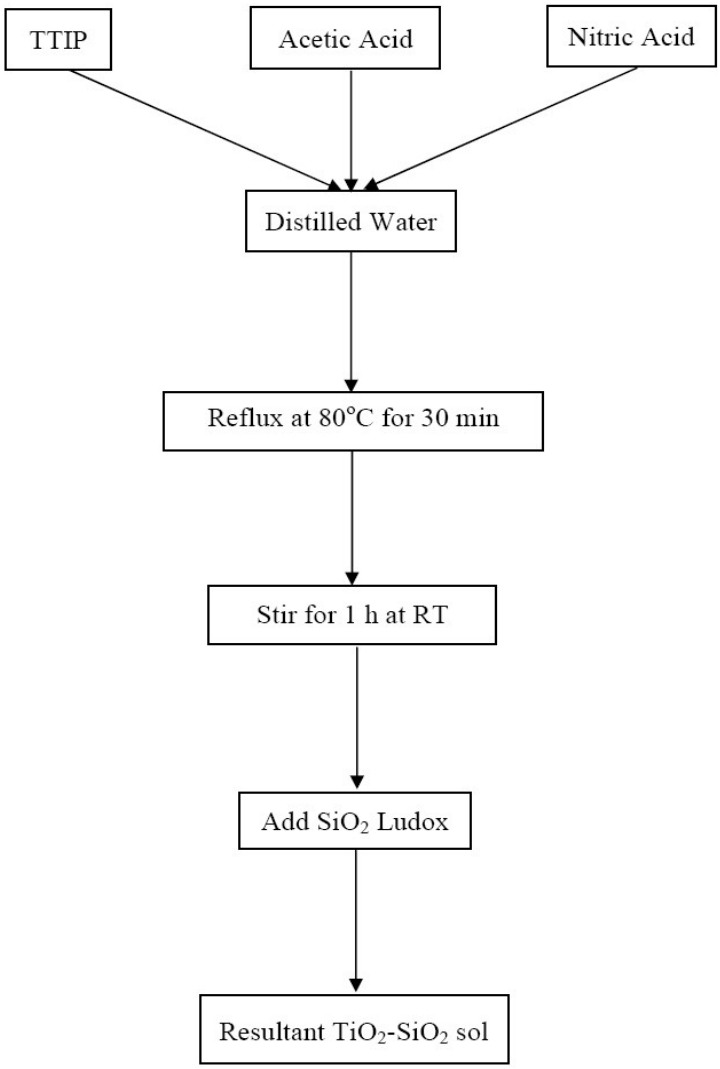


Figure 3.1 Flow chart for the preparation of titanium dioxide-silicon dioxide ludox colloidal solution

On the other hand, the growth medium for *E. coli* called nutrient broth was prepared (Appendix D). Resultant broth was autoclaved at 121 oC for 15 minutes to sterilize before the cultivate procedure. *E. coli* used in the experiments was cultured over 16 hours in a rotary-shaker that is fixed at 170 rpm and 35°C.

Each 50 ml broth was centrifuged at 10,000 rpm over 4 minutes to colled *E. coli* cells from the cultivation medium. The supernatant fluid was removed away

before adding 5 ml of distilled water to the sediment and stirred properly to suspend bacteria. Then this suspension was added to the prepared TiO_2 water based sol, pH value of which was adjusted to 7-9 by adding the proper amount of ammonia solution. To test the effect of number of cells per unit volume of TiO_2-SiO_2 thin film on surface area, and photocatalytic activity, different amount of *E. coli* centrifuged from Luria broth (LB) medium was added into TiO_2-SiO_2 mixture.

For this purpose, a single colony of *E. coli* cell was inoculated in 400 ml, 200 ml, 100 ml, 50 ml and 20 ml of nutrient broth. They were grown at 37° C in an incubator shaker and centrifuged as explained above. Thereafter harvested *E. coli* from 50 ml broth was reconstituted with 5 ml distilled water and added to the 100 ml solution. In case of 400 ml broth, *E. coli* centrifuged from 50 ml broth and 5 ml distilled water was added at different times until the whole required amount was added. The compositions of the prepared colloidal solutions which comprised TiO_2-SiO_2 and *E. coli* in diverse concentrations are shown in Table 3.1.

Table 3.1 Preparation of *E. coli* doped TiO_2 solutions of different concentrations

Sample	Amount of LB Broth (ml)	TiO_2-SiO_2 colloidal solution (ml)	Amount of Distilled Water Added (ml)	Final Volume of TiO_2-SiO_2 Colloidal Solution (ml)	TiO_2 : *E. coli* Ratio in the Sol (Appropriate Ratio)
1	400 (50x8)	100	40 (5x8)	140	0.71 : 1.71
2	200 (50x4)	100	20 (5x4)	120	0.83 : 1
3	100 (50x2)	100	10 (5x2)	110	0.91 : 0.54
4	50	100	5	105	0.95 : 0.29
5	20	100	2	102	0.98 : 0.12
6	0	100	0	100	1 : 0

From the growth curve of *E. coli* XL1-blue given in the Appendix E, the colony forming unit was observed about $1.2x10^9$ per mililiter. For the sample indicated as x1 E-coli contains $2x10^9$ cfu/ml. The colony forming unit in the other solutions were also obtained (Appendix E).

The resultant *E. coli* doped TiO_2-SiO_2 coating solution of three different *E. coli* ratio (*E. coli* x 1, *E. coli* x 0.29, *E. coli* x 0) can be seen from the Figure 3.2.



(a) **(b)** **(c)**

Figure 3.2 *E. coli* doped TiO_2-SiO_2 coating solution of (a)*E. coli* x 1, (b)*E. coli* x 0.29 and (c)*E. coli* x 0

3.4. Coating the Films

Thin films of *E. coli* – TiO_2 - SiO_2 were deposited over Pyrex glass plates by a dip coating technique which is described in section 2.4.2. Pretreated Pyrex glass substrates were dipped into the coating solution at constant speed of 0.14 cm/s, hold in the solution for one minute and removed from the solution with 0.05 cm/s, respectively. This procedure was repeated to acquire multilayer coatings. The equipment has a microprocessor controller and operates with minimal vibration rate for smooth and homogeneous coating. Experimental setup for dip coating technique which was used in the studies is exhibited in the Figure 3.3.



Figure 3.3 Experimental setup for dip coating

E. coli suspension was added to TiO_2 sol as described in previous section and substrates were coated by using TiO_2-*E. coli* mixed sol.

In order to alter the amorphous structure to the crystalline form and complete removal of organic residuals, samples were calcined at 500 ºC for 30 minutes in tube (Protherm 1000W, PTF 12/50/250) furnace under air flow. The samples were removed after 30 minutes calcination.

3.5. Analysis of the Films

3.5.1. Spectroscopic Analysis

Double beam UV-visible spectroscopy (Thermo Electron Corporation, Nicolet Evolution 100) was used for the band gap measurements of the samples. The

bare substrate was placed in the referance beam and difference spectrum were collected in absorbance(A) units.

3.5.2. Surface Area Analysis of the Films

The specific surface area plays an important role in photocatalytic activity of thin films. The N_2 adsorption (BET) technique is very versatile method for both surface area and pore size distribution of catalyst samples. However, this method requires a considerable amount of sample and is not suitable for the characterization of thin films. The weight of catalyst per substrate was determined by subtracting the average weight of bare substrate from the weight of samples. The amount of catalyst per sample is only several milligrams and even the weight measurement has very large standart deviation. In one study [141], 30 samples placed in a BET apparatus to perform a BET measurement. The other methods such as surface acustic wave method is very indirect and requires precise calibration with known samples.The other methods of surface area determination are based on adsorption of organic probe molecules such as methylene blue as suggested by Giles et al [142-144].

Methylene blue (MB) can be used for surface are determination for oxides, was selected as a solute in this study to determine the surface area of the films by using Langmuir isotherms [145]. Methylene blue was chosen since its known chemical properties, molecular area and strong adsorption onto solids [146]. The structure of MB demonstrated in Figure 3.4.

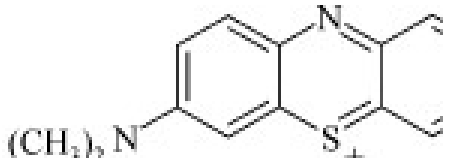


Figure 3.4 The structure of methylene blue

The method of adsorption of methylene blue in liquid phase for the specific surface area determination is based on the differences between initial and equilibrium concentrations of methylene blue solution. It should be assumed that methylene blue is adsorbed on the surface with kinetic and equilibrium relations appropriate to Langmuir theory given in the equation 3.1.

$$\frac{C_E}{x/m} = \frac{1}{kx_m} + \frac{C_E}{x_m} \qquad \textbf{(3.1)}$$

where

C_E : Equilibrium concentration of methylene blue remaining in the solution, mg/lt

x/m : Quantity of methylene blue adsorbed per unit area of substrate mg/cm^2

x_m : Adsorption capacity (solute monolayer capacity) per unit area of substrate Langmuir constant, mg/cm^2

k : Bonding energy constant, Langmuir Constant

For all adsorption isoherms of mehylene blue onto thin film, the plot of $\frac{C_E}{x/m}$ versus C_E gives a straight line with slope equal to $\frac{1}{x_m}$ and intercept equal to $\frac{1}{kx_m}$.

The specific surface area was calculated by the following equation:

$$S = \frac{L \times A_{MB} \times x_m}{N \times M_w} \qquad \textbf{(3.2)}$$

where

A_{MB} : Molecular area of methylene blue adsorbed on the surface, literature data:1.2 nm^2

L : Avogadro's number, 1/mol

N : Coverage factor, literature data: 1

M_w : Molecular weight g/mol

[146, 147]

Adsorption measurements for all samples were carried out as follows: Coated glass samples were placed in 20 ml of methylene blue solution of known (1 ppm, 2 ppm, 3 ppm) concentration. This sample containing solution was maintained at 35 ^oC for 24 hours. This time was determined by a series of measurements at 35 ^oC and it was concluded that adsorbing solution reached complete equilibrium within 24 hours. Photographs of the adsorbing solution and the solid after 24 hours are given in Figure 3.5.

The methylene blue uptake onto the sample surface was calculated from the difference between the initial (t = 0) and final (t = 24 hours) adsorption value. The initial and eqilibrium absorbance data of the prepared solution were reported by means of Thermo Electron Corporation, Nicolet Evolution 100 spectrophotometer by using the wavelength value of 611 nm for MB solution that is taken from the literature [148].



Figure 3.5 Photographs of the (a) adsorbing solutions in the presence of solid after 24 hours and (b) the solids removed from the MB solution after 24 hours

On the measurements, samples are broken into smaller pieces and the area of each part was determined by counting the squares of graph paper placed under the sample. At least three measurements were carried out for each sample in order to increase accuarcy. The solutions having different methylene blue concentrations were used on the surface area determinations. Thin films of known dimensions were maintained in the MB solution of 1 ppm, 2 ppm and 3 ppm, respectively.

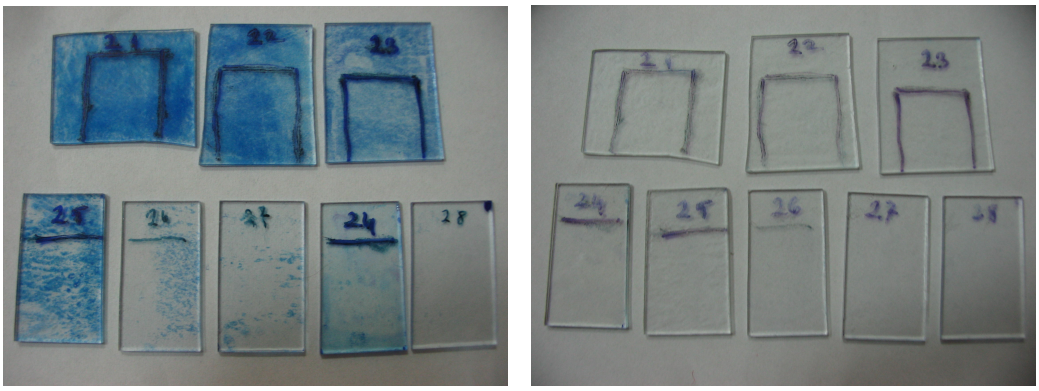
3.5.3. Self Cleaning Activity

The discoloration of both methylene blue solution (0.04 mg/ml) and methyl orange solution (10mg/ml) was detected. These solutions were droped on to the coated pyrex glass samples for which two sets were prepared in the same analysis. While, one of these sample was irradiated with simulated sunlight (Suntest solar simulator with a dose of 300 W/m^2), the other one was kept in dark place. Then these two samples were compared to observe the bleaching of the spots over several hours. [140]

In addition, spectroscopic analysis of the thin films stained with the ~ 80 µl of 150-210 ppm methylene blue solutions was performed by using the unstained film as a reference. These samples were also irradiated with Suntest solar simulator. The absorbance value of the spotted films were taken at several time intervals (30-60 minutes) by using the fixed wavelength of 661 nm and the analysis was kept on until the spot on the film was disappear and the absorbance data reached to constant values.

3.5.4. Measurement of Photocatalytic Activity

The photocatalytic degradation of any organic substance proceeds via the formation of free radicals $\bullet O^-_3$ and •OH having high oxidation-reduction potential as introduced in the Chapter 2.4. In this study, the degradation of methylene blue was tested for photocatalytic activity measuremets. For this purpose, the samples were immersed in the methylene blue solution of 3 ppm and waited for 24 hours to reach the complete adsorption equilibrium conditions. Afterwards, they were put out of the solution (Figure 3.9 (b)) and then dried in a dark place at room temperature overnight. After recording the initial absorbances at 661 nm, the films were subjected to 300 W/m^2 artificial solar irradiation. The absorbance data measurements, observed under the same conditions, were kept on intermittently with UV-Visible Spectrophotometer until all the adsorbed methylene blue was decomposed (Figure 3.6). The initial absorbance was defined as 1 as for initial concentration and the ratio of initial value and other absorbances measured after irradiation were converted to concentration change between 1 and 0.



(a) (b)

Figure 3.6 Thin films (a) maintained in methylene blue solution for 24 hours and then dried (b) radiated with Suntest solar simulator until the recorded absorbance data reached to constant value.

3.5.5. Contact Angle Measurement

Apart from the photocatalytic purification, TiO_2 containing thin films exhibits photoinduced superhydrophilic properties on the coating surface. Film hydrophilicity was determined qualitatively by measuring the contact angle with the optical contact angle and surface tension meter (KSV CAM System). The motorized syringe (Hamilton, 10 ml), was used to drop a controlled volume of ultrapure water. The measurements were performed at room conditions. The drop image was acquired by a CCD camera attached to the microscope, then transferred to the computer for processing with an image analysis software.

3.5.6. Surface Morphology and Thickness Measurement

The surface morphology of the thin films were examined by SEM. Before being examined on a QUANTA 400F Field Emission scanning electron microscopy

(SEM) and JEOL JSM 6060 scanning electron microscopy samples were first coated with carbon and gold to achieve sufficient conductivity during analysis. Electron microscopy studies, which allows to determine film morphology and local surrounding is an effective characterization for this study for establishing ordering parameters of the structure such as surface porosity, cracking and homogenity.

For characterization of film thickness the Dektak 6M stylus profiller was used since by this profiller measurable step height can be adjusted to less than few nanometers. It is a semi-manual instrument which gives profile data of a sample by the help of a stylus in contact with the sample which is moved horizontally across the sample surface. Hereby, the thickness of the thin film can be estimated from the profile data of the film layers.

3.5.7. Film Roughness Measurement

Surface roughness of an *E. coli* doped TiO_2-SiO_2 coated glass substrate was measured by Nanosurf Easyscan 2 Atomic Force Microscope (AFM). By moving the metal tip of AFM across the surface at a constant reference level, the tunneling current, which changes with the surface height variation, can be measured and the corresponding topographic structure of the surface was obtained. The scan size by AFM can be chosen any value up to 8 μm. Each measurement contains 512 X 512 data points. During the measurement, errors can easily occur by external vibration, improper engagement of the tip on the sample. The roughness of the samples was directly computed from their AFM images.

3.5.8. Surface Area, Pore Size Distribution, XRD and TGA Analysis for Powder Form

The prepared solution which was used for thin film coating procedure then dried at room temperature. The dried portion was hammered to obtain powder which

was calcinated at 500ºC for 30 minnutes. Finally, the powder was dehydrated in a vacuumed incubator over 24 hours. The powder was analyzed for its surface area and pore size distribution using Micromeritics Gemini V.

The BET surface areas of the sample were obtained from N_2 adsorption/desorption isotherms determined at liquid nitrogen temperature on an automatic analyzer (Micromeritics). The samples were outgassed for 24 h under vacuum at 100°C prior to analysis.

X-ray diffraction (XRD) patterns of powder samples were recorded on a Philips PW 1729 X-ray Diffractometer using nickel-filtered Cu KR radiation over the range of $5° < 2\theta < 75°$ in 0.05° steps with a 1 s counting time per step.

Thermogravimetric analyse (TGA) of powder samples were recorded at the heating rate of 10 $^{o}C.min^{-1}$. by utilizing Shimadzu DTG-60H to determine thermal stability and fraction of volatile components by monitoring the weight change that occurs as a specimen is heated. The measurement is performed under nitrogen atmosphere to slow down oxidation.

CHAPTER 4

RESULTS AND DISCUSSION

The photocatalytic activity of titanium dioxide strongly relies on its crystallinity and specific surface area which is cited in the Section 2.5. Consequently, the anatase phase with large surface area is desired in photocatalytic applications. Thus, efforts have been put into the formation of anatase phases with large surface area in this study. The limited surface area of glassy TiO_2 thin films was improved by the addition of SiO_2, which is also enhance the thermal stability. The viability of the use of microorganisms as 3D templates was also examined.

The photocatalytic activities of *Esherichia coli* indentated thin films were tested and the surfaces were characterized by scanning electron microscopy (SEM), X-ray diffraction (XRD), contact angle indication, UV-spectrometer, BET and pore size distribution analysis were used to observe the surface morphology, phases in the system, superhydrophilicity, porosity, absorbance and thicknesses of the thin films. Suntest solar light simulator was used as irradiation source.

4.1. Measurements of Photocatalytic Activities

In order to increase the photocatalytic activity for these thin films, it was decided to increase the surface area hence the porosity of the surface since a larger surface area enables the simultaneous adsorption of more molecules and increases the probability of the charge carriers transport to the surface. Therefore, improving the synthesis routes and developing recepies producing smaller particles, porous particles and materials with higher surface area are promising methods to increase photocatalytic efficiency. For this purpose,

organic materials might be added to the sol-gel formulations as molecular or macroscopic templates such as poly(ethylene glycol) [149], activated carbon and some non-surfactant organic compounds as diolates and glycerine [49] . These organic molecules have to be removed from the thin film with thermal methods such as calcination, evaporation or extraction (dissolution or supercritical extraction) methods. The structure, shape and size of the voids depends on the template and its interaction with the gel phase [49] produced by template which have the same size as the removed molecules as templates.

E. coli was selected as the 3D template material since it is easy to grow under laboratory conditions, can survive and grow with or without oxygen and its cell wall structure is known [140, 150]. The cells are about 2 μm long and 0.5 μm in diameter, which would supply rough surface for the resultant titania-silica ludox solution.

The cultivated *E. coli* cells were added to the water based titania solution after the pH value was adjusted between 8-9 not to damage the *E. coli* cells before gelation or film formation. The pH value was adjusted by using a weak base solution such as ammonia. On the other hand, the films were dried at 30-35 ºC instead of drying at 100-110 ºC to conserve the 3D shape of the cells. Moreover, the centrifuged cells concentrate was first suspended in a small amount of water and then appended to the solution by stirring vigourously for producing homogenous coating solution and therefore homogenous thin film on the substrate.

Photocatalytic degradation of methylene blue solution and the effect of methylene blue concentration on photocatalytic performance were tested by using *E. coli* templated thin film samples. Degradation of methylene blue was first tested on the thin films that were prepared by adding *E. coli*, centrifuged from 200 ml broth, into the 100 ml TiO_2-SiO_2 sol (x1 *E. coli*:x0.83 TiO_2) obtained by using sol-gel method. The amount of 80 μl methylene blue solutions

of different concentration (150 - 200 mg/l) were stained onto the film surfaces (Figure 4.1). These samples were dried at room temperature and subsequently, they were radiated by a solar light simulator with a dose of 300 W/m^2. At regular intervals samples were analyzed at 661 nm with a UV–VIS spectrophotometer to determine the concentration of MB. From Figure 4.1, apart from the MB concentaration difference, all the samples were unstained for a certain time period (4 hours).

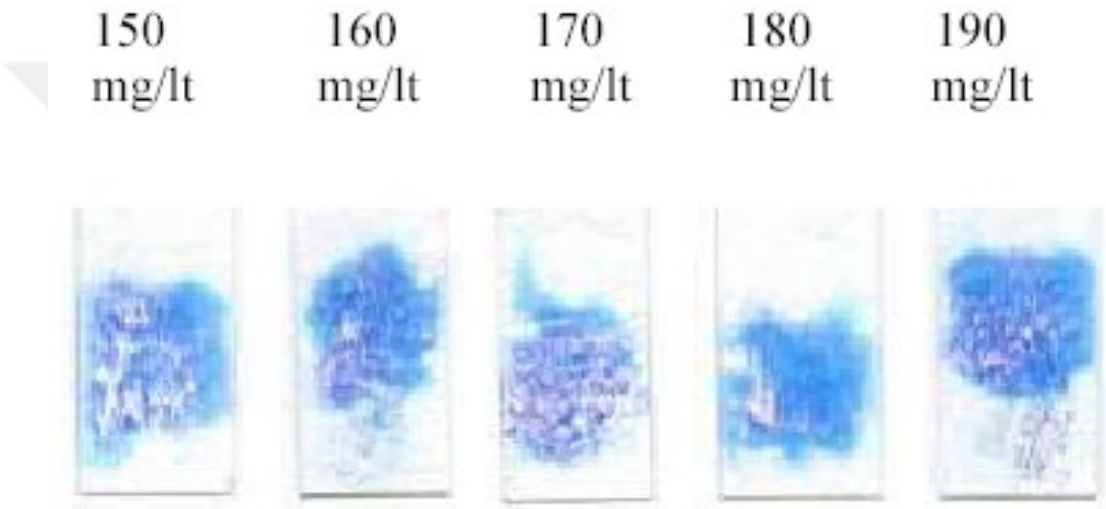


Figure 4.1 Thin films which contained *E. coli*:TiO_2 at a rate of 1:0.83, were stained with the methylene blue solution which had concentrations between the range of 150 mg/lt-210 mg/lt (a) kept in dark place (b) radiated with Suntest solar simulator for 4 hours.

Preliminary experiments done with the stains of 20-150mg/l methylene blue solutions under 300 W/m^2 irradiation result with the complete degradation within one hour. In order to measure activity data with time, solutions within higher

concentration range having 150-200 mg/l were used. The methylene blue concentration on the samples were obtained by the absorbance measurement and by comparing with the unstained glass. The absorbance of the methylene blue stain at 661 nm of each sample was followed with respect to the time by measuring the methylene blue concentration in 15 minute time intervals. The photocatalytic activity was examined quantitatively by measuring the absorbance values at 661 nm wavelength as introduced in Section 3.6.4.

From the absorbance data for the films that were prepared by adding *E. coli*, centrifuged from 200 ml broth into the 100 ml TiO_2-SiO_2 sol (x1 *E. coli*:x0.83 TiO_2), concentration change of MB stains can be obtained. Figure 4.2 demonstrates that under the solar irradiation nearly half of the concentration change occured at the end of 2 hours for all the samples.

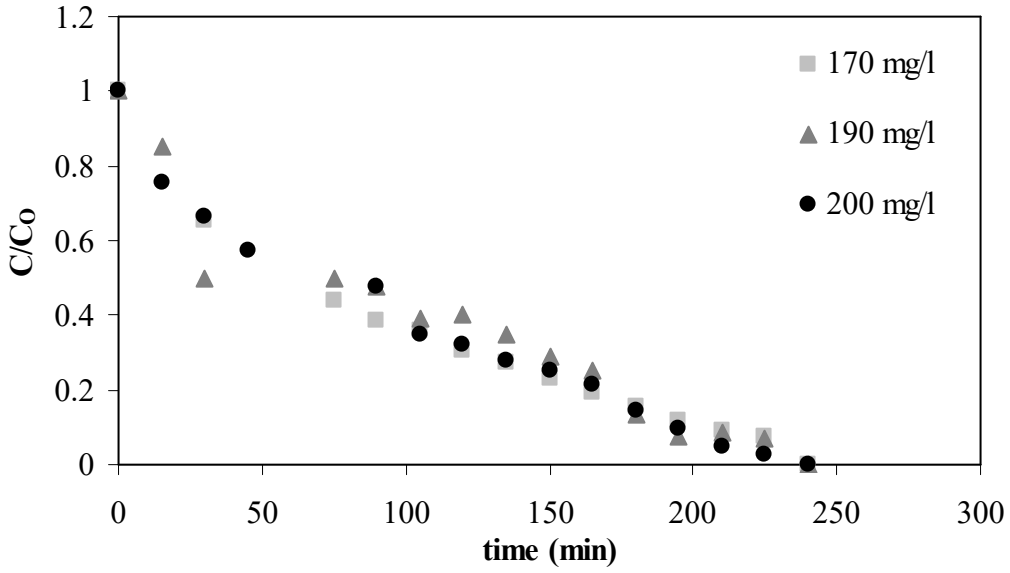


Figure 4.2 Concentration change of methylene blue for the *E. coli* doped titanium dioxide coated thin films subjected to 300 W/m^2 artificial solar irradiation.

On account of the *E. coli* addition to the coating solution has favorable effect on photocatalytic activity of the thin films, it was decided to investigate the influence of *E. coli* concentration on photocatalytic activity. Therefore, *E. coli* cells were grown in 400ml, 200 ml, 100 ml, 50 ml and 20 ml of nutrient broths which were incubated on a rotary shaker at 37 °C for 16 h. Then from each broth *E. coli* cells were harvested by centrifugation and added to the prepared 200 ml TiO_2-SiO_2 ludox sol as the detailed procedure was represented in Section 3.3.

The methylene blue stains were applied to the samples as described previously and the rate of change of absorbance of methylene blue concentration on stain was followed with respect to time under irradiation. Concentration change of methylene blue stain of 210 mg/l with respect to time over the surface of the thin films with different *E. coli* loadings on titania are shown in Figure 4.3. The data for concentration change of methylene blue stains of 210 mg/l, 190 mg/l, 180 mg/l and 170 mg/l are given in the Appendix C.

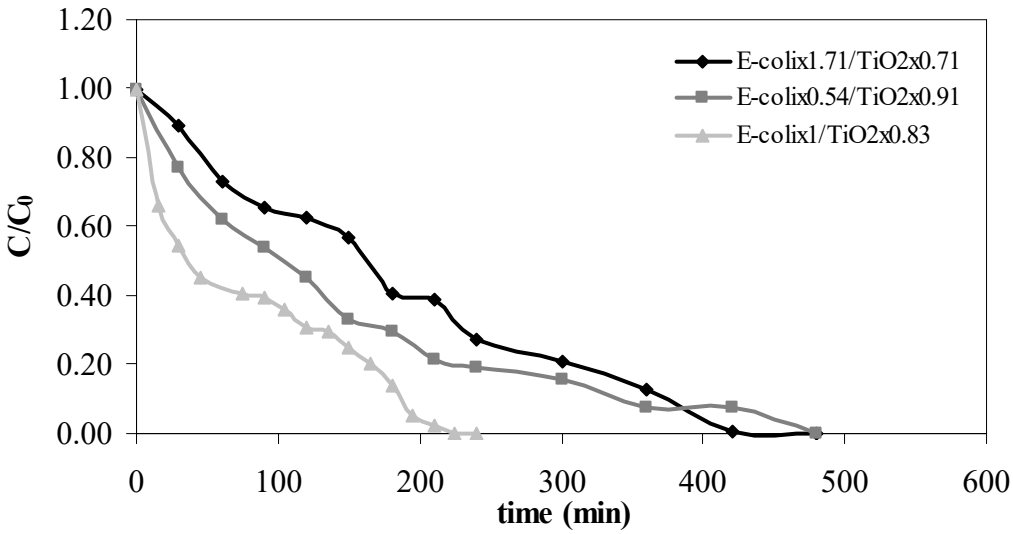


Figure 4.3 Concentration change of methylene blue stained on the surface of the thin films with different *E. coli* and titania content under 300W/m^2 irradiation.

Figure 4.3 shows that the samples having *E. coli* loadings of 1 performed better than 0.54. However, the x1.71 *E. coli* loading have limited activity compared to the other two samples

The same experiment was repeated with the methylene blue solution of 4 ppm instead of methylene blue stain. The thin films with different *E. coli* loadings on titania (x0-x1.71) were immersed into the methylene blue solution and kept at 35 ºC for 24 hours. When the samples were dried, the rate of change of absorbance of methylene blue solution was followed with respect to time under irradiation.

Concentration change of methylene blue solution with respect to time over the surface of the thin films with different *E. coli* loadings on titania are shown in Figure 4.4. The data for concentration change is given in the Appendix C.

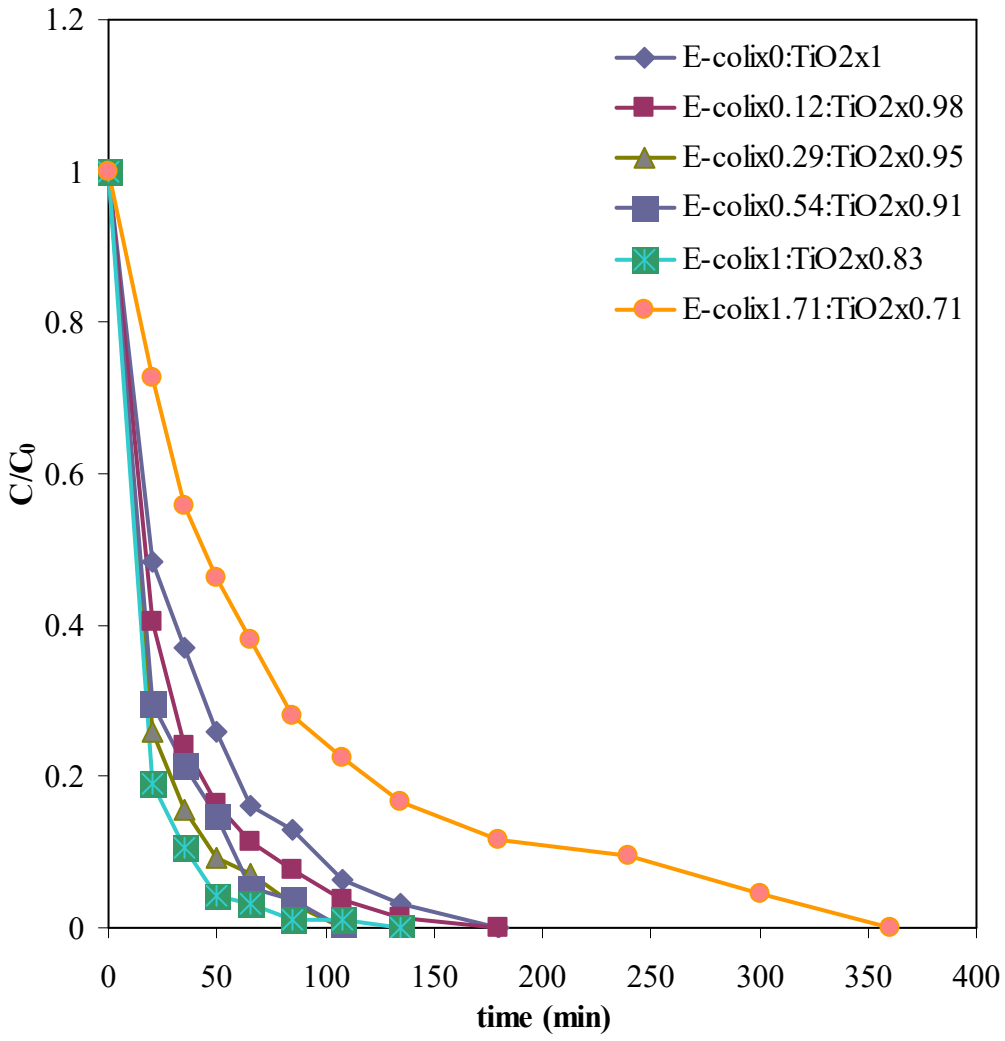


Figure 4.4 Concentration change of methylene blue solution on the surface of the thin films with different *E. coli* and titania content under 300W/m^2 irradiation

Figure 4.4 shows that all the samples having *E. coli* loadings between 0.29 – 1 performed better than pure TiO_2. However, the 1.71: 0.71 loading has limited activity compared to pure TiO_2. These results imply that, 80% of the methylene blue can be degraded within 20 minutes under 300W/m^2 irraditaion.

The initial degradation rate, determined from time vs. MB solution concentration change which can be seen in the Figure 4.3 and Figure 4.4 is illustrated in Figure 4.5 and Figure 4.6, respectively. It was found that the initial decomposition rate increases with *E. coli* loading and reaches to a maximum with 1:0.83 loaded sample. Further loading of *E. coli* did not contribute to the activity. Regarding the experimental results shown in Figure 4.5 and Figure 4.6, it can be ellucidated that the *E. coli* content on the film surface (Table 4.1) and the decomposition rate of methylene blue increases proportionally to a certain extend. The error bars shows in the line graph below and the mean values, deviation and errors are given in the Appendix C.

Table 4.1 *E. coli* doped TiO_2 solutions of different concentrations

Sample	**Amount of LB Broth (ml)**	**TiO_2-SiO_2 colloidal solution (ml)**	**Amount of Distilled Water Aded (ml)**	**Final Volume of TiO_2-SiO_2 Colloidal Solution (ml)**	**TiO_2 : *E. coli* Ratio in the Sol (Appropriate Ratio)**
1	0	100	0	100	1 : 0
2	20	100	2	102	0.98 : 0.12
3	50	100	5	105	0.95 : 0.29
4	100 (50x2)	100	10 (5x2)	110	0.91 : 0.54
5	200 (50x4)	100	20 (5x4)	120	0.83 : 1
6	400 (50x8)	100	40 (5x8)	140	0.71 : 1.71

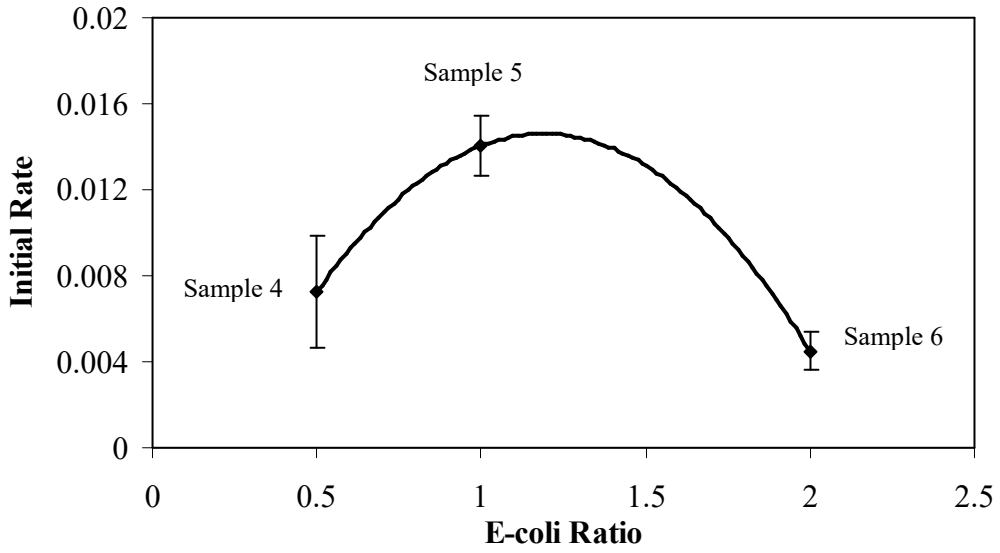


Figure 4.5 The initial degradation rate of methylene blue which is the avarage of four different data for various *E. coli* (x0.54-x1.71) contents.

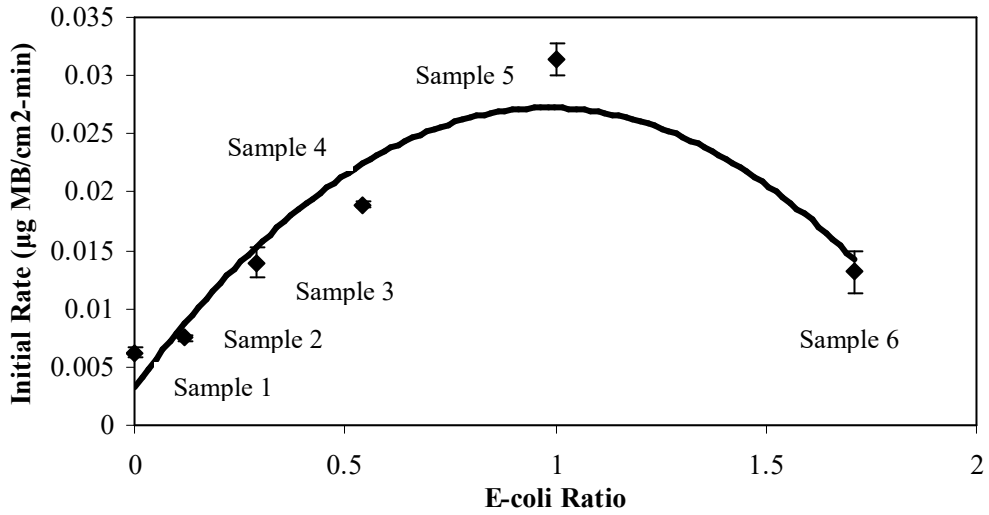


Figure 4.6 The initial degradation rate of methylene blue which is the avarage of two different data for various *E. coli* (x0-x1.71) content.

The increase of photocatalytic activity by loading *E. coli* culture to the TiO_2 formulation might be attributed to several factors. As it is described in Chapter 2, the photocatalytic efficiency of semiconductors can be enhanced by the red shift of band gap (absorbance of photons with smaller energy i.e visible light), the enhancement by surface area and porosity. In order to elucidate the increase of photocatalytic activity with *E. coli* addition, the band gap and surface area of the samples were determined.

4.2. Optical Absorption of the Films

The UV-Vis absorbance spectrum of thin films were investigated in the wavelength range of 190nm-900nm.

Band gap of the thin films produced from with *E. coli* loaded TiO_2 colloidal solutions are presented in Figure 4.8. As observed from the UV-Visible spectra, *E. coli* doped titanium dioxide has spectral analysis at 320 nm which indicates that there is a blue shift compared with the literature value of 380 nm for pure TiO_2 semiconductor. All samples show almost the same peak level and spectral analysis as seen from the UV-Visible spectra given in Figure 4.7. that indicates the *E. coli* loading has no effect on the crystallinity of the samples and their chemical structure which might alter their electronic energy level.

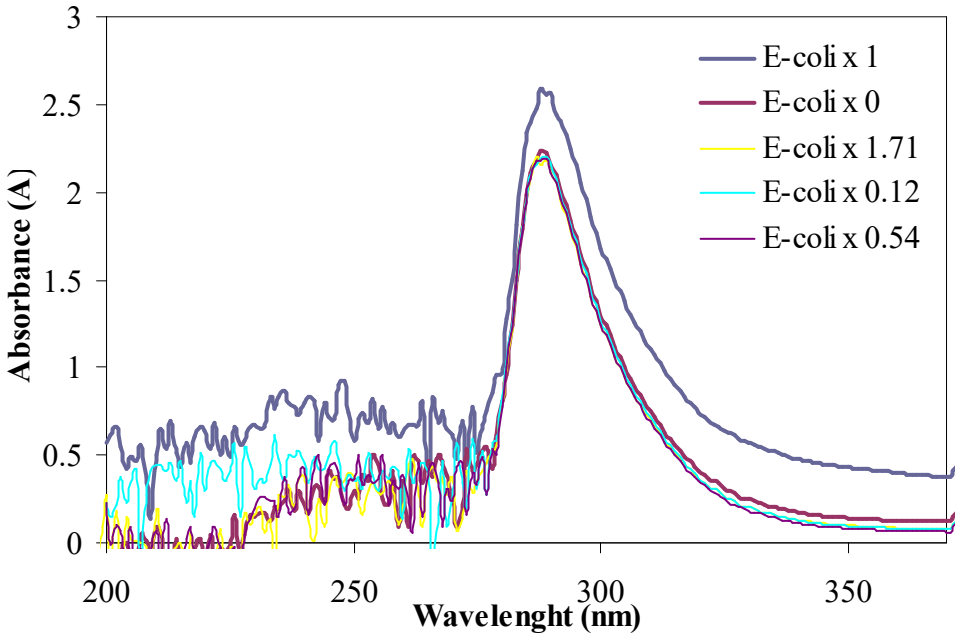


Figure 4.7 Absorbance spectra of *E. coli* doped and undoped TiO_2 - SiO_2 coated films.

4.3. Surface Area Measurements

4.3.1. Surface Area Determination of the Powders

The measurement of surface area by BET method requires 20-500 mg of samples depending on the surface area. However, the thin films applied onto the glass substrates are very thin and weights less than 3 mg each. The surface area of the thin film samples were carried out by using methylene blue adsorption technique as described in Chapter 3.

4.3.2. Surface Area Determination of the Films

In order to calculate surface area of the crack free *E. coli* doped thin films, the Langmuir adsorption technique was utilized which was explained in part 3.6.2.

The specific surface area values for six types of thin films were calculated as a result of three measurements. If the weight of the samples is not known, the adsorption of methylene blue only allows the determination of relative surface area which is defined as the area of thin film per unit area of the substrate if the substrate surface is homogeneously coated (Appendix B).

On the measurements, thin films with the known substrate area were kept in solution for 24 hours to reach the equilibrium concentration in methylene blue solution and the measurement was performed with three different solution concentration (1 ppm, 2ppm and 3 ppm). The adsorption data were analyzed according to the Langmuir equation by assuming monolayer adsorption:

$$\frac{C_E}{x/m} = \frac{1}{kx_m} + \frac{C_E}{x_m}$$

The equilibrium concentration of methylene blue (C_E) could be obtained from the absorbance data taken in 24 hours. Quantity of methylene blue adsorbed per unit weight of adsorbent x/m could also be found from the known substrate area and calculated equilibrium concentration. The plot of $\frac{C_E}{x/m}$ versus C_E gives a straight line which was fitted to these data points and from the slope of this regression line ($\frac{1}{x_m}$) and surface area of the films were calculated. As an example for the sample of TiO_2 rate is 0.71 and *E. coli* rate is 1.71, the $\frac{1}{x_m}$ value was found as 981.16 from the adsorption isotherm that was shown in the Figure 4.8. The statistical measurement of how well a regression line approximates to three different data points (R-square) was calculated as 0.9914 which indicating the data points provides good predictions. Langmuir isotherms and surface area calculations are given in Appendix B.

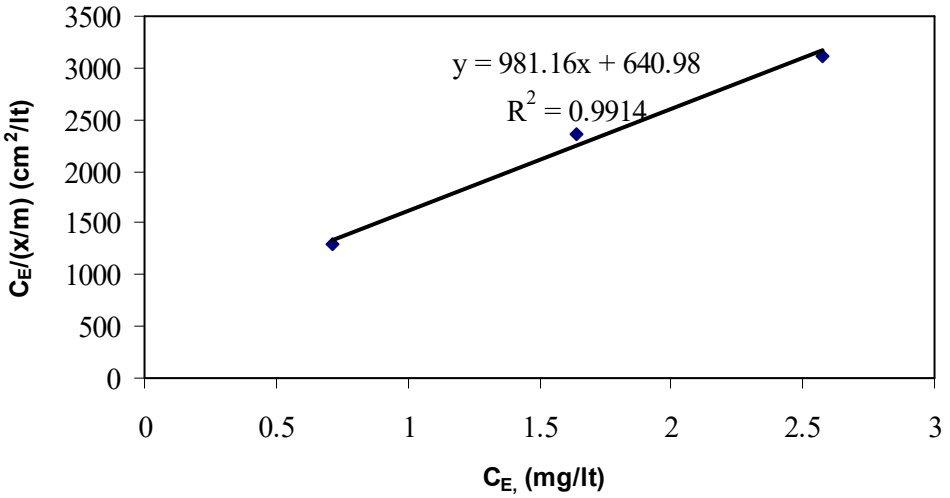


Figure 4.8 Adsorption isotherm for the sample of TiO_2 rate is 0.71 and *E. coli* rate is 1.71

Then, the surface area was calculated from the below equation:

$$S = \frac{L \times A_{MB} \times x_m}{N}$$

Surface area calculations for all the samples are also given in Appendix B and surface area measurement results are tabulated in Table 4.2

Table 4.2 Relative Surface area of the thin films with different concentrations

Sample	Surface Area (cm^2/cm^2)
E. coli x 0	4.3
TiO_2 x 1	
E. coli x 0.12	5.0
TiO_2 x 0.98	
E. coli x 0.29	8.8
TiO_2 x 0.95	
E. coli x 0.54	10.4
TiO_2 x 0.91	
E. coli x 1	15.1
TiO_2 x 0.83	
E. coli x 1.71	19.7
TiO_2 x 0.71	

As it is given in Table 4.2, *E. coli* loading enhances the surface area in a great extend. The bare TiO_2 thin film coated sample has limited surface area ($4.3 m^2/g$) and by addition of *E. coli*, relative surface area increased proportionally. As expected, the maximum adsorption surface area was observed for the film with the maximum *E. coli* content, 19.69 cm^2/cm^2. It might be interesting to compare the specific surface area obtained by absorption of methylene blue and the initial rate of methylene blue degradation (Figure 4.9).

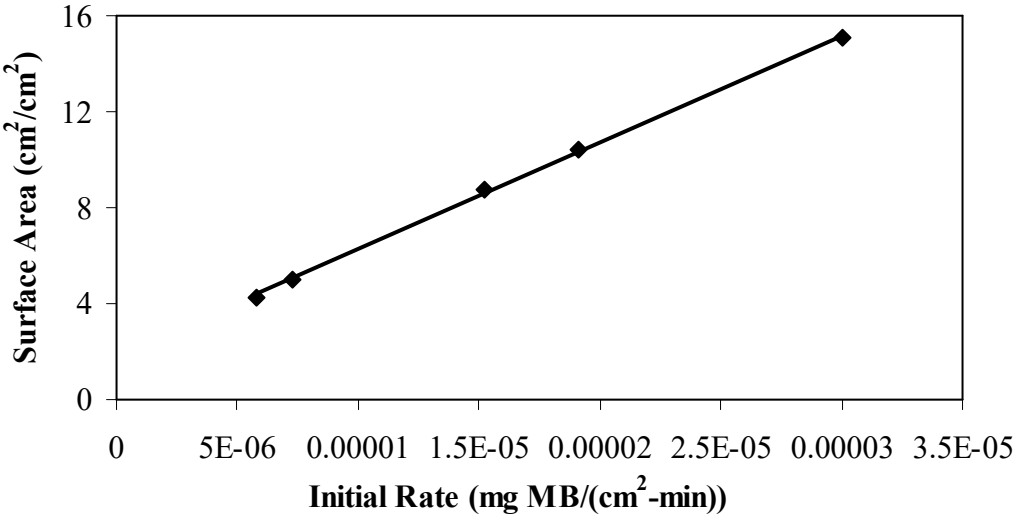


Figure 4.9 Relationship between the initial rate of MB degredation and the surface area of the thin films.

The increase in the decomposition rate by *E. coli* loading might be explained by the increase of surface area of the thin films which is rather harder (Figure 4.9). On the other hand, the sample involving higher *E. coli* with the higher surface area than the other films showed the weakest photolysis (Figure 4.5 and Figure 4.6). This could be due to the two reasons: Firstly, this sample consists of the lowest amount of TiO_2 which has an important effect on percentage of methylene blue decomposition. Secondly, the film might not satisfy the requirement of the transparency. Thus, obtaining films with optimum transperancy, surface area and high photocatalytic activity, hydrophilicity was aimed in this study.

In order to ensure the surface imprinting, and better understanding the effect of *E. coli* addition to the sol-gel method, the same recepie was followed and the solution obtained by sol-gel method was dried without coating. The gel obtained was calcined under the same tempereture and BET surface area of the powder samples were measured by using N_2 adsorption/desorption method.

The BET surface area of the samples is summarized in the Table 4.3. The specific surface area of the pure TiO_2 was determined as 229 m^2/g (BET) method. However, the *E. coli* loading into TiO_2 did not contribute to the surface area of the powder samples (Table 4.3) compared to the relative surface area determined for thin films (Table 4.2). These results might be explaining interaction of cell wall on the gel surface on drying step yielding higher surface area.

Table 4.3 Surface area of the powder samples with different concentrations

Sample	Surface Area (m^2/g)
E. coli x 0	229
TiO_2 x 1	
E. coli x 0,29	230
TiO_2 x 0.95	
E. coli x 0.54	231
TiO_2 x 0.91	
E. coli x 1	236
TiO_2 x 0.83	

4.4. Film morphology

4.4.1. Surface SEM Images of the *E. coli* doped TiO_2 Thin Films

The recepie and coating method have to yield crack free, transparent, homogeneous and continous thin films. Thus, the surface imaging might contribute important clues about the recepie and the success of the method.

In the present study, the porosity and surface morphology of the thin films was modified by utilizing *Escherichia coli* as 3D templates. *E. coli* is an rod-shaped

bacterium propelled by long, rapidly rotating flagella (Figure 4.10) is commonly found in the lower intestine of warm-blooded animals.

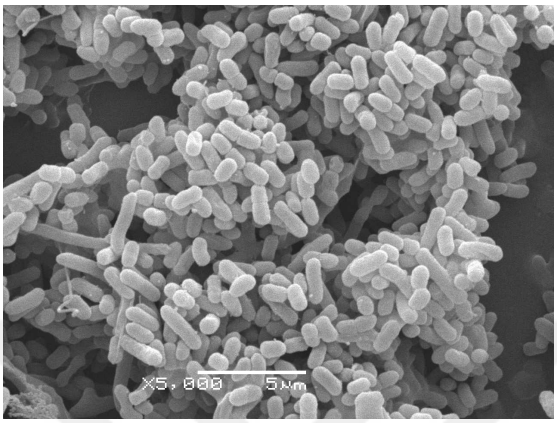


Figure 4.10 Cluster of *E. coli* cells magnified 5,000 times

E. coli can survive and grow in the presence of oxygen (although it can also grow without oxygen), which makes it a useful experimental model organism in the laboratory. The cells are about 2 μm in lenght and 0.5 μm in diameter, with a cell volume of 0.6 - 0.7 μm^3 [151].

E. coli is the well-understood bacterium in the world, and is an extremely important model organism in many fields of research, due to its unique properties. For instance, it is easy to grow under laboratory conditions. Even though many different varieties, called strains of the species exist that have different characteristics while some are safe model organisms, others can cause potentially deadly disease, research strains are very safe to work with. In addition, as compared with other bacteria, *E. coli* grows quickly. Optimum growth of *E. coli* which can be driven by aerobic or anaerobic respiration occurs at 37°C, but some laboratory strains can multiply at temperatures of up to 49°C [140, 150]. As *E. coli* is the part of the common micro flora of large intestine, it

could be defined that the optimum pH of E coli growing in a culture at 37ºC is 7.0-8.0.

On the preparation procedure of *E. coli* doped TiO_2-SiO_2 ludox solution, NH_4OH was employed to adjust the pH of the solution between 7.0-8.0 before adding *E. coli*-distilled water suspension to the sol due to the fact that aside from temperature, the pH of the organisms environment exerts the greatest influence on its growth. [152].

Scanning electron micrographs of the thin film surfaces having 0.71 : 1.71, 0.94 : 0.54, 0.95 : 0.29 and 1 : 0 TiO_2 : *E. coli* proportions presented in Figure 4.11, Figure 4.12, Figure 4.13 and Figure 4.14 respectively. From these SEM images one could observe that cracked, nonhomogenous and rough surfaces were produced by applying the TiO_2-SiO_2-*E. coli* solutions with higher pH. The cracks on the thin film surfaces are mostly interpreted as the result of shrinkages during drying and calcination steps. Such surface structures are not acceptable although satisfactory photocatalytical activity was obtained and they seem defect free to a naked eye.

Our previous study with the same formulations having acidic (low pH values) structure yielded crack free, continous but amorphous (glassy) thin films as it is given in Figure 4.11.

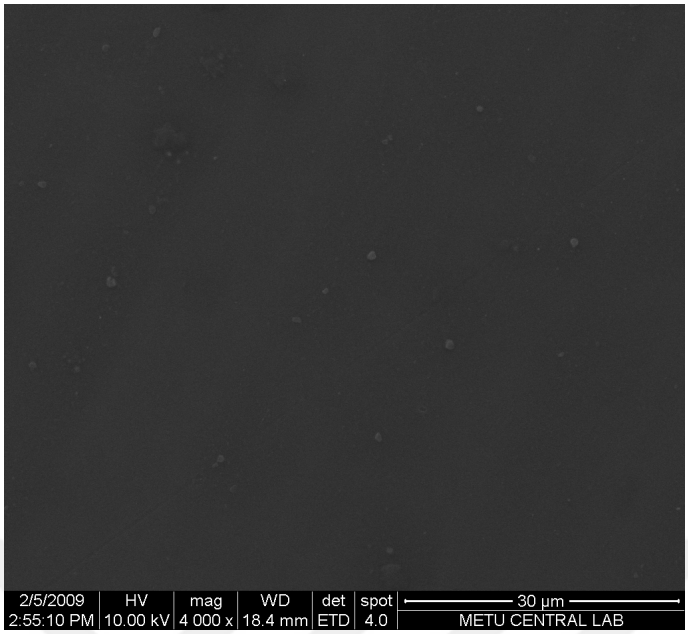


Figure 4.11 SEM surface image of TiO_2–SiO_2 layer of pH≈2

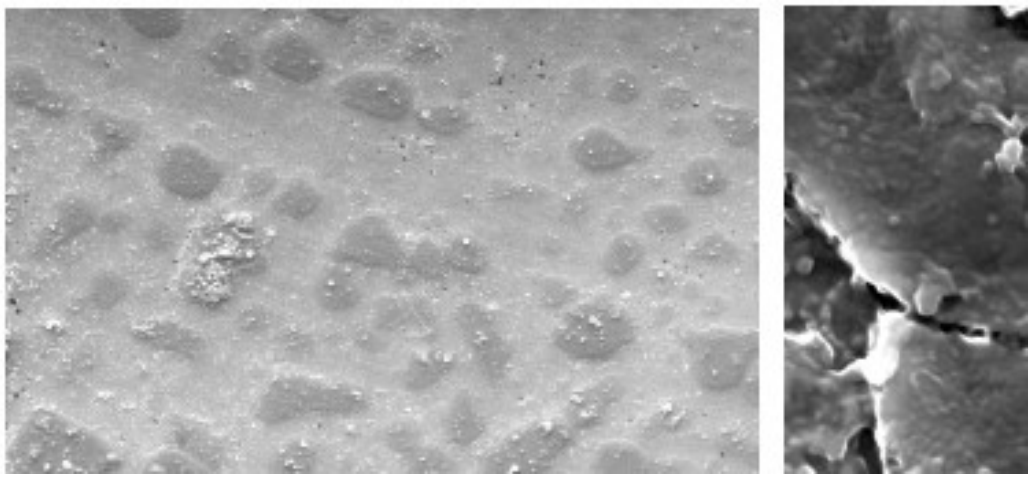


Figure 4.12 SEM surface image of the cracked titania layer of pH≈8

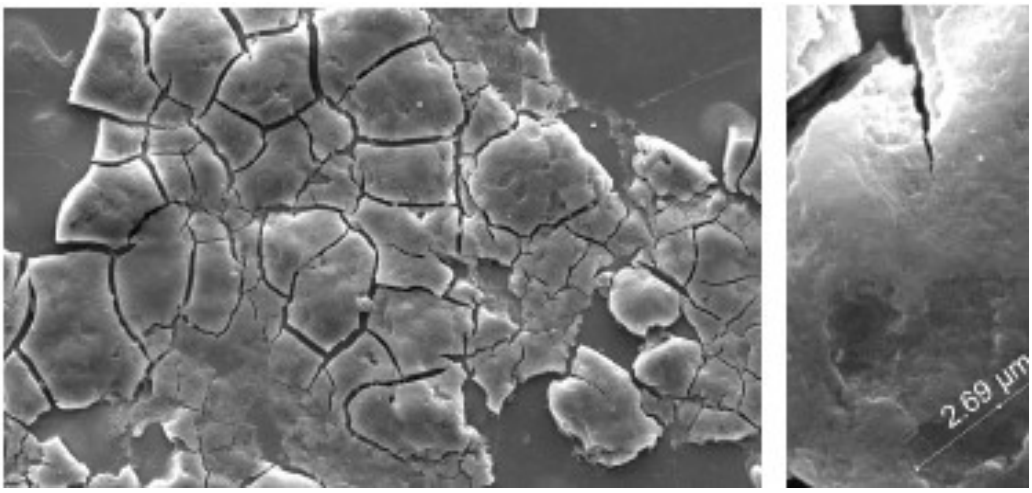


Figure 4.13 SEM surface image of the cracked titania layer doped with *E. coli* x 0.29

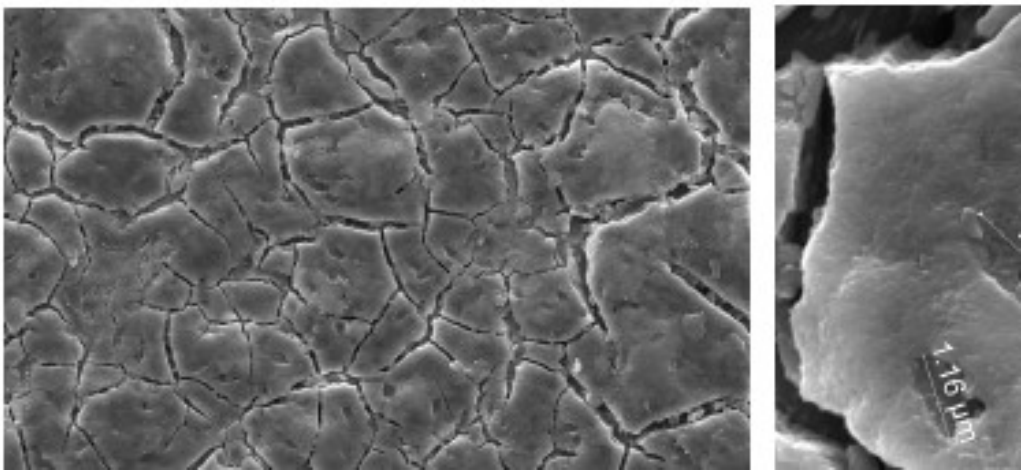


Figure 4.14 SEM surface image of the cracked titania layer doped with *E. coli* x 0.54

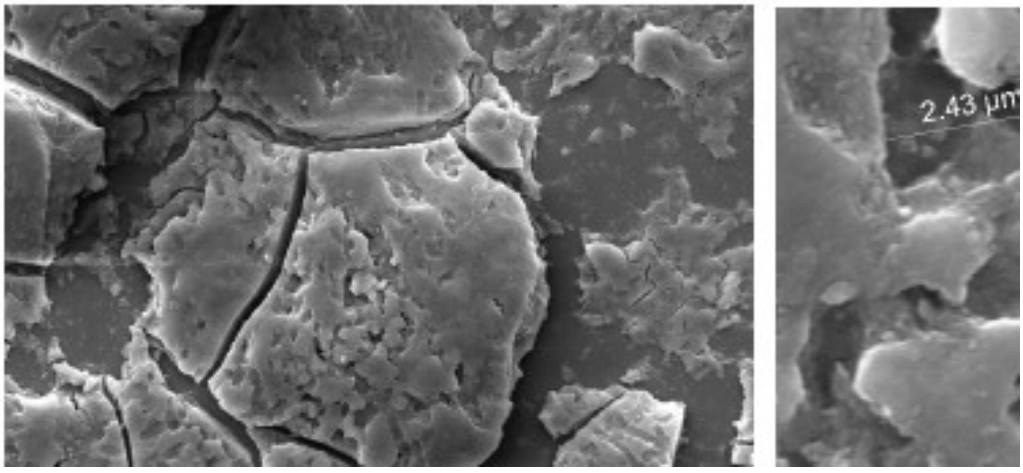


Figure 4.15 SEM surface image of the cracked titania layer doped with *E. coli* x 1

The micrographs show that *E. coli* addition promoted the surface roughness however increasing the pH from 1-2 to 7-8 could trigger the forming of crack in TiO_2 film since cracking was observed for all the films with high pH while the surface of the film coated with the sol of low pH was very smooth. The SEM images of the cracking samples can be observed in the Figure 4.12, 4.13, 4.14, 4.15. The cracks in TiO_2 film are disadvantage in extending the use-life of coated photocatalyst because the flakes can break away from the substrate surface in the progress using.

The flocculation and sedimentation was formed in the solution by the addition of ammonia and observing the cracked film surfaces in the SEM micrographs, could be considered as the change in the pH of the colloidal solution is the critical point for influencing the colloidal system. By the addition of the ammonia to balance the repulsive and attractive forces that exist between the particles in a colloidal dispersion may adhere to one another and form aggregates of successively increasing size that may settle out under the influence of gravity.

The very slowly and dropwise addition of ammonia to the colloidal stock solution controls the colloidal stability by conditioning the combination of Van der Waals, electrostatic, and repulsive-attractive interaction potentials of the system. As it was expected only few cracks appear in the doped TiO_2 which can be observed from the Figure 4.16, 4.17, 4.18, 4.19, 4.20, 4.21.

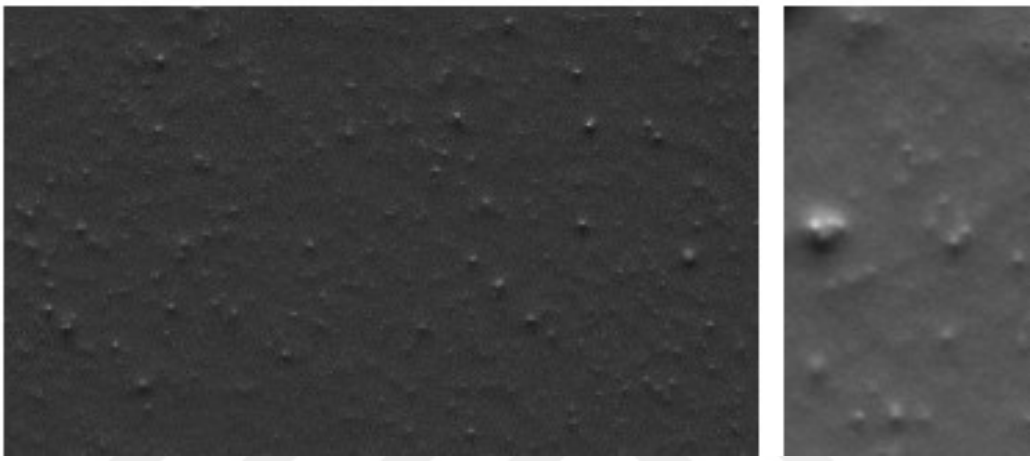


Figure 4.16 SEM surface image of the crack free titania layer of pH≈8, indicating a low porosity level

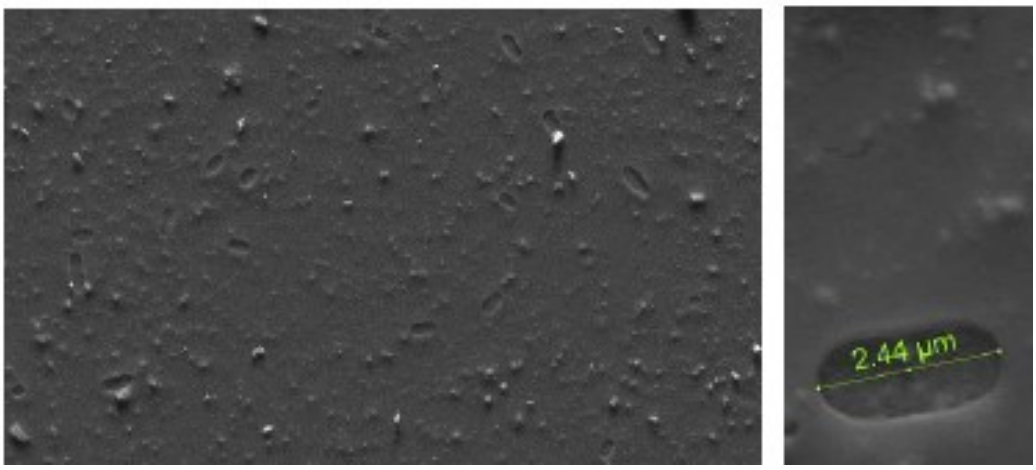


Figure 4.17 SEM surface image of the crack free titania layer doped with *E. coli* x 0,12

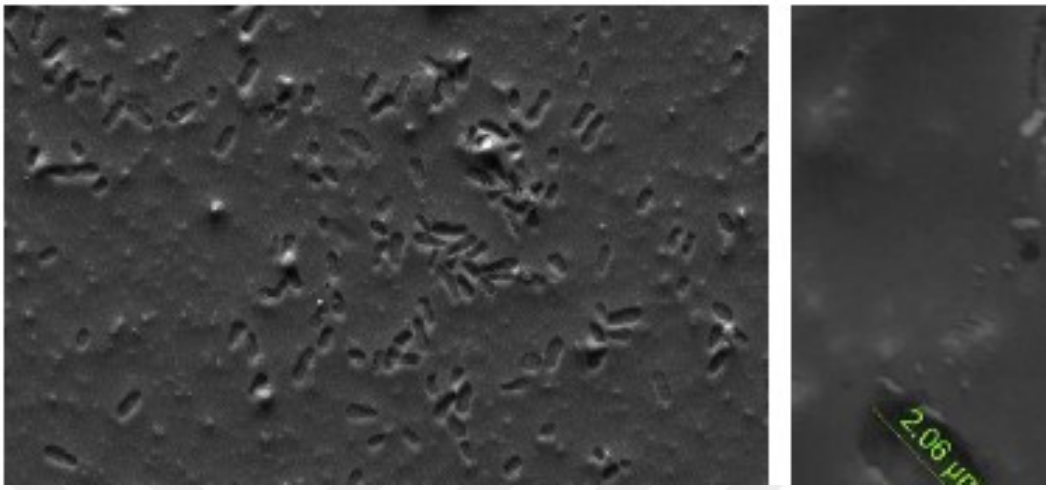


Figure 4.18 SEM surface image of the crack free titania layer doped with *E. coli* x 0,29

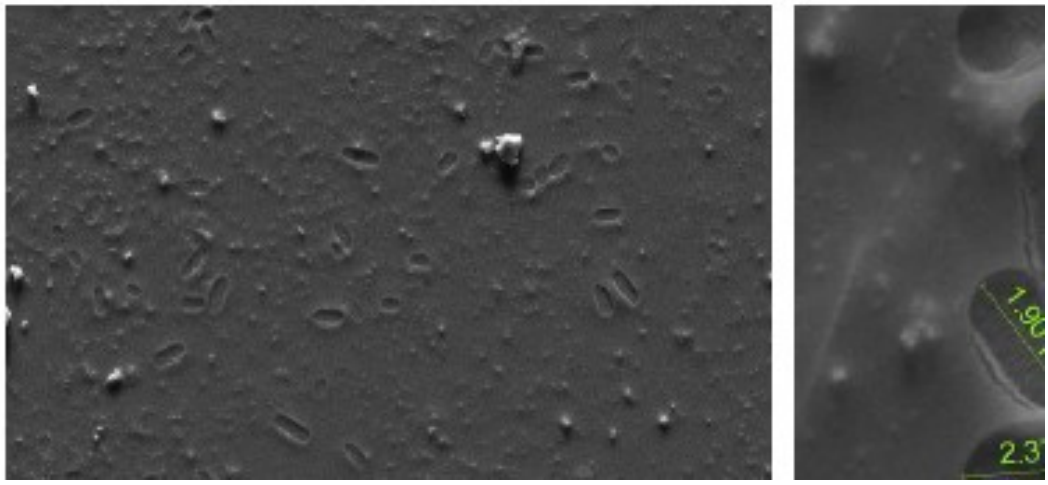


Figure 4.19 SEM surface image of the crack free titania layer doped with E coli x 0,54

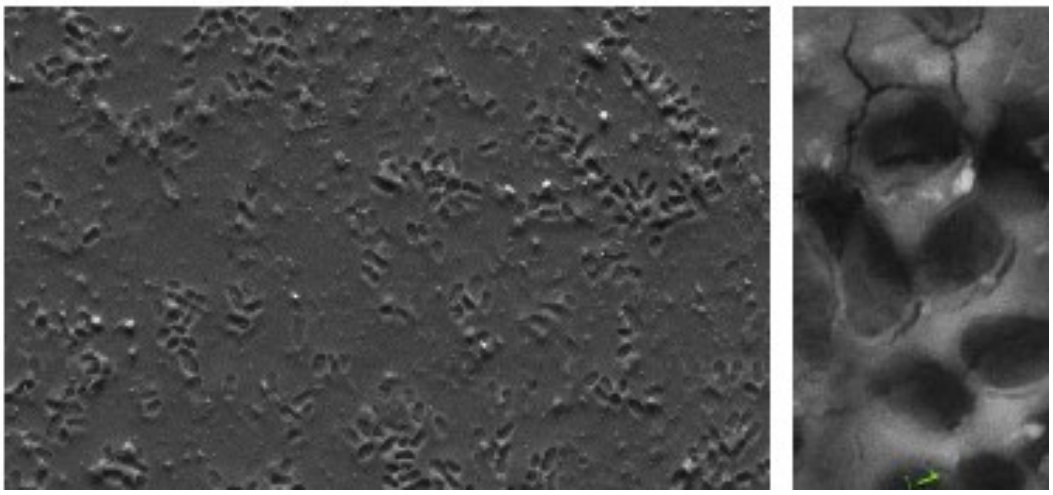


Figure 4.20 SEM surface image of the crack free titania layer doped with *E. coli* x 1

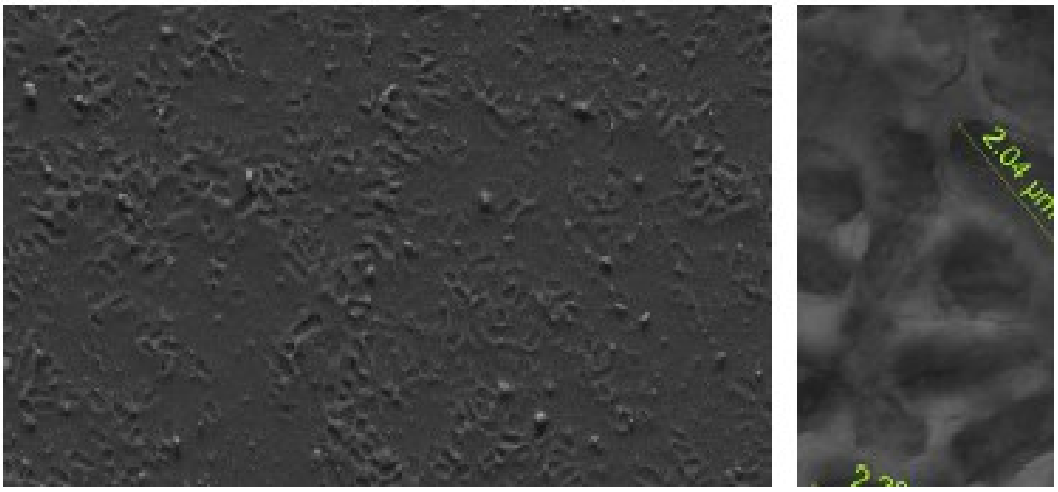


Figure 4.21 SEM surface image of the crack free titania layer doped with *E. coli* x 1.71 indicating a high porosity level

It should be noted that the film morphology shown in Figure 4.16 changes significantly with the appendant *E. coli* ratio used during the dip coating processing. TiO_2 films of synthesized without or with relatively low amount of

E. coli (images of Figure 4.16 and 4.17) appear to be smooth and non-porous. However, the surfaces of TiO_2 film shown in Figure 4.20 and 4.21 become rougher as the *E. coli* concenration increases in the coating solution. Obviously the structure of the films depends on the *E. coli* volume in the TiO_2-SiO_2 sol during the film formation: the higher the *E. coli* added, the larger the surface area of the structure formed.

From the micrographs, dimples size of about 1.5-3 μm can be roughly estimated which confirms the size of *E. coli* cell which leave indentation as 3D template when heat treated at high temperatures. Moreover, all of the TiO_2 nanocrystals obtained, either *E. coli*-doped at different concentrations or not, form micrometer-sized aggregates that can be seen from the Figures.

The thin films were achieved by repeating 3 coating cycles followed by drying procedure as explained in Chapter 3. The overlaped *E. coli* indentations which can be observed from the Figure 4.22, point out the repeated coating layers. It can be observed that, besides the outer layer, titanium interlayer improves the surface quality since the overlapping case provokes the increase in the roughness and area of the film surface.

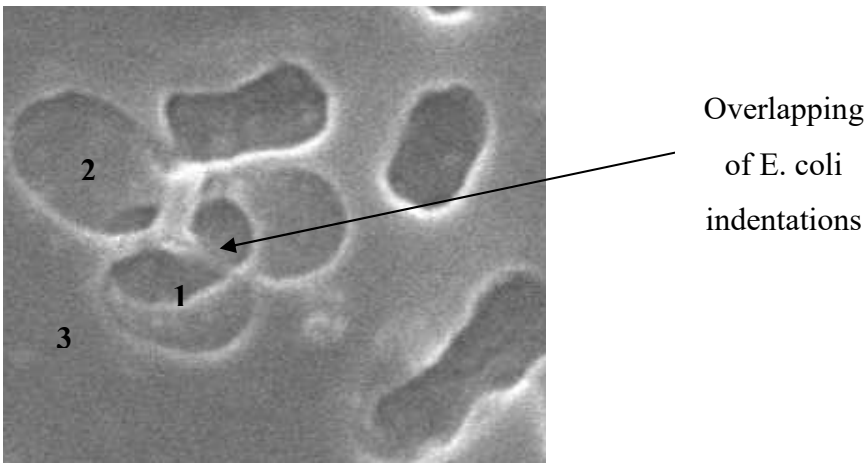


Figure 4.22 SEM surface view of the overlaped *E. coli* bacteria sink into three-layered film.

4.4.2. Cross Sectional SEM Images of Thin Films

In general, the films formed by using sol-gel method are relatively thin depending on the viscosity, contact angle and density of the colloidal solution. Improving film thickness can be achieved through the succesive dip coating processes. [153] However, dip coating cycles can be a tedious and costly procedure. On the other hand, thick films are often fragile, which raises a problem with respect to their long-term mechanical stability. In addition, photocatalysis requires thick films of several hundreds of nm, while photo-induced superhydrophilicity involves a very thin active layer at the outer surface of the film [154]. As a consequence, to reach optimum film thickness both for photocatalytic activity and hydrophilicity is another important parameter to be considered [155].

The film thickness of *E. coli* doped TiO_2 films were measured by thickness profilemeter. Films dip coated by three layers and the height of steps formed by each layer were observed by Stylus Profiller. It can be seen from the Table 4.4 that the average film thickness value is found to be around 160 nm for these samples. Since the samples were three times dip coated, the thickness value for all of them were very close.

Table 4.4 *E. coli* doped TiO_2 film thickness with three dip coating layers

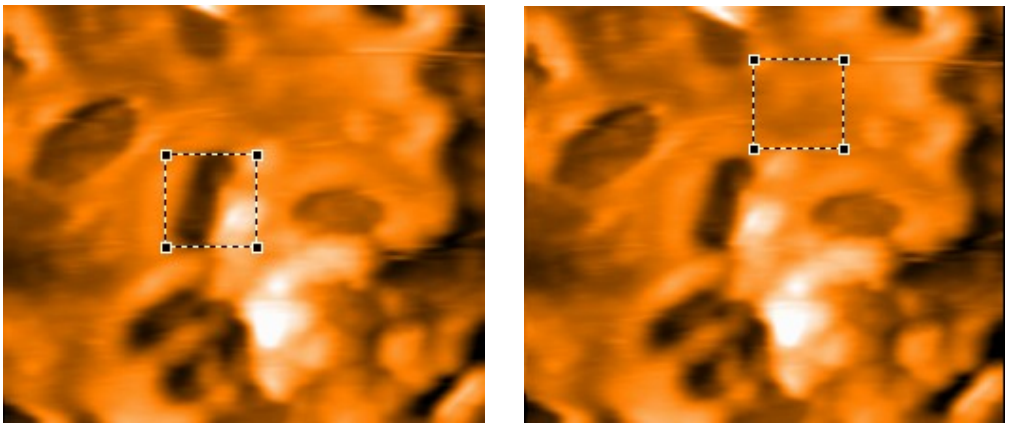
Sample	Thickness (nm)
E. coli x 0	166
TiO_2 x 1	
E. coli x 0.12	169
TiO_2 x 0.98	
E. coli x 0,29	160
TiO_2 x 0.95	
E. coli x 0.54	168
TiO_2 x 0.91	
E. coli x 1	164
TiO_2 x 0.83	
E. coli x 1.71	162
TiO_2 x 0.71	

4.5. Film roughness

SEM image of the *E. coli* doped film layers exhibit that 2-3 micron sized dimples were created at the surface due to the *E. coli* cells. These indents on the film show rougher surface than the other parts. The analysis of the indents was carried out by atomic force microscope with the tapping mode.

Typical average roughness value for the unindented surface of x1.71 *E. coli*: x0.71 TiO_2 film was found about 18.8 nm. The atomic force microscopy (AFM) measurement of surface roughness on the indentation was 126.7 nm for the same sample. As observed from the micrographs, the indents have rougher surface than the other parts on the film. The scanned area of several micrometers

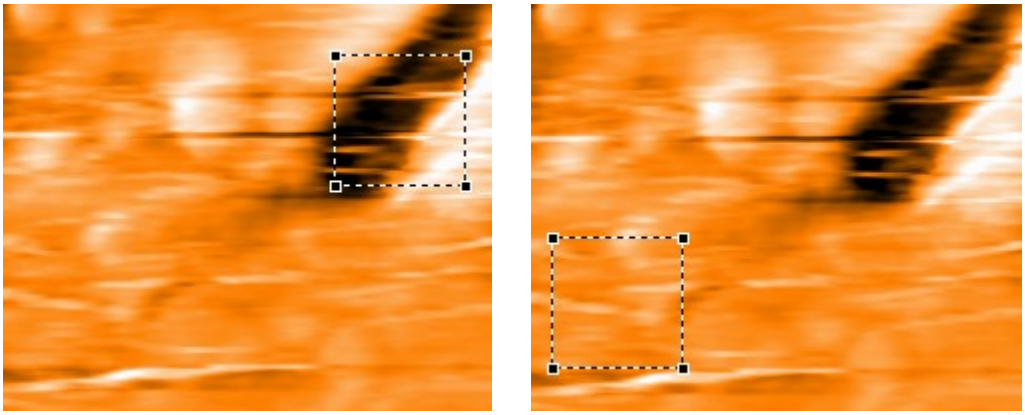
concerned to the indent and unindent site on the film are presented in Figure 4.23 (a) and (b), respectively.



(a) (b)

Figure 4.23 AFM image of the (a) interior part of the *E. coli* gap and (b) outer part of the *E. coli* gap for the film with the rate of 1.71(*E. coli*) and 0.71 (TiO_2).

The films deposited by using 0.12:0.98 (*E. coli*:TiO_2) exhibited the same result. As it was expected a lower average surface roughness (about 19.8 nm) was obtained at the outer part of the *E. coli* gap (unindent part) on the film (Figure 4.24 (a)) and rougher surface (about 127.1 nm) was achieved at the outer part of the *E. coli* gap (Figure 4.23 (b)) by the AFM roughness measurements.



(a) (b)

Figure 4.24 AFM image of the (a) interior part of the *E. coli* gap and (b) outer part of the *E. coli* gap for the film with the rate of 0.12 (*E. coli*) and 0.98 (TiO_2).

The increase of the surface roughness among the indent and unindent surface is about 6-7 times for all the samples. The result of AFM analysis is in good agreement with SEM observation that the *E. coli* indentation create rougher surface. This could be due to the outer membrane morphology of the bacteria. According to Meincken et. al., the average surface corrugation (roughness) of an untreated *E. coli* cell was determined to be 2.41 ± 1.37 nm and it was observed that the membrane roughness can increase correlated with some chemicals [162]. In the present study, *E. coli* cells were added to the TiO_2-SiO_2 solution which is similar to the case in the study of M. Meincken. Furthermore, the nanosized titania crystalls remained on the surface after calcination could also enhance the porosity of the film surface.

In case of need to compare the surface roughness measurement belongs to the two films of different *E. coli*:TiO_2 content, it was observed that film with higher thickness (about 169 nm) exhibits a higher roughness than the film with lower thickness (about 160 nm).

Surface roughness is a critical parameter in the thin film coatings especially in determining the performance of photocatalytic and hydrophilicity mechanism. However, the photocatalytic activities of the prepared films not only depend on the surface roughness of films, but also depend on the amount of loaded photocatalyst as mentioned before.

4.6. Characterization of Hydrophilic Property

The hydrophilic properties are well known to be enhanced by fine roughness [156]. In other words, to improve the hydrophilic property, controling the microstructure and chemical property of the film surface is significant. Infact with the increase of chemically absorbed –OH on the surface, certainly the hydrophilic property is enhanced [157].

The superhydrophilicity of thin films were evaluated by the measurement of water contact angle on the surface from five different points. Thin films were conditioned in dark at 23.5ºC and 65% humidity for 24 hours before the measurement to reduce photoinduced superhydrophilicity effect. The average contact angle data was calculated from the both right and left side value of five different measurements. The contact angle for pretreated substrate was shown in Table 4.5.

Table 4.5 Contact angle measurements of pretreated substrate

Pretreated Pyrex Glass	
Left	Right
64.19º	64.23º
64.21º	

It has been reported that porous TiO_2 film always presents the very low contact angle. Yu et al. reported that a porous TiO_2 film which was prepared by a simple polyethylene glycol (PEG) modified sol–gel method showed excellent hydrophilicity with CA < 5° without UV light irradiation.

The wetting property of *E. coli* modified mesoporous TiO_2 films as investigated. Mean values of contact angles of the *E. coli* doped TiO_2-SiO_2 Ludox cracked and crack free films are summarized in Table 4.6 and Table 4.7, respectively.

It was observed that cracking surfaces resulting in the decline of hydrophilicity. Crack free thin films of titanium dioxide became super-hydrophilic with a contact angle below five degrees without UV light irradiation. In addition, hydrophilicity increased with the increasing of *E. coli* content of the film. That is, highly hydrophilic surfaces of the films could be attributed to their nanostructural morphologies such as high porosity and roughness.

Table 4.6 Contact angle measurements of *E. coli* doped TiO_2-SiO_2 coated cracked thin films

TiO_2 x 0.71 E.coli x 1.71		**TiO_2 x 0.83 E.coli x 1**		**TiO_2 x 0.91 E.coli x 0.54**		**TiO_2 x 0.95 E.coli x 0.29**		**TiO_2 x 0,98 E.coli x 0.12**		**TiO_2 x1 E.coli x 0**	
Left	Right	Left	Right	Left	Right	Left	Right	Left	Right	Left	Right
17.15º	18.19º	12.41º	12.60º	21.24º	23.53º	10.40º	9.79º	5.70º	5.54º	10.10º	8.65º
17.67º		12.51º		22.39º		10.09º		5.62º		9.38º	

Table 4.7 Contact angle measurements of *E. coli* doped TiO_2-SiO_2 coated crack free thin films

TiO_2 x 0.71 E.coli x 1.71		**TiO_2 x 0.83 E.coli x 1**		**TiO_2 x 0.91 E.coli x 0.54**		**TiO_2 x 0.95 E.coli x 0.29**		**TiO_2 x 0,98 E.coli x 0.12**		**TiO_2 x1 E.coli x 0**	
Left	Right	Left	Right	Left	Right	Left	Right	Left	Right	Left	Right
1.77º	2.09º	2.36º	2.14º	2.93º	2.91º	2.46º	2.36º	3.38º	3.36º	6.11º	6.04º
1.93º		2.25º		2.92º		2.41º		3.37º		5.91º	

4.7. Thermal Analysis of the *E. coli* Doped Thin Films

In order to determine the best conditions for pyrolysis and annealing of the thin films, thermal analysis was performed on the titanium dioxide powders. The differential thermal analysis (DTA) was performed to investigate the exothermic reactions and the curves for thermogravimetric analysis (TGA) were drawn to see the weight losses upon increasing temperature.

Shown in Fig. 4.25, 4.26 and 4.27 are the thermogravimetric analysis (TGA) spectrum for the *E. coli* doped TiO_2-SiO_2 powders. TGA curves indicate a weight loss of 4-6 % for all the titania powders containing different concentrations of *E. coli* that exhibit the total content of the residual water and some organic groups in the mesoporous titanium dioxide was about 4-6 wt %. Moreover, for the powders the exothermic peaks are in the temperature range of 400 - 430 ^{o}C that can be seen from the DTA curves and not much weight loss could be observed in the TG curve after that temperature range. This can be due to the fact that crystallization of *E. coli* doped TiO_2 powder started over 400^{o}C. In addition, as all the samples of diverse compositions display the same curves without any distinct peak, it can be concluded that calcination temperature was not changing root and increasing temperature did not demonstrate any effect on the formula.

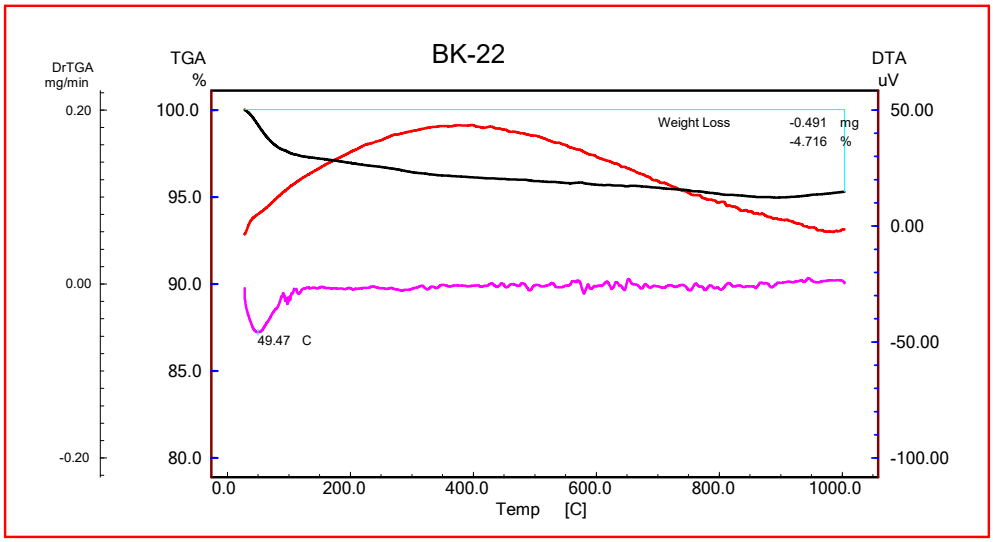


Figure 4.25 Differential thermal analysis (DTA) and thermogravimetric analysis (TGA) curves of *E. coli* doped TiO_2 powders with composition of *E. coli* x 1 and TiO_2 x 0.83

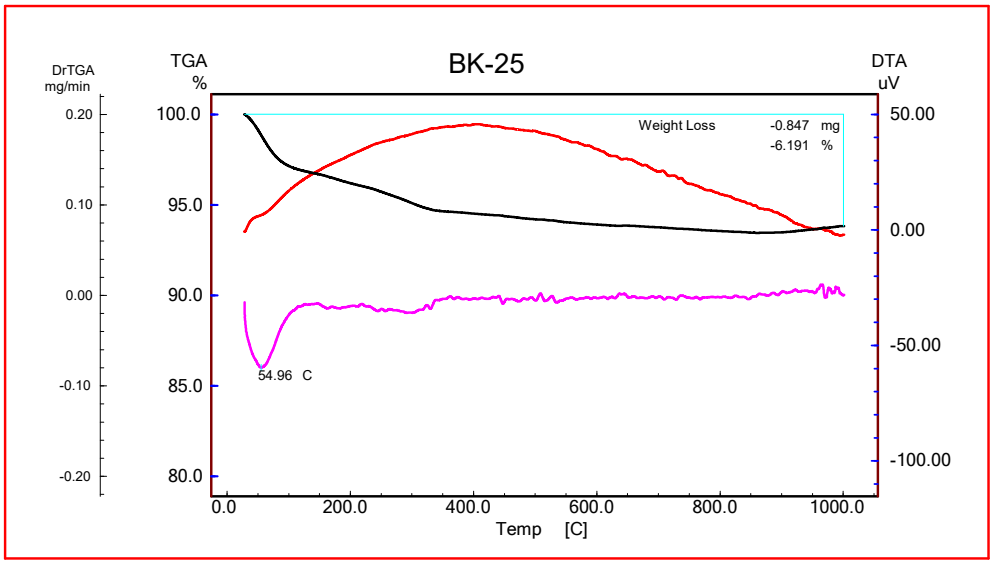


Figure 4.26 Differential thermal analysis (DTA) and thermogravimetric analysis (TGA) curve of *E. coli* doped TiO_2 powders with composition of *E. coli* x 0.29 and TiO_2 x 0.95

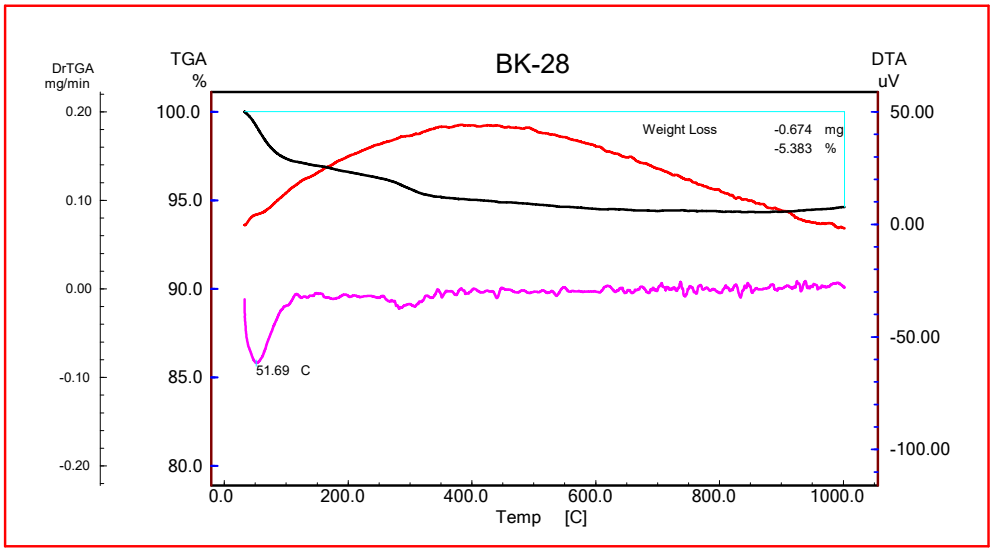


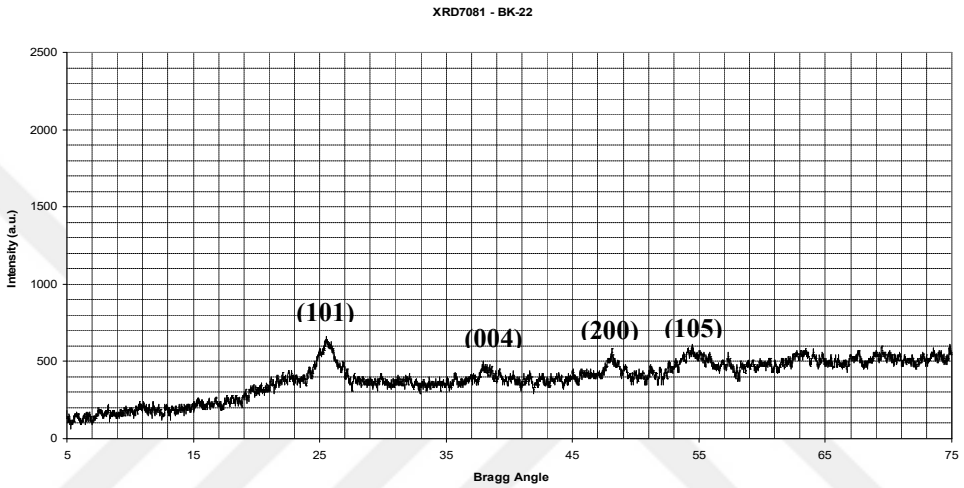
Figure 4.27 Differential thermal analysis (DTA) and thermogravimetric analysis (TGA) curve of *E. coli* doped TiO_2 powders with composition of *E. coli* x 0 and TiO_2 x 1

4.8. Crystalline Film Formation

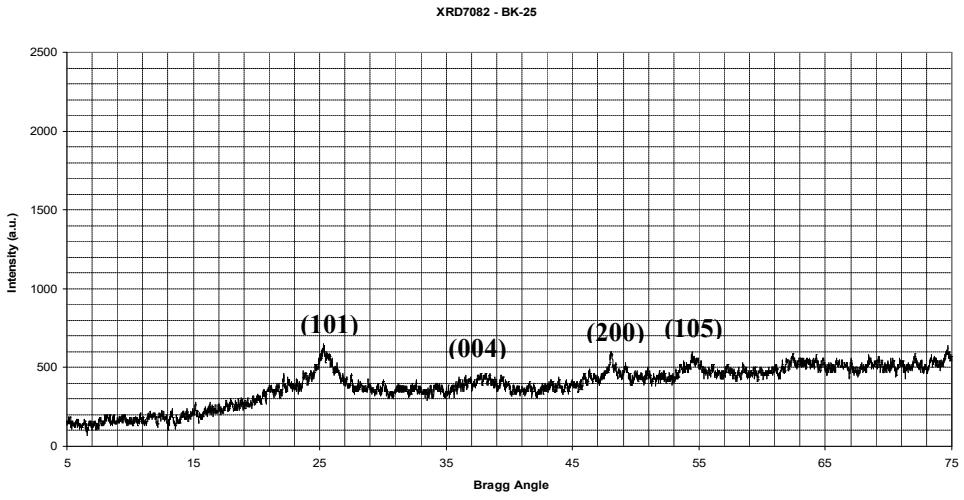
X-ray diffraction studies were performed on the *E. coli* doped titanium dioxide powder. The effect of TiO_2:*E. coli* rate on crystalline formation have been investigated. In order to see whether TiO_2:*E. coli* ratio contributes to the inhibitory effect on any crystalline formation, two diverse rate were selected.

Figure 4.28 (a) and (b) shows the powder XRD patterns of two TiO_2 samples calcinated at 500 ^oC for 30 minutes. The structure phases observed were all anatase. The spectra display a rather intense diffraction peak at $2\theta = 25.528^o$, which corresponds to anatase (101) plane of TiO_2. The other peaks at $2\theta = 37.791^o, 48.052^o$ and 53.902^o indicate the anatase (004), (200) and (105) planes of TiO_2 respectively [158, 159]. Furthermore, no additional peaks of other impurities were detected. This result illustrated that the synthesized powders and thin films by this method were pure anatase TiO_2. As shown by the XRD

diffraction patterns plotted in the figures, as the quotient of TiO_2:*E. coli* changes from 0.83:1 to 0.95:0.29 in the solution, a phase transformation into the crystalline anatase phase occurred with the same intensity. For the two samples, peak intensities are very weak. This can be attributed to the rapid reactions due to increase in pH of the solution. [160]



(a)



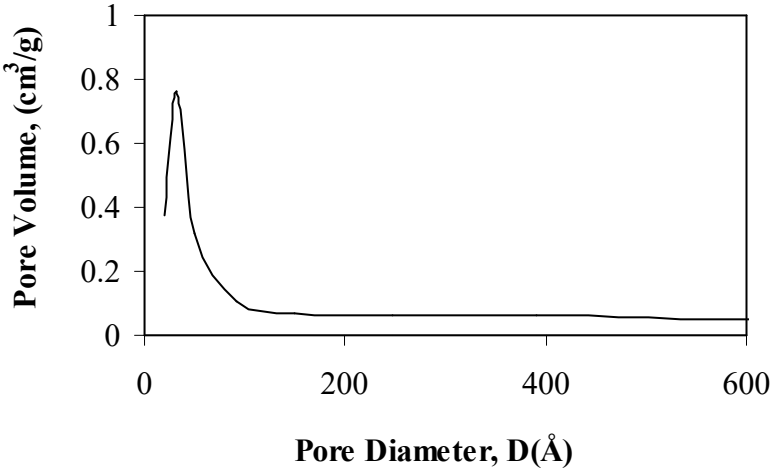
(b)

Figure 4.28 Powder X-ray diffraction patterns for (a) *E. coli* x 1 and TiO_2 x 0.83 and (b) *E. coli* x 0.29 and TiO_2 x 0.95

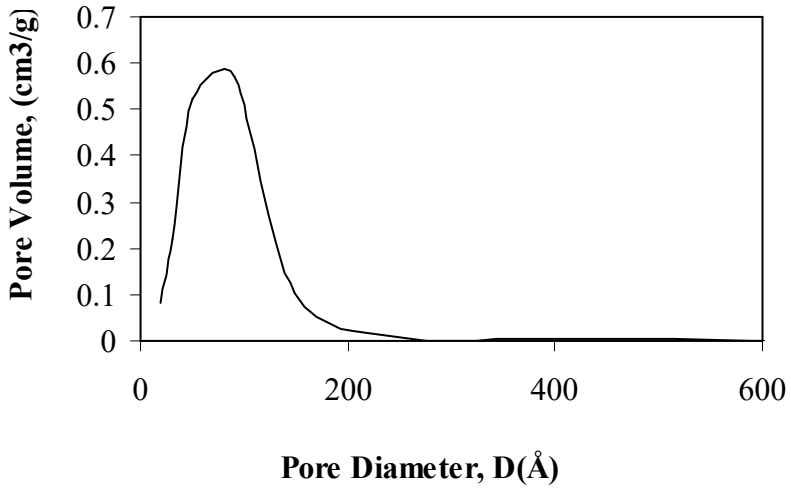
4.9. Pore Size Distribution Measurements

Pore size distribution is based on the adsorption branch of the hysteresis loop, because the desorption branch of the powder TiO_2 samples may have possibility for the reduction of the BET surface area comes from the pore blocking effect that is the probability of cloging some smaller pores by a larger exchange cation. [161]

Figure 4.29 represents the pore size distribution of the TiO_2 powders involving different *E. coli* amount. It can be observed that the *E. coli* content in the film gives rise to increase in pore size and widening in pore size distribution. Namely, the average pore size is smaller and the pore size distribution is narrower for samples which contain x0 *E. coli*. The formation of larger pores can be associated with the *E. coli* addition since such larger pores were observed for the films containing *E. coli* as can be seen from the Figure 4.29 (b).



(a)



(b)

Figure 4.29 Pore size distribution curves of TiO_2 films which include: (a) *E. coli* x 0 and (b) *E. coli* x 1

CHAPTER 5

CONCLUSIONS

In this study, titanium dioxide thin films were produced by dip coating sol-gel method on pretreated pyrex glass substrate. For the optimization of the microstructural and photocatalytic investigations, different process parameters such as composition of the solution and the surface area were applied. In order to increase the surface area of the films *Esherichia coli* was used as 3D templates.

Substrates coated with *E. coli* doped TiO_2-SiO_2 ludox solution of different composition at 0.14 cm/s dipping speed and 0.05 removing speed, reached about 160 nm thickness for three layer coating of all different compositions.

The microstructure of the coatings reveals pores throughout the coatings and the pores increase as the *E. coli* content in the film increases. Additionally, the multilayered structure also improves the surface quality of the *E. coli* doped film via enhanced ovelapping of the gaps occur at different layers.

Roughness measurements on the surface of the film showed that the roughness of *E. coli* gap is about 6-7 times higher than the other parts. These high roughness measurements were because of the titania nanocrystals dispersed on the surface and the outer cell membrane morphology of the *E. coli*. Moreover, the film with higher thickness (about 169 nm) exhibits a higher roughness than the film with lower thickness (about 160 nm).

The higher concentration of *E. coli* cells on the film provokes the surface area. Surface area of the film which did not contain *E. coli* was found as 4.28 cm^2/cm^2, whereas the surface area of the films which contains different amounts of *E. coli* increases up to 19.69 cm^2/cm^2. In addition, the pore size distribution

curves of the powder samples show that larger pores were observed for the powders containing more *E. coli* bacteria.

The surface area gain by *E. coli* doping resulted in higher photocatalytic activity under visible light up to a certain concentration of *E. coli*:TiO_2. The maximum (x1.71) *E. coli* promoted TiO_2 thin films, accomodated the lowest amount of titania on the surface, displayed lower activity when compared with the other samples. The best photocatalytic activity was achieved by the sample which contains *E. coli* at the rate of 1 and TiO_2 at the rate of 0.83 on the surface and with the surface area of 15.05 cm^2/cm^2 .

While adjusting the mixed oxide solution pH ammonia ammonia was added very slowly by stirring to balance of attractive and repulsive forces and prevent the agglomeration. Crack-free TiO_2 thin films were obtained by means of using unprecipitated solution. The addition of higher *E. coli* bacteria to the solution results in few cracks. However, no flake of layers was observable.

Crack free thin films of titanium dioxide became super-hydrophilic with a water contact angle below five degrees without UV light irradiation. The hydrophilic properties were enhanced by the increasing *E. coli* content and also the fine roughness of the film.

From the X-Ray diffraction analysis a slight peak was detected at 25.3° assigned to (101) lattice plane of anatase TiO_2. In addition, from the TGA-DTA curves of the powder samples it was observed that samples revealed 4-6% total weight loss on heating attributed to the release of adsorbed water and removal of little residual, crystallization of *E. coli* doped TiO_2 powder started over 400 ºC and increasing temperature has no effect on the formula attributed to the silicon dioxide content of the film.

CHAPTER 6

FURTHER SUGGESTIONS

In order to increase surface area other bacterial templates with smaller size than *E. coli* should be investigated. The microorganism should also be nonpathogenic and easy to grow under laboratory conditions as *E. coli* strain.

The homogenity of the films should be enhanced. For instance magnetotactic bacteria can be applied as 3-D template instead of *E. coli*. Magnetotactic bacteria are able to align in parallel to magnetic field since they contain tiny magnetic iron particles and more regular indentations can be carved out on the surface.

Antimicrobial activity should be tested for the films containing different amount of *E. coli* and TiO_2. In this manner one can have idea about antimicrobial properties of the samples in addition to the photocatalytic and wetting properties.

REFERENCES

1. O. Carp, C.L. Huisman, A. Reller, Progress in Solid State Chemistry **32** (2004), 33–177.

2. T.-S. Yang C.-B. Shiu, M.-S. Wong, Surface Science **548** (2004), 75–82.

3. C.Y. Wang, D.W. Bahnemann, J.K. Dohrmann, Chemical Communications **16** (2000) 1539.

4. A. Sclafani, L. Palmisano, E. Davi, New Journal of Chemistry **14** (1990), 265.

5. G. Bertrand, N. Berger-Keller, C. Meunier, C. Coddet, Surface & Coatings Technology **200** (2006), 5013–5019.

6. K.K. Saini, S. D. Sharma, Chanderkant, M. Kar, D. Singh, C.P. Sharma, Journal of Non-Crystalline Solids **353** (2007), 2469–2473.

7. J. Chen, C. S. Poon, Building and Environment **44** (2009), 1899–1906.

8. S. Mozia, A. W. Morawski, M. Toyoda, M. Inagaki, Desalination **241** (2009), 97-105.

9. A. Sobczyk-Guzenda, M. Gazicki-Lipman, H. Szymanowski, J. Kowalski, P. Wojciechowski, Thin Solid Films **31** (2009), 5409-5414.

10. Y. M. Jeong, J.K. Lee, H. W. Jun, G.R. Kim, Y. Choe, Journal of Industrial and Engineering Chemistry **15** (2009), 202-206.

11. J. O. Carneiro, V. Teixeria, A. Potinha, A. Magahaes, P. Coutinho, C.J. Tavares, R. Newton, Materials Science and Engineering B **138** (2007), 144-150.

12. M.R. Hoffmann, S.T. Martin, W. Choi, D.W. Bahnemann, Chemical Reviews **95** (1995), 69-96.

13. A. Mills, A. Lepre, N. Elliot, S. Bhopal, O.P. Parkin, S.A. O'Neill, Journal of Photochemistry and Photobiology A **160** (2003), 213.

14. O. Zywitzki, T. Modes, P. Frach, D. Glöss, Surface & Coatings Technology **202** (2008), 2488–2493.

15. S.X. Liu, Z.P. Qu, X.W. Han, C.L. Sun, Catalysis Today **93–95** (2004), 877–884.

16. K.K. Saini, S. D. Sharma, Chanderkant, M. Kar, D. Singh, C.P. Sharma, Journal of Non-Crystalline Solids **353** (2007), 2469–2473.

17. D.R. Uhlmann, T. Suratwala, K. Davidson, J.M. Boulton, G. Teowee, Journal of Non-Crystalline Solids **218** (1997), 113-122.

18. A.S. Grove, Physics and Technology of Semiconductor Devices, John Wiley & Sons, New York, (1967).

19. A. H. Seidman and S. L. Marshall, Semiconductor Fundamentals, John Wiley and Sons, New York, (1963).

20. D. A. Neamen, Semiconductor Physics and Devices, McGraw Hill, New York, (2003).

21. V. Parmon, Catalysis Today **39** (1997), 137.

22. D. S. Bhatkhande, V. G. Pangarkar, A. Beenackers, Journal of Chemical Technology and Biotechnology **77** (2001), 102-116.

23. A. J. Nozik, R. Meming, Journal of Physical Chemistry **100** (1996), 13061.

24. H. Zhang, J.F. Banfield, Journal of Physical Chemistry B **104** (2000) 3481-3487.

25. A. Fujishima, X. Zhang, D. A. Tryk, Surface Science Reports **63** (2008), 515-582.

26. T.-S. Yang, C.-B. Shiu, M.-S. Wong, Surface Science **548** (2004), 75–82.

27. M. Ramamoorthy, D. Vanderbilt, R.D. King-Smith, Physical Review B **49** (1994), 16721.

28. V. Shklover, M.K. Nazeeruddin, S.M. Zakeeruddin, C. Barbe, A. Kay, T. Haibach, W. Steurer, R. Hermann, H.U. Nissen, M. Gratzel, Chemistry of Materials **9** (1997), 430-439.

29. B.K. Erdural, A. Yürüm, U. Bakır, G. Karakaş, Journal of Nanoscience and Nanotechnology **8** (2008), 878-886.

30. A. Fujishima, T.N. Rao, D.A. Tryk, Electrochimica Acta **45** (2000), 4683.

31. H. Jensen, K.D. Joensen, J.-E. Jorgensen, J.S. Pedersen, E.G. Sogaard, Journal of Nanoparticle Research **6** (2004), 519–526.

32. M. Kang, S.-Y. Lee, C.-H. Chung, S.M. Cho, G.Y. Han, B.-W. Kim, K.J. Yoon, Journal of Photochemistry and Photobiology A **144** (2001), 185–191.

33. J. Yu, J. Xiong, B. Cheng, S. Liu, Applied Catalysis B: Environment **60** (2005), 211–221.

34. O. Carp, C.L. Huisman, A. Reller, Prog. Solid State Chem. **32** (2004), 33–177.

35. G. L. Puma, A. Bono, D. Krishnaiah, J. G. Collin, Journal of Hazardous Materials **157** (2008) 209–219.

36. M.G. Nolan, M.E. Pemble, D.W. Sheel, H.M. Yates, Thin Solid Films **515** (2006), 1956–1962.

37. C.J. Tavares , S.M. Marques , L. Rebouta , S. Lanceros-Méndez , V. Sencadas , C.M. Costa, E. Alves, A.J. Fernandes, Thin Solid Films **517** (2008), 1161–1166.

38. P. Frach, D. GloX, Chr. Metzner, T. Modes, B. Scheffel, O. Zywitzki, Vacuum **80** (2006), 679–683.

39. L.E. Scriven, Mater. Res. Symp. Proc. **121** (1988), 717.

40. C.J. Brinker, A.J. Hurd, P.R. Schunk, G.C. Frye, C.S. Ashley, J. Non-Crystalline Solids **147/148,** (1992) 424.

41. A. Erkan, Investigation of Thin Semiconductor Coatings and Their Antimicrobial Properties, MSc Thesis, METU, Ankara, (2005).

42. H. Choi, E. Stathatos, D.D. Dionysiou, Thin Solid Films **510** (2006), 107.

43. G. L. Pumaa, A. Bonob, D. Krishnaiah, J. G. Collin, Journal of Hazardous Materials **157** (2008), 209–219.

44. A.I. Kontos, Thin Solid Films **515** (2007), 7370–7375.

45. L. Lasa, B. Serrano, M. Salaices, Photocatalytic Reaction Engineering, Springer Science + Business Media, New York, (2005).

46. Y. Takata, S. Hidaka, M. Masuda, T. Ito, International Journal of Energy Research **27** (2003), 111.

47. A. Fujishima, K. Hashimoto, T. Watanabe, TiO_2 Photocatalysis-Fundamentals and Applications, BKC, Tokyo, (1999).

48. K.S. Guan, B.J. Lu, Y.S. Yin, Surface and Coatings Technology **173** (2003) 219– 223.

49. O. Carp, C.L. Huisman, A. Reller, Progress in Solid State Chemistry **32** (2004), 33–177.

50. M. Machida, K. Norimoto, T. Watanabe, K. Hashimoto, A. Fujishima, Journal of Materials Science **34** (1999) 2569– 2574.

51. J.G. Yu, J.C. Yu, G.R. Zhong, J.J. Han, Q.N. Zhao, Journal of Materials Science Letters **20** (2001) 1745–1748.

52. X.T. Gao, I.E. Wachs, Catalalysis Today **51** (1999) 233– 254.

53. C. Murata, H. Yoshida, J. Kumagai, T. Hattori, Journal of Physical Chemistry B **107** (2003) 4364–4373.

54. C. Anderson, A.J. Bard, Journal of Physical Chemistry **99** (1995) 9882–9885.

55. K.S. Guan, B.J. Lu, Y.S. Yin, Surface and Coating Technology **173** (2003) 219– 223.

56. X. Zhao, Q. Zhao, J. Yu, B. Liu, Journal of Non-Crystalline Solids **354** (2008) 1424–1430.

57. V. Shpovalov, E.V. Stefanovich, T.N. Truog, Surface Science Letters **498** (2002) 103– 108.

58. T. Watanabe, Bull. Ceram. Soc. Jpn. **31** (1996) 837– 840.

59. A. Nakajima, K. Hashimoto, T. Watanabe, Langmuir **16** (2000), 7044-7047.

60. J. Shi, J. Zheng, P. Wu, Journal of Hazardous Materials, **161** (2009), 416.

61. R. Doong, S. Chang, Y. Hung, I. Kao, Seperation and Purification Technology **58** (2007), 192.

62. J. Yu, J.C. Yu and X. Zhao, Journal of Sol-Gel Science and Technology **24** (2002), 95.

63. Z. Li, B. Hou, Y. Xu, D. Wu, Y. Sun, Journal of Colloid and Interface Science **288** (2005), 149–154.

64. C. Yu, J. C. Yu, M. Chan, Journal of Solid State Chemistry **182** (2009), 1061–1069.

65. D. Robert, J.V. Weber, Journal of Cleaner Production **6** (1998), 335-338.

66. Y. Ao, J. Xu, D. Fu, C. Yuan, Applied Surface Science **255** (2008), 3137–3140.

67. C.Y. Kuo and H.Y. Lin, Journal of Hazardous Materials **165** (2009), 1243–1247.

68. M.R. Hoffmann, S.T. Martin, W. Choi, D.W. Bahnemann, Chemical Reviews **95** (1995), 69.

69. D. S. Bhatkhande, V. G. Pangarkar, A. Beenackers, Journal of Chemical Technology and Biotechnology **77** (2001), 102-116.

70. M. Ni, M. K. H. Leung, D. Y. C. Leung, K. Sumathy, Renewable and Sustainable Energy Reviews **11** (2007), 401–425.

71. X. G. Hou, M. D. Huang, X. L. Wu, A.-D. Liu, Chemical Engineering Journal **146** (2009), 42–48.

72. M.J. Uddin, F. Cesano, D. Scarano, F. Bonino, G. Agostini, G. Spoto, S. Bordiga, A. Zecchina, Journal of Photochemistry and Photobiology A: Chemistry **199** (2008), 64–72.

73. G. Mele, G. Ciccarella, G. Vasapollo, E. Garcia-Lopez, L. Palmisano, M. Schiavello, Applied Catalysis B-Environent **38** (2002), 309–319.

74. A. Corma, P. Serna, H. Garcia, Journal of the American Chemical Society **129** (2007), 6358–6359.

75. P. Löbl, M. Huppertz, D. Mergel, Thin Solid Films **251** (1994), 72.

76. G. Zhao, S.Utsumi, H. Kozuka, T. Yoko, Journal of Materials Science **33** (1998), 3655-3659.

77. R. Wang, N. Sakai, A. Fujishima, T. Watanabe, K. Hashimoto, Journal of Physical Chemistry B **103** (1999), 2188.

78. D. D. Beck, R. W. Siegel, Journal of Materials Research **7** (1992), 2840.

79. J.F. Porter, Y. Li, C.K. Cahn, Journal of Material Science **34** (1999) 1523–1531.

80. C. Su, B. Y. Hong, C. M. Tseng, Catalsis Today, **96** (2004), 119-126.

81. M. Inagaki, R. Nonaka, B. Tryba, A.W. Morawski, Proceedings of 4th International Conference Oils and Environment AUZO 2005, June 20–23, Gdansk, Poland, (2005), 325–332.

82. Z. Li, B. Hou, Y. Xu, D. Wu, Y. Sun, Journal of Colloid and Interface Science **288** (2005), 149–154.

83. A. Nakajima, S. Koizumi, T. Watanabe, K. Hashimoto, Journal of Photochemistry and Photobiology A Chemistry **146** (2001), 129.

84. A. Vittadini, A. Selloni, F.O. Rotzinger, M. Grätzel, Physical Review Letters **81** (1998), 2954.

85. O. Zywitzki, T. Modes, P. Frach, D. Glöss, Surface & Coatings Technology **202** (2008), 2488–2493.

86. A. Fujishima, X. Zhang, Comptes Rendus Chimie **9** (2006), 750–760.

87. X.Y. Deng, Y.H. Yue, Z. Gao, Applied Catalalysis B **39** (2002), 135.

88. I. Sopyan, M. Watanabe, S. Murasawa, K. Hashimoto and A. Fujishima. Journal of Photochemistry and Photobiology A: Chemistry **98** (1996), 79.

89. R. Wang, K. Hashimoto, A. Fujishima, M. Chikuni, E. Kojima, A. Kitamura, M. Shimohigoshi, T. Watanabe, Advanced Materials **10** (1998) 135-138.

90. P.S. Patil, Materials Chemistry Physics **59** (1999) 185.

91. H.K. Pulker, Coating on Glass, Elsevier, New York, (1999).

92. D.R. Uhlmann, J.M. Boulton, G. Teowee, L.W. Weisenbach, B.J.J. Zelinski, SPIE Proc. **1328** (1990), 270.

93. C.J. Brinker, G.W. Scherer, Sol-Gel Science: The Physics and Chemistry of Sol-Gel Processing, Academic Press, San Diego, CA, (1990).

94. C. Lee, Surface and Coatings Technology **173** (2003), 192–200.

95. Karuppuchamy N. Suzuki, S. Ito, T. Endo, Current Applied Physics **9** (2009), 243–248.

96. T. S. Yang, C.B. Shiu, M. S. Wong, Surface Science **548** (2004), 75-82.

97. L. D. Landau, B. G. Levich, Acta Physiochim. U.R.S.S. **17** (1942), 42-54.

98. C. J. Brinker, A. J. Hurd, K. J. Ward, Ultrastructure Processing of Advanced Ceramics, Wiley, New York (1988).

99. H. Schmidt, Sol-gel production : proceedings of the First Conference on Application and Commercialization of of Sol-Gel Processing **(**Saarbrücken, Germany), Trans Tech Pubications, NH, (1998).

100. J. Yang, D. Li, H.Wang, X.Wang, X. Yang, L. Lu, Materials Letters **50** (2001) 230–234.

101. S.H. Oh, D.J. Kim, S.H. Hahn, E.J. Kim, Materials Letters **57** (2003) 4151–4155.

102. M. Sasani Ghamsari, A.R. Bahramian, Materials Letters **62** (2008), 361–364.

103. N.-L. Wu, Bull. Coll. Eng., N.T.U. **84** (2002), 85.

104. C.J. Brinker, A.J. Hurd, P.R. Schunk, G.C. Frye and C.S. Ashley, Journal of Non-Crystalline Solids **147-148** (1992) 424-436.

105. H. Yin, Y. Wada, T. Kitamura, S. Kambe, S. Murasawa, H. Mori, T. Sakata, S. Yanagida, Journal of Materials Chemistry **11** (2001) 1694.

106. C. Su, B.-Y. Hong, C.-M. Tseng, Catalysis Today **96** (2004) 119–126.

107. H. Hieber, Thin Solid Films, **37** (1976) 335.

108. T. S. Chow., Journal of Physics: Condensed Matter **10** (1998), 445.

109.K. Hashimoto, H. Irie, A. Fujishima, Japan. Journal of Applied Physics **44** (2005) 8269-8285.

110.A. Bozzi, T. Yuranova, I. Guasaquillo, D. Laub, J. Kiwi, Journal of Photochemistry and Photobiology A: Chemistry **174** (2005) 156-164.

111.A. Bozzi, T. Yuranova, J. Kiwi, Journal of Photochemistry and Photobiology A: Chemistry **172** (2005), 27-34.

112.X.T. Zhang, O. Sato, M. Taguchi, Y. Einaga, T. Murakami, A. Fujishima, Chemistry of Materials **17** (2005), 696-700.

113. X. Zhang, A. Fujishima, M. Jin, A.V. Emeline, T. Murakami, Journal of Physical Chemistry B **110** (2006), 25142-25148.

114.S.N. Frank, A.J. Bard, Journal of the American Chemical Society **99** (1977), 303-304.

115. S.N. Frank, A.J. Bard, Journal of Physical Chemistry **81** (1977), 1484-1488.

116.D. Bahnemann, Solar Energy **77** (2004), 445-459.

117.A. Fujishima, T.N. Rao, D.A. Tryk, Journal of Photochemistry and Photobiology C **1** (2000), 1-21.

118.T. Ibusuki, K. Takeuchi, Journal of Molecular Catalysis **88** (1994), 93-102.

119.H. Ichiura, T. Kitaoka, H. Tanaka, Chemosphere **51** (2003), 855-860.

120.Y. Takata, S. Hidaka, J.M. Cao, T. Nakamura, H. Yamamoto, M. Masuda, T. Ito, Energy **30** (2005), 209-220.

121.A. Fujishima, D.A. Tryk, T. Watanabe, K. Hashimoto, International Glass Reviews (1998) 114-116.

122.T. Watanabe, A. Nakajima, R. Wang, M. Minabe, S. Koizumi, A. Fujishima, K. Hashimoto, Thin Solid Films **351** (1999), 260-263.

123.Y. Takata, S. Hidaka, M. Masuda, T. Ito, International Journal of Energy Research **27** (2003), 111-119.

124.Y. Takata, S. Hidaka, J.M. Cao, K. Tanaka, M. Masuda, T. Ito, T. Watanabe, M. Shimohigoshi, Thermal Science Engineering **8** (2000), 33-41.

125.Y. Ohko, S. Saitoh, T. Tatsuma, A. Fujishima, Journal of the Electrochemical Society **148** (2001), 24-28.

126.T. Tatsuma, S. Saitoh, Y. Ohko, A. Fujishima, Chemistry of Materials **13** (2001), 2838-2842.

127.P. Ngaotrakanwiwat, T. Tatsuma, S. Saitoh, Y. Ohko, A. Fujishima, Physical Chemistry Chemical Physics **5** (2003), 3234-3237.

128.T. Tatsuma, S. Saitoh, P. Ngaotrakanwiwat, Y. Ohko, A. Fujishima, Langmuir **18** (2002), 7777-7779.

129.P. Ngaotrakanwiwat, S. Saitoh, Y. Ohko, T. Tatsuma, A. Fujishima, Journal of the Electrochemical Society **150** (2003), 1405-1407.

130.M.C. Lee, W. Choi, Journal of Physical Chemistry B **106** (2002), 11818-11822.

131.Y. Ishikawa, Y. Matsumoto, Y. Nishida, S. Taniguchi, J. Watanabe, Journal of American Chemical Society **125** (2003), 6558-6562.

132.T. Tatsuma, W. Kubo, A. Fujishima, Langmuir **18** (2002), 9632-9634.

133.Y. Ohko, T. Tatsuma, T. Fujii, K. Naoi, C. Niwa, Y. Kubota, A. Fujishima, Nature Materials **2** (2003), 29-31.

134.K. Kawahara, K. Suzuki, Y. Ohko, T. Tatsuma, Chemistry Chemical Physics **7** (2005), 3851-3855.

135.R. Gorges, S. Meyer, G. Kreisel, Journal of Photochemistry and Photobiology A: Chemistry **167** (2004), 95-99.

136.K. Naoi, Y. Ohko, T. Tatsuma, Journal of the American Chemical Society **126** (2004), 3664-3668.

137.A. Erkan, U. Bakir, G. Karakas, Journal of Photochemistry and Photobiology A: Chemistry **184** (2006), 313–321.

138. P.F. Schwarz, N.J. Turro, S.H. Bossmann, A.M. Braun, A.-M.A. Abdel Wahab, H. Durr, Journal of Physical Chemistry B **101** (1997), 7127–7134.

139. Q. Liu, X. Wu, B. Wang, Q. Liu, Materials Research Bulletin **37** (2002), 2255-2262.

140. T. Yuranova, R. Mosteo, J. Bandara, D. Laub, J. Kiwi, Journal of Molecular Catalysis A: Chemical **244** (2006), 160–167.

141. Y. Ao, J. Xu, D. Fu, C. Yuan, Applied Surface Science **255** (2008), 3137–3140.

142. C. H. Giles and S. N. Nakhwa, Journal of Applied Chemistry, **12**, 266-272 (1962).

143. C. H. Giles, A. P. D'Silva and I. A. Easton, Journal of Colloid Interface Science (1974) **47**, 766-777.

144. C. H. Giles, Adsorption from Solution at the Solid-Liquid Interface, Academic Press, London, (1983).

145. C. Kaewprasit, E. Hequet, N. Abidi, J. P. Gourlot, Journal of Cotton Science **2** (1998), 164-173.

146. Inel O. and Tumsek F., Turkish Journal of Chemistry **24** (2000) 9-20.

147. T. Wu, G. Liu, J. Zhao, H. Hidaka, N. Serpone, Journal of Physical Chemistry B **102** (1998), 5845-5851.

148. K. Tadanaga, N. Katata, T. Minami, Journal of the American Ceramical Society **80** (1997), 1040.

149. E. Stathatos, P. Lianos, P. Falaros, Progress in Colloid and Polymer Science (2001) **118,** 96-99.

150. W. J. Ingledew, R. K. Poole, Microbiology Reviews **48** (1984), 222–271.

151. U. Fotadar, P. Zaveloff, L. Terracio, Journal of Basic Microbiology **45** (2005), 403–404.

152. E. J.A. Pope, S. Sakka, L. C. Klein, Sol-Gel Science and Technology, The American Ceramic Society, Ohio, Volume 55, (1994) 13.

153. A. Mills, G. Hill, M. Crow, S. Hodgen, Journal of Applied Electrochemistry **35** (2005) 641.

154. M. Langlet, S. Permpoon, D. Riassetto, G. Berthome, E. Pernot, J.C. Joud, Journal of Photochemistry and Photobiology A **181** (2006), 203.

155. Y. Chen, D. D. Dionysiou, Applied Catalysis B: Environmental **69** (2006), 24–33.

156. J. Yu, X. Zhao, Q. Zhao, G. Wang, Materials Chemistry and Physics **68** (2001), 253–259.

157. Y. Takata, S. Hidaka, M. Masuda, T. Ito, International Journal of Energy Research **27** (2003), 93-186.

158. S. Yamabi, H. Imai, Chemistry of Materials **14** (2002), 609-614.

159. J. Winkler, Titanium Dioxide, Vincentz Network GmbH & Co. KG, Hannover, (2003).

160. R.S. Mane, O. S. Joo, W. J. Lee, S. H. Han, Micron **38** (2007), 85–90.

161. J. F. Lee, C. K. Lee, L. C. Juang, Journal of Colloid and Interface Science **217** (1999), 172–176.

162.G. Seber, Preparation of Antimicrobial Biodegredable Films from the Agricultural Biowaste, MSc Thesis, METU, Ankara, (in press).

APPENDIX A

SAMPLE CALCULATIONS FOR THE TITANIUM DIOXIDE AND *E. COLI* CONCENTRATION IN THE SOLUTIONS

A.1. Titanium Dioxide Rate Calculation in the Solution

According to the procedure given in part 3.3.4, 2.5 ml titanium tetra-isopropoxide (TTIP) was used for 100 ml sol synthesis.

Density of titanium tetra-isopropoxide is:

$\rho\ C_{12}H_{28}O_4Ti = 0.95\ g/ml$

Mass of titanium n-butoxide added is:

$$Mass\ of\ C_{12}H_{28}O_4Ti = 2.5ml \times 0.95\frac{gr}{ml} = 2.375gr$$

Since molecular weight of titanium tetra-isopropoxide is 284.23 gr /mol,

$$2.375gr \times \left(284.23\frac{gr}{mol}\right)^{-1} = 8.36\times10^{-3}\ mol\ Ti\ means:$$

$$8.36 \times 10^{-3}\ mol\ TiO_2$$

Since molecular weight of titanium dioxide is 79.87 gr /mol,

$$Mass\ of\ TiO_2 = 79.87\frac{gr}{mol} \times \left(8.36\times10^{-3}\ molTiO_2\right) = 0.667gr\ \ TiO_2\ in\ the\ 100\ ml\ solution.$$

The sol was then diluted with distilled water ad *E. coli* suspension of which different concentrations:

The *E. coli* which was centrifuged from 50 ml broth was resuspended with 5 ml water. Therefore, the 100 ml sol was distilled with 40 ml water when the *E. coli* which was centrifuged from 400 ml broth was added. Similarly, for 200 ml broth 20 ml water, for 100 ml broth 10 ml water, for 50 ml broth 5 ml water and for 20 ml of broth 2 ml of water was added to the sol. This was also explained in the Table 3.1.

The rate of titania in these solutions are calculated as follows:

For 140 ml sol:

$$1.334gr \times \frac{100ml}{140ml} = 0.953gr \ \ TiO_2 \ in \ the \ 140 \ ml \ sol$$

$$\frac{0.943grTiO_2}{1.334grTiO_2} = 0.71$$

For 120 ml sol:

$$1.334gr \times \frac{100ml}{120ml} = 1.112gr \ TiO_2 \ in \ the \ 120 \ ml \ sol$$

$$\frac{1.112grTiO_2}{1.334grTiO_2} = 0.83$$

For 110 ml sol:

$$1.334gr \times \frac{100ml}{110ml} = 1.213gr \ TiO_2 \ in \ the \ 110 \ ml \ sol$$

$$\frac{1.213grTiO_2}{1.334grTiO_2} = 0.91$$

For 105 ml sol:

$$1.334gr \times \frac{100ml}{105ml} = 1.270gr \ TiO_2 \ in \ the \ 105 \ \ ml \ sol$$

$$\frac{1.270 gr TiO_2}{1.334 gr TiO_2} = 0.95$$

For 102 ml sol:

$$1.334 gr \times \frac{100 ml}{102 ml} = 1.308 gr\ TiO_2 \text{ in the 102 ml sol}$$

$$\frac{1.308 gr TiO_2}{1.334 gr TiO_2} = 0.98$$

For 100 ml sol:

1.334 gr TiO_2 in the 100 ml sol/1.334 TiO_2 in the 100 ml sol = 1

A.2. *E. coli* Rate Calculation in the Solution

In this study, the *E. coli* amount is calculated on the basis of the broth volume. Therefore the rates of the *E. coli* in the solutions are found as follows:

For 140 ml sol:

$$\frac{400 ml broth(E-coli)}{140 ml solution} = \frac{2.875 \frac{E-coli}{solution}}{1.667 \frac{E-coli}{solution}} = 1.71$$

For 120 ml sol:

$$\frac{200 ml broth(E-coli)}{120 ml solution} = \frac{1.667 \frac{E-coli}{solution}}{1.667 \frac{E-coli}{solution}} = 1$$

For 110 ml sol:

$$\frac{100 ml broth(E-coli)}{110 ml solution} = \frac{0.909 \frac{E-coli}{solution}}{1.667 \frac{E-coli}{solution}} = 0.54$$

For 105 ml sol:

$$\frac{50 ml broth(E-coli)}{105 ml solution} = {}^{0.476\frac{E-coli}{solution}}\Big/_{1.667\frac{E-coli}{solution}} = 0.29$$

For 102 ml sol:

$$\frac{20 ml broth(E-coli)}{102 ml solution} = {}^{0.196\frac{E-coli}{solution}}\Big/_{1.667\frac{E-coli}{solution}} = 0.12$$

APPENDIX B

CALCULATIONS FOR SURFACE AREA MEASUREMENTS

Methylene blue solution with 2 ppm, 3 ppm and 4 ppm concentration was prepeared for surface area measurements. TiO_2 coated thin film of known concentration was immersed into 20 ml methylene blue solution. At the end of 24 hours, absorbances of methylene blue were measured. This procedure was repeated for 1ppm, 2ppm and 3ppm concentration of methlene blue.

For the sample of TiO_2 rate is 0.83 and *E. coli* rate is 1 in the solution, the surface area is calculated as follows:

First of all the prepared methylene blue of 1 ppm, 2ppm and 3ppm concentration were measured and observed as 0.275, 0.486 and 0.723 at 661 nm respectively.

Then the area of the sample is calculated. Area were multiplied by 2 in order to have the area coated since both sides of the glass substrate were coated.

Area of the sample: $\left(25mm \times 20.5mm\right) \times \frac{1cm^2}{100mm^2} \times 2 = 10.25cm^2$

At the end of 24 hours, absorbances of methylene blue of 1 ppm, 2ppm and 3ppm concentration were remeasured to analyze the concentration difference. The absorbance values were found 0.181 for 1 ppm, 0.409 for 2ppm and 0.627 for 3ppm methylene blur solution.
Afterwards corresponding concentration values were calculated as:

C_E *(for 1ppm)* $= \frac{0.181}{0.275} \times 1 \frac{mg}{lt} = 0.658182 \frac{mg}{lt}$

$$C_E \text{ (for 2ppm)} = \frac{0.409}{0.486} \times 2 \frac{mg}{lt} = 1.683128 \frac{mg}{lt}$$

$$C_E \text{ (for 3ppm)} = \frac{0.627}{0.723} \times 3 \frac{mg}{lt} = 2.602166 \frac{mg}{lt}$$

Adsorbed methylene blue on the surface was measured by using concentration of the solution and knowing the initial solute amount solved in water.

Initial solutes solved in 20 ml water for different MB concentration were:

$$1mg \times \frac{20ml}{1000ml} = 0.02mg \ \ methylene\ blue$$

$$2mg \times \frac{20ml}{1000ml} = 0.04mg\ methylene\ blue$$

$$3mg \times \frac{20ml}{1000ml} = 0.06mg\ methylene\ blue$$

Adsorbed methylene blue on the surface is the difference between the initial amount of solute and the amount of solute remaining in the MB sol after 24 hours.

$$For\ 1\ ppm\ MB\ sol: x = 0.02mg - 0.678 \frac{mg}{lt} \times \frac{1lt}{1000mg} \times 20ml = 0.006836mg$$

$$For\ 2\ ppm\ MB\ sol: x = 0.04mg - 1.683 \frac{mg}{lt} \times \frac{1lt}{1000mg} \times 20ml = 0.006337mg$$

$$For\ 3\ ppm\ MB\ sol: x = 0.06mg - 2.602 \frac{mg}{lt} \times \frac{1lt}{1000mg} \times 20ml = 0.007967mg$$

x/m (quantity of methylene blue adsorbed per unit volume of adsorbent) was calculated by dividing adsorbed amount of methylene blue to the coated area of the sample:

For 1 ppm MB sol: $\frac{x}{m} = \frac{0.006836}{10.75} = 0.000636 \frac{mg}{cm^2}$

For 2 ppm MB sol: $\frac{x}{m} = \frac{0.006337}{10.75} = 0.00059 \frac{mg}{cm^2}$

For 3 ppm MB sol: $\frac{x}{m} = \frac{0.007967}{10.75} = 0.000741 \frac{mg}{cm^2}$

Then $\frac{C_E}{x/m}$ values were calculated from the obtained data above.

For 1 ppm MB sol: $\frac{C_E}{x/m} = \frac{0.658182 \frac{mg}{lt}}{0.000636 \frac{mg}{cm^2}} = 1034.973$

For 2 ppm MB sol: $\frac{C_E}{x/m} = \frac{1.683128 \frac{mg}{lt}}{0.00059 \frac{mg}{cm^2}} = 2855.032$

For 3 ppm MB sol: $\frac{C_E}{x/m} = \frac{2.60166 \frac{mg}{lt}}{0.000741 \frac{mg}{cm^2}} = 3510.547$

From the below equation the plot of $\frac{C_E}{x/m}$ versus C_E gives a straight line with slope equal to $\frac{1}{x_m}$ and intercept equal to $\frac{1}{kx_m}$.

$$\frac{C_E}{x/m} = \frac{1}{kx_m} + \frac{C_E}{x_m}$$

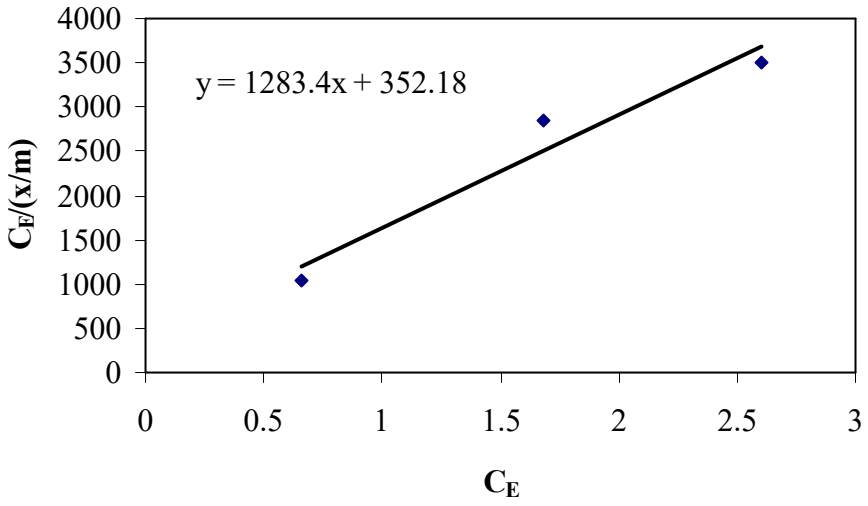


Figure B.1 Adsorption isotherm for the sample of TiO_2 rate is 0.83 and *E. coli* rate is 1

From this plot $\frac{1}{x_m}$ is found as 1283.4 and x_m is found as 0.001505.

Finally, specific surface area in terms of cm^2/cm^2 was calculated according to equation:

$$S = \frac{L \times A_{MB} \times x_m}{N \times M_w}$$

$$S = \frac{6.02 \times 10^{23}\, mol^{-1} \times 1.2 nm^2 \times \frac{1 cm^2}{10^{-18} nm^2} \times 0.001505 \frac{mg}{cm^2}}{1 \times 373.9 \frac{g}{mol} \times \frac{1000 mg}{1 g}}$$

$$S = 15.05429 cm^2 / cm^2$$

During the calculations, cross-sectional area of methylene blue adsorbed on the surface (A_{MB}) was taken as 1.2 nm^2 while coverage factor (N) was taken as 1 [146].

For the sample of TiO_2 rate is 0.71 and *E. coli* rate is 1.71 in the solution, area, amounts of adsorbed methylene blue, regression coefficients for each sample are tabulated below.

Table B.1 Data required to calculate surface area measurement for the sample of TiO_2 rate is 0.71 and *E. coli* rate is 1.71

MB Conc (ppm)	**Area (cm2)**	**Abs (24h)**	**C_E (mg/lt)**	**x (mg)**	**x/m (mg/cm2)**	**C_E/(x/m)**
1	10.25	0.197	0.716364	0.005673	0.000553	1294.391
2	10.25	0.399	1.641975	0.00716	0.000699	2350.431
3	10.25	0.621	2.576763	0.008465	0.000826	3120.221

From the given data in the Table B.1 curves for fitting parameters to Langmuir isotherms are obtained and the surface area is calculated.

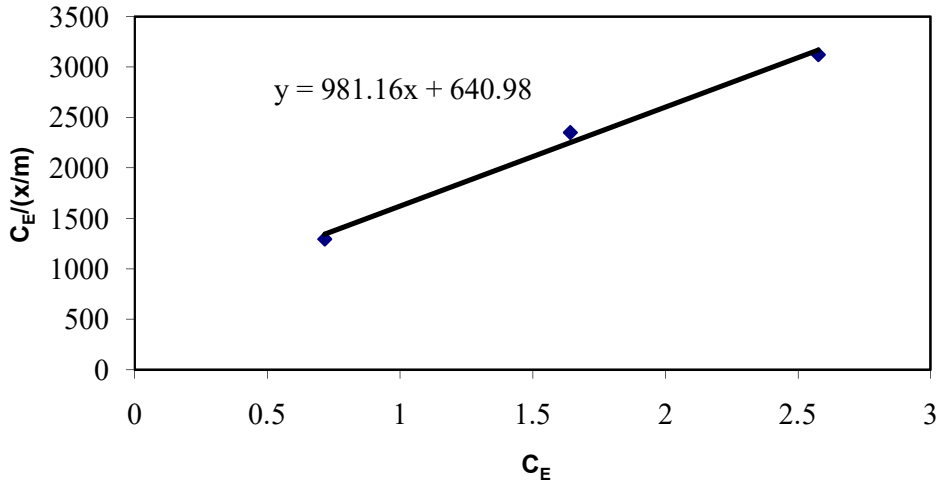


Figure B.2 Adsorption isotherm for the sample of TiO_2 rate is 0.71 and *E. coli* rate is 1.71

From this plot $\frac{1}{x_m}$ is found as 981.16 and x_m is found as 0.0010192.

Then specific surface area in terms of cm^2/cm^2 was calculated according to equation:

$$S = \frac{6.02\times10^{23}\,mol^{-1}\times1.2nm^2\times\frac{1cm^2}{10^{-18}nm^2}\times0.0010192\frac{mg}{cm^2}}{373.9\frac{g}{mol}\times\frac{1000mg}{1g}}$$

$$S = 19.69166cm^2/cm^2$$

For the sample of TiO_2 rate is 0.91 and *E. coli* rate is 0.54 in the solution, area, amounts of adsorbed methylene blue, regression coefficients for each sample are tabulated below.

Table B.2 Data required to calculate surface area measurement for the sample of TiO_2 rate is 0.91 and *E. coli* rate is 0.54

MB Conc (ppm)	Area (cm^2)	Abs (24h)	C_E (mg/lt)	x (mg)	x/m (mg/cm^2)	$C_E/(x/m)$
1	9	0.436	1.794239	0.004115	0.000457	3924
2	9	0.207	0.752727	0.004945	0.000549	1369.853
3	9	0.664	2.755187	0.004896	0.000544	5064.407

From the given data in the Table B.2 curves for fitting parameters to Langmuir isotherms are obtained and the surface area is calculated.

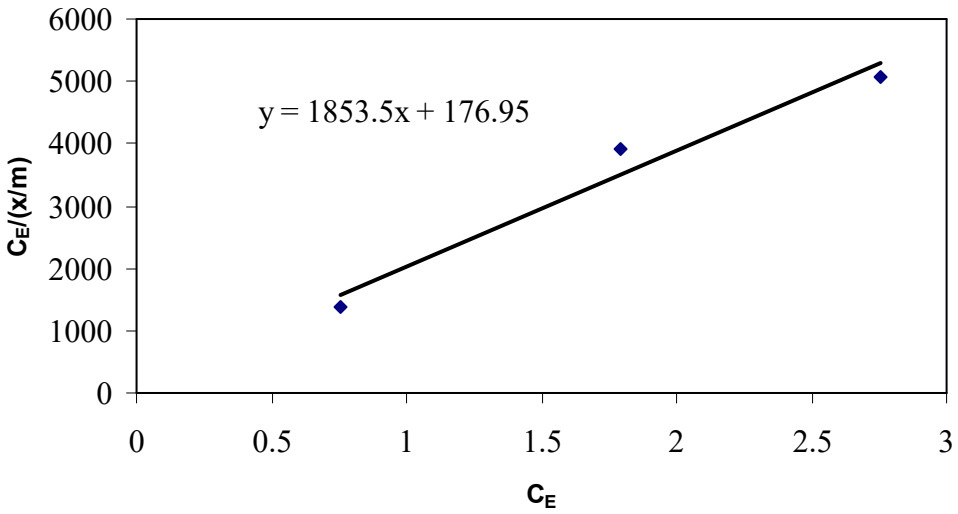


Figure B.3 Adsorption isotherm for the sample of TiO_2 rate is 0.91 and *E. coli* rate is 0.54

From this plot $\frac{1}{x_m}$ is found as 1853.1 and x_m is found as 0.0005395

Then specific surface area in terms of cm^2/cm^2 was calculated according to equation:

$$S = \frac{6.02 \times 10^{23} mol^{-1} \times 1.2 nm^2 \times \frac{1 cm^2}{10^{-18} nm^2} \times 0.0005395 \frac{mg}{cm^2}}{373.9 \frac{g}{mol} \times \frac{1000 mg}{1 g}}$$

$$S = 10.42389 cm^2 / cm^2$$

For the sample of TiO_2 rate is 0.95 and *E. coli* rate is 0.29 in the solution, area, amounts of adsorbed methylene blue, regression coefficients for each sample are tabulated below.

Table B.3 Data required to calculate surface area measurement for the sample of TiO_2 rate is 0.95 and *E. coli* rate is 0.29

MB Conc (ppm)	**Area (cm^2)**	**Abs (24h)**	**C_E (mg/lt)**	**x (mg)**	**x/m (mg/cm^2)**	**$C_E/(x/m)$**
1	13.75	0.415	1.707819	0.005844	0.000425	4018.486
2	13.75	0.213	0.774545	0.004509	0.000328	2361.895
3	13.75	0.655	2.717842	0.005643	0.00041	6622.243

From the given data in the Table B.3 curves for fitting parameters to Langmuir isotherms are obtained and the surface area is calculated.

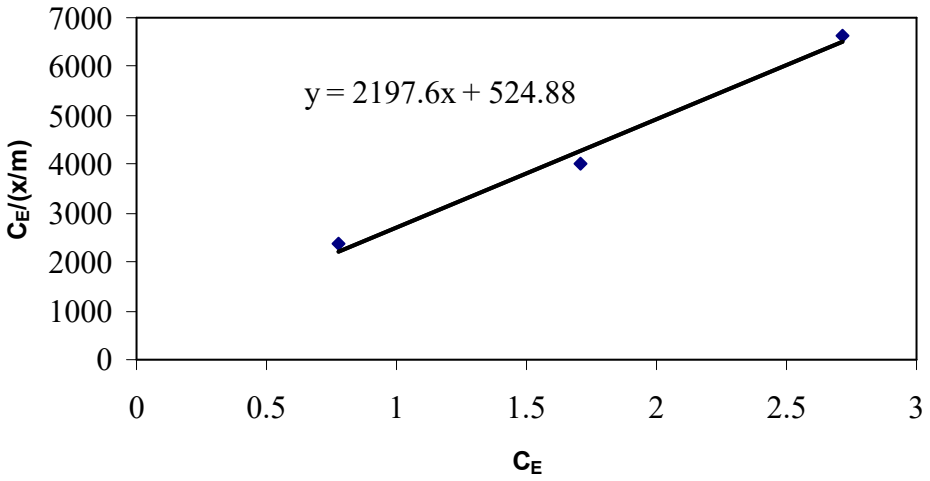


Figure B.4 Adsorption isotherm for the sample of TiO_2 rate is 0.95 and *E. coli* rate is 0.29

From this plot $\frac{1}{x_m}$ is found as 2197.6 and x_m is found as 0.000455.

Then specific surface area in terms of cm^2/cm^2 was calculated according to equation:

$$S = \frac{6.02 \times 10^{23} mol^{-1} \times 1.2 nm^2 \times \frac{1 cm^2}{10^{-18} nm^2} \times 0.000455 \frac{mg}{cm^2}}{373.9 \frac{g}{mol} \times \frac{1000 mg}{1 g}}$$

$$S = 8.7917155 cm^2 / cm^2$$

For the sample of TiO_2 rate is 0.98 and *E. coli* rate is 0.12 in the solution, area, amounts of adsorbed methylene blue, regression coefficients for each sample are tabulated below.

Table B.4 Data required to calculate surface area measurement for the sample of TiO_2 rate is 0.98 and *E. coli* rate is 0.12

MB Conc (ppm)	Area (cm^2)	Abs (24h)	C_E (mg/lt)	x (mg)	x/m (mg/cm^2)	$C_E/(x/m)$
1	9.5	0.454	1.868313	0.002634	0.000277	6739.063
2	9.5	0.247	0.898182	0.002036	0.000214	4190.179
3	9.5	0.695	2.883817	0.002324	0.000245	11790.18

From the given data in the Table B.4 curves for fitting parameters to Langmuir isotherms are obtained and the surface area is calculated.

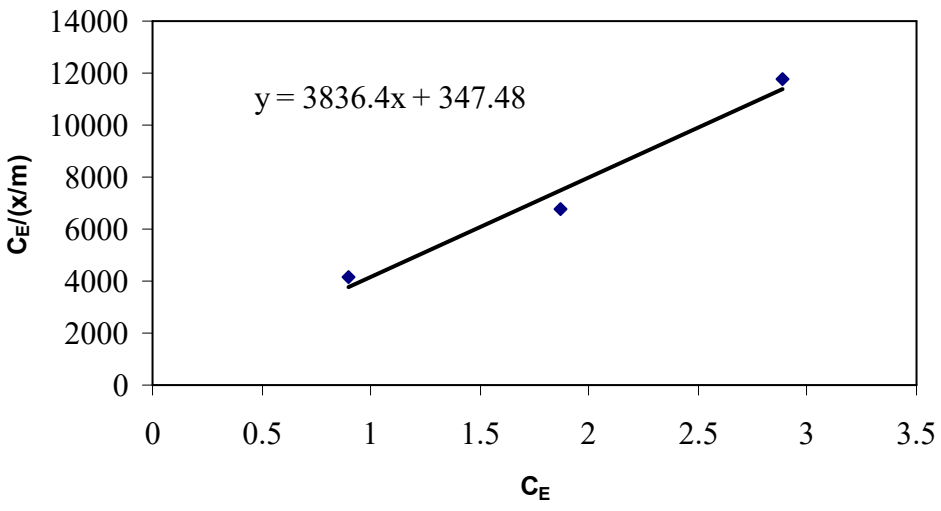


Figure B.5 Adsorption isotherm for the sample of TiO_2 rate is 0.98 and *E. coli* rate is 0.12

From this plot $\frac{1}{x_m}$ is found as 3836.4 and x_m is found as 0.0002627.

Then specific surface area in terms of cm^2/cm^2 was calculated according to equation:

$$S = \frac{6.02\times10^{23}\,mol^{-1}\times1.2nm^2\times\frac{1cm^2}{10^{-18}nm^2}\times0.0002627\frac{mg}{cm^2}}{373.9\frac{g}{mol}\times\frac{1000mg}{1g}}$$

$$S = 5.0361469cm^2/cm^2$$

For the sample of TiO_2 rate is 1 and contained no *E. coli* in the solution, area, amounts of adsorbed methylene blue, regression coefficients for each sample are tabulated below.

Table B.5 Data required to calculate surface area measurement for the sample of TiO_2 rate is 1 and *E. coli* rate is 0

MB Conc (ppm)	**Area (cm2)**	**Abs (24h)**	**C_E (mg/lt)**	**x (mg)**	**x/m (mg/cm2)**	**C_E/(x/m)**
1	13.75	0.452	1.860082	0.002798	0.000204	9139.706
2	13.75	0.232	0.843636	0.003127	0.000227	3709.302
3	13.75	0.686	2.846473	0.003071	0.000223	12746.62

From the given data in the Table B.5 curves for fitting parameters to Langmuir isotherms are obtained and the surface area is calculated.

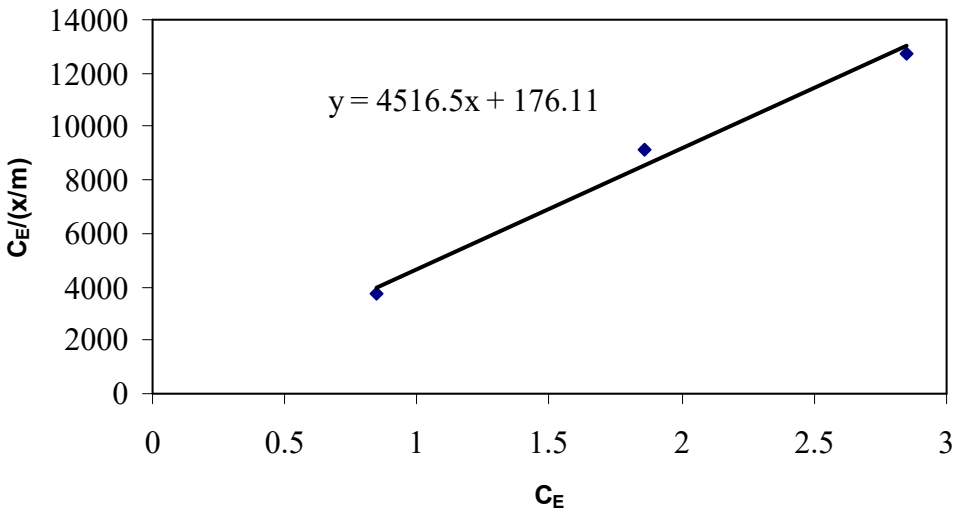


Figure B.6 Adsorption isotherm for the sample of TiO_2 rate is 1

From this plot $\frac{1}{x_m}$ is found as 4516.5 and x_m is found as 0.0002214.

Then specific surface area in terms of cm^2/cm^2 was calculated according to equation:

$$S = \frac{6.02\times10^{23}\,mol^{-1}\times1.2nm^2\times\frac{1cm^2}{10^{-18}nm^2}\times0.0002214\frac{mg}{cm^2}}{373.9\frac{g}{mol}\times\frac{1000mg}{1g}}$$

$$S = 4.2777978cm^2/cm^2$$

APPENDIX C

DATA OF PHOTOCATALYTIC ACTIVITY MEASUREMENTS

Table C.1 Concentration change of methylene blue stain with the concentartion of 170 mg/lt for the *E. coli* doped titanium dioxide coated thin films subjected to 300 W/m^2 artificial solar irradiation.

Irradiation Time (min)	**C/C_0 Ecolix1.71/ TiO_2x0.71**	**Irradiation Time (min)**	**C/C_0 Ecolix1/ TiO_2x0.83**	**Irradiation Time (min)**	**C/C_0 Ecolix0.54/ TiO_2x0.91**
0	1.00	0	1.00	0	1.00
30	0.86	15	0.47	30	0.79
60	0.79	30	0.42	60	0.69
90	0.75	75	0.38	90	0.62
120	0.71	90	0.32	120	0.39
150	0.67	105	0.29	150	0.28
180	0.54	120	0.23	180	0.25
210	0.35	135	0.20	210	0.11
240	0.21	150	0.14	240	0.11
300	0.14	165	0.17	300	0.07
360	0.14	180	0.14	360	0.07
420	0	195	0.10	420	0
480	0	210	0.04	480	0
		225	0		
		240	0		

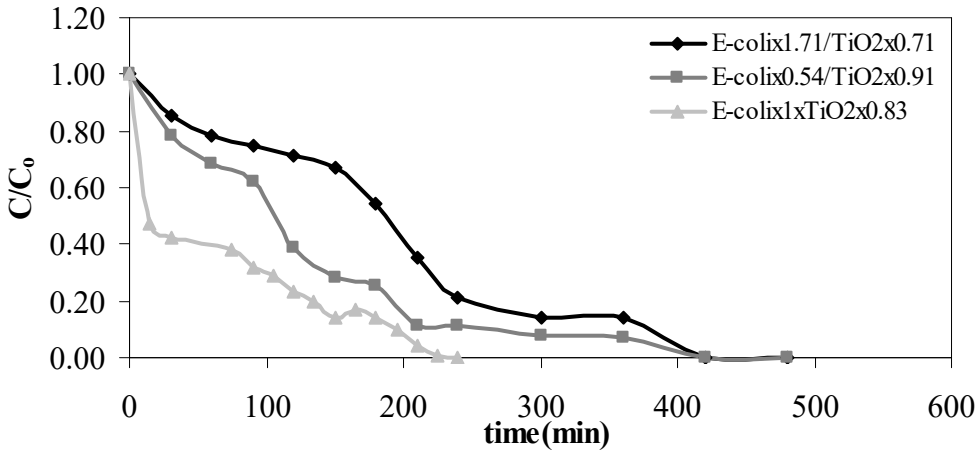


Figure C.1 Concentration change of methylene blue (170 mg/lt) solution on the surface of the thin films with different *E. coli* and titania content.

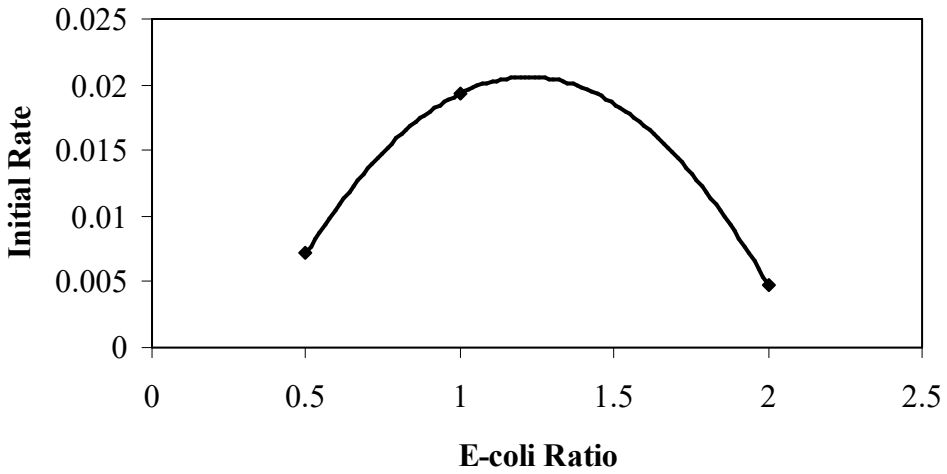


Figure C.2 The initial degradation rate of methylene blue solution (170 mg/lt) for various *E. coli* content.

Table C.2 Concentration change of methylene blue stain with the concentartion of 180 mg/lt for the *E. coli* doped titanium dioxide coated thin films subjected to 300 W/m^2 artificial solar irradiation.

Irradiation Time (min)	**C/C_0 Ecolix1.71/ TiO_2x0.71**	**Irradiation Time (min)**	**C/C_0 Ecolix1/ TiO_2x0.83**	**Irradiation Time (min)**	**C/C_0 Ecolix0.54/ TiO_2x0.91**
0	1.00	0	1.00	0	1.00
30	0.83	15	0.87	30	0.56
60	0.58	30	0.53	60	0.37
90	0.54	45	0.16	90	0.30
120	0.46	60	0.11	120	0.20
150	0.26	75	0.07	150	0.13
180	0.28	90	0.03	180	0.09
210	0.28	195	0.02	210	0.08
240	0.26	210	0	240	0.05
300	0.19			300	0.03
360	0.08			360	0
420	0			420	0
480	0			480	0

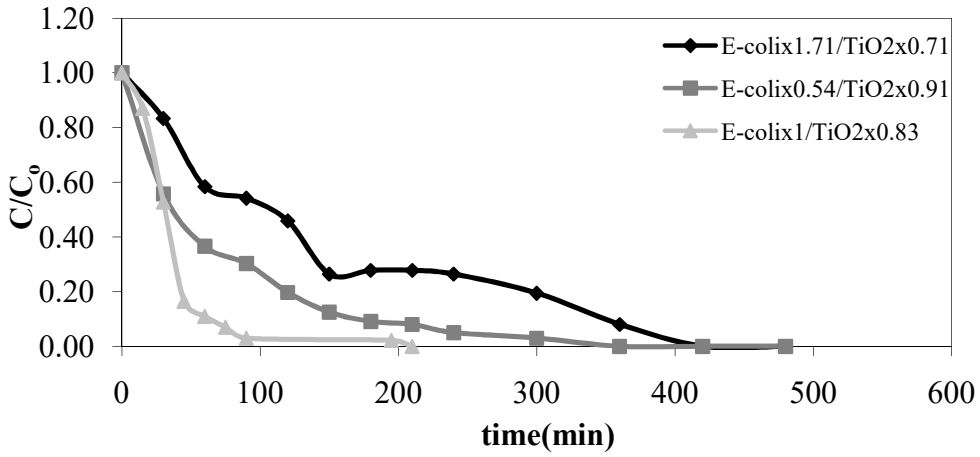


Figure C.3 Concentration change of methylene blue solution (180 mg/lt) on the surface of the thin films with different *E. coli* and titania content.

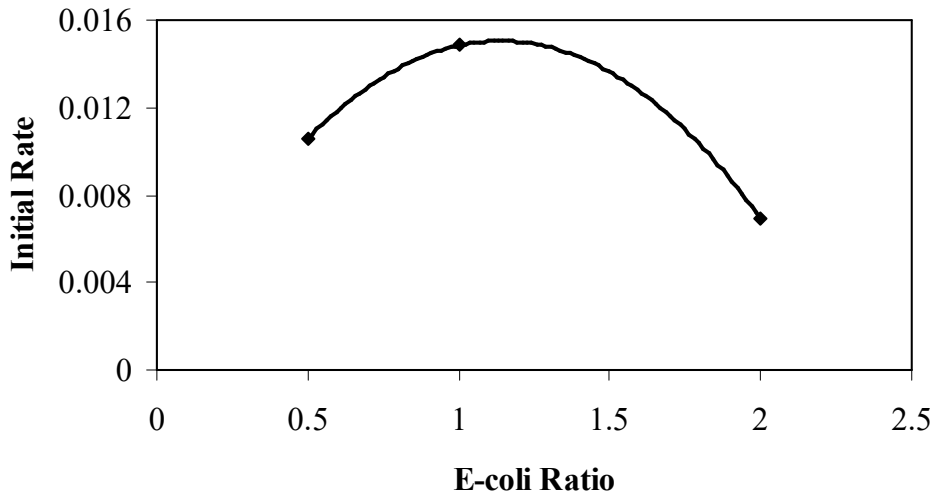


Figure C.4 The initial degradation rate of methylene blue solution (180 mg/lt) for various *E. coli* content.

Table C.3 Concentration change of methylene blue stain with the concentartion of 190 mg/lt for the *E. coli* doped titanium dioxide coated thin films subjected to 300 W/m^2 artificial solar irradiation.

Irradiation Time (min)	**C/C_0 Ecolix1.71/ TiO_2x0.71**	**Irradiation Time (min)**	**C/C_0 Ecolix1/ TiO_2x0.83**	**Irradiation Time (min)**	**C/C_0 Ecolix0.54/ TiO_2x0.91**
0	1.00	0	1.00	0	1.00
30	1.00	30	0.79	15	0.85
60	0.81	60	0.73	30	0.57
120	0.66	90	0.68	75	0.47
150	0.58	120	0.51	90	0.39
180	0.46	150	0.31	105	0.38
210	0.42	180	0.27	120	0.33
240	0.36	210	0.26	135	0.28
300	0.31	240	0.21	150	0.23
360	0.23	300	0.18	165	0.11
420	0.07	360	0.09	180	0.06
480	0	420	0.03	195	0.06
		480	0	210	0.05
				240	0

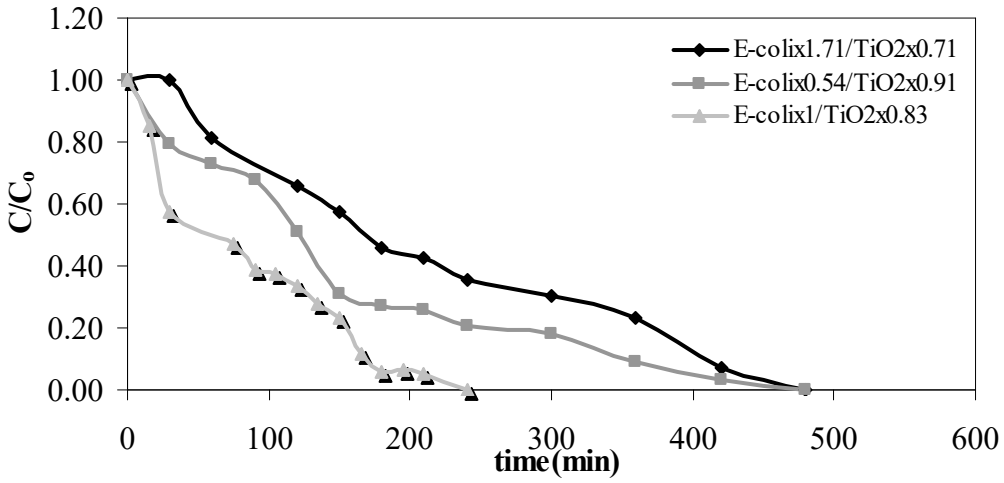


Figure C.5 Concentration change of methylene blue solution (190 mg/lt) on the surface of the thin films with different *E. coli* and titania content.

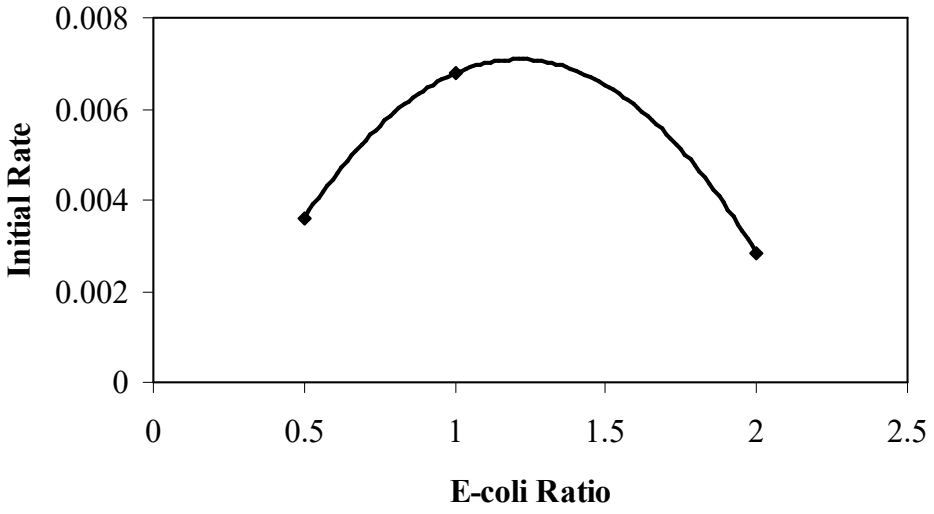


Figure C.6 The initial degradation rate of methylene blue solution (190 mg/lt) for various *E. coli* content.

Table C.4 Concentration change of methylene blue stain with the concentartion of 210 mg/lt for the *E. coli* doped titanium dioxide coated thin films subjected to 300 W/m^2 artificial solar irradiation.

Irradiation Time (min)	**C/C_0 Ecolix1.71/ TiO_2x0.71**	**Irradiation Time (min)**	**C/C_0 Ecolix1/ TiO_2x0.83**	**Irradiation Time (min)**	**C/C_0 Ecolix0.54/ TiO_2x0.91**
0	1.00	0	1.00	0	1.00
30	0.90	15	0.66	30	0.77
60	0.73	30	0.54	60	0.62
90	0.66	45	0.45	90	0.54
120	0.63	75	0.41	120	0.45
150	0.57	90	0.39	150	0.33
180	0.40	105	0.36	180	0.29
210	0.39	120	0.31	210	0.22
240	0.27	135	0.29	240	0.19
300	0.21	150	0.25	300	0.16
360	0.13	165	0.20	360	0.08
420	0.01	180	0.14	420	0.07
480	0	195	0.05	480	0
		210	0.02		
		225	0		
		240	0		

Table C.5 Concentration change of methylene blue solution for the *E. coli* doped (x0-x0.12-x0.29) titanium dioxide (x1-x0.98-x0.95) coated thin films subjected to 300 W/m^2 artificial solar irradiation.

Irradiation Time (min)	**C/C_0 Ecolix0/ TiO_2x1**	**C/C_0 Ecolix0.12/ TiO_2x0.98**	**C/C_0 Ecolix0.29/ TiO_2x0.95**
0	1	1	1
20	0.48387	0.40506	0.25773
35	0.37097	0.24051	0.15464
50	0.25806	0.16456	0.09278
65	0.16129	0.11392	0.07216
85	0.12903	0.07595	0.03093
108	0.06452	0.03797	0
135	0.03226	0.01266	
180	0	0	

Table C.6 Concentration change of methylene blue solution for the *E. coli* doped (x0.54-x1-x1.71) titanium dioxide (x0.91-x0.83-x0.71) coated thin films subjected to 300 W/m^2 artificial solar irradiation.

Irradiation Time (min)	**C/C$_0$ Ecolix0.54/ TiO$_2$x0.91**	**C/C$_0$ Ecolix1/ TiO$_2$x0.83**	**C/C$_0$ Ecolix1.71/ TiO$_2$x0.71**
0	1	1	1
20	0.2962963	0.18947368	0.72625698
35	0.21481481	0.10526316	0.55865922
50	0.14814815	0.04210526	0.46368715
65	0.05185185	0.03157895	0.37988827
85	0.03703704	0.01052632	0.27932961
108	0	0.01052632	0.22346369
135		0	0.16759777
180			0.11731844
240			0.09497207
300			0.04469274
360			0

Table C.7 Mean, standart deviation and error value of the *E. coli* doped (x0.54-x1-x1.71) titanium dioxide coated thin films.

	E. coli x0.54	*E. coli* x1	*E. coli* x1.71
Initial Rate	0.00713246	0.01933333	0.0047619
	0.01057692	0.01483516	0.00694444
	0.0036075	0.00677699	0.00282486
	0.00766667	0.01521739	0.00348259
Mean	0.00724589	0.01404072	0.00450345
Standart Deviation	0.00285911	0.00525323	0.00181522
Standart Error	0.00142956	0.00262661	0.00090761

Table C.8 Mean, standart deviation and error value of the *E. coli* doped (x0.12-x0.29-x0.54-x1-x1.71) and undoped titanium dioxide coated thin films.

	E. coli x0	*E. coli* x0.12	*E. coli* x0.29	*E. coli* x0.54	*E. coli* x1	*E. coli* x1.71
Inıtial Rate (μg MB/(cm^2-min))	0.005763	0.007276	0.015232	0.019142	0.030034	0.011303
	0.006614	0.007697	0.01264	0.018747	0.032774	0.01501
Mean	0.006189	0.007487	0.013936	0.018944	0.031404	0.013157
Standart Deviation	0.000602	0.000298	0.001833	0.000279	0.001938	0.002621
Standart Error	0.000426	0.000211	0.001296	0.000197	0.00137	0.001854

APPENDIX D

PREPARATION OF NUTRIENT BROTH

Nutrient broth was prepared by adding 2 g tryptone, 1 g yeast extract and 2 g sodium chloride into 200 ml water that was stirred until obtaining a limpid liquid. Resultant broth was autoclaved to sterilize before the cultivate procedure. *E. coli* bacteria used in the experiments was cultured over 16 hours in a rotary-shaker that is fixed at 170 rpm and 35ºC (Figure D.1).

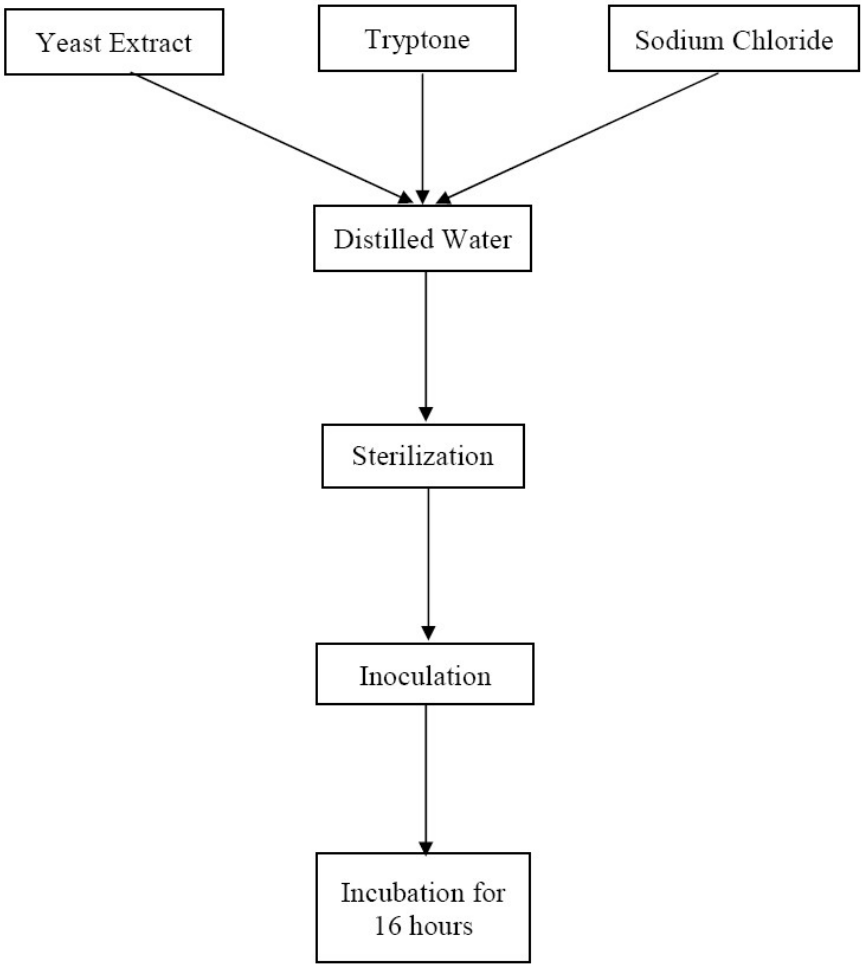


Figure D.1 Flow chart for the preparation of *E. coli* culture

APPENDIX E

GROWTH CURVE

The S-shaped curve that describes the bacteria's growth in a constant environment. The bacteria grow exponentially, then they reach the maximum of the environments resources, and then start decaying. In this study *E-coli* was centrifuged at 16th hour when the maximum amount was reached (Figure E.1).

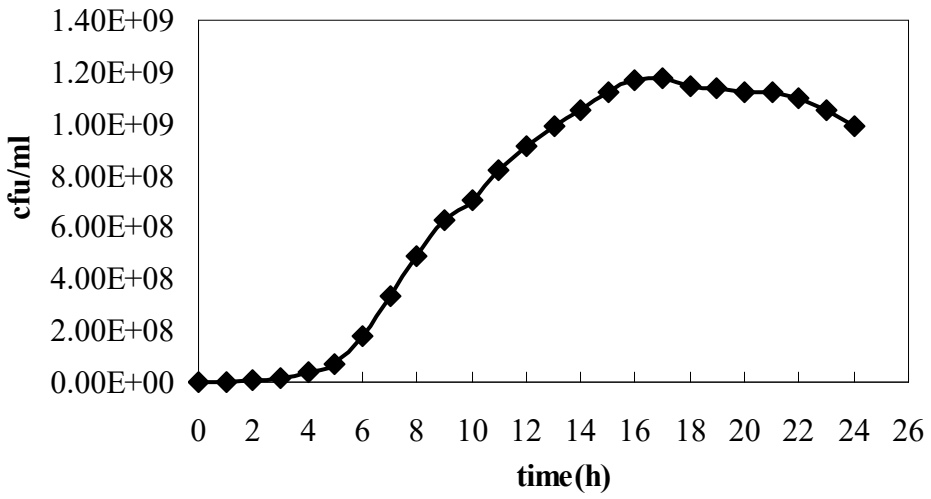


Figure E.1 Growth curve of *E. coli* XL1-blue [162]

The colony forming unit was observed as 1.2x10^9 per mililiter from the growth curve given in the . The colony forming unit in the solutions were calculated as follows:

For x1.71 *E-coli*;

$$1.2\times10^9\ \frac{cfu}{ml}\times\frac{400mlbroth}{140mlsol}=3.4\times10^9\ \frac{cfu}{ml}$$

For x1 *E-coli*;

$$1.2\times10^{9}\ \frac{cfu}{ml}\times\frac{200mlbroth}{120mlsol}=2\times10^{9}\ \frac{cfu}{ml}$$

For x0.54 *E-coli*;

$$1.2\times10^{9}\ \frac{cfu}{ml}\times\frac{100mlbroth}{110mlsol}=1.1\times10^{9}\ \frac{cfu}{ml}$$

For x0.29 *E-coli*;

$$1.2\times10^{9}\ \frac{cfu}{ml}\times\frac{50mlbroth}{105mlsol}=0.6\times10^{9}\ \frac{cfu}{ml}$$